University of Nevada, Reno

Experimental Seismic Evaluation of Ceiling-Piping-Partition Nonstructural Systems

A thesis submitted in partial fulfillment of the
requirements for the degree of Master of Science in
Civil and Environmental Engineering

by

Craig K. Jenkins

Dr. E. “Manos” Maragakis / Thesis Advisor

December, 2015

THE GRADUATE SCHOOL

We recommend that the thesis
prepared under our supervision by

CRAIG K. JENKINS

Entitled

Experimental Seismic Evaluation of Ceiling-Piping-Partition Nonstructural Systems

be accepted in partial fulfillment of the
requirements for the degree of

MASTER OF SCIENCE

E. "Manos" Maragakis, Ph.D., Dean, Advisor

Ahmad Itani, Ph.D., Chair, Committee Member

John Anderson, Ph.D., Graduate School Representative

David W. Zeh, Ph.D., Dean, Graduate School

December, 2015

ABSTRACT

The seismic performance of nonstructural components plays a significant role during and after an earthquake. Damage to these systems can leave buildings inoperable, causing economic losses and extensive downtime. Therefore, it is necessary to better understand the response of these systems in order to enhance the seismic resilience of buildings.

A series of full-scale system-level experiments conducted at the University of Nevada, Reno Network for Earthquake Engineering Simulation site aimed to investigate the seismic performance of integrated ceiling-piping-partition systems. A full-scale, two-story, two-by-one bay steel braced-frame test-bed structure that spanned over three biaxial shake tables was used to house the nonstructural systems. The test-bed structure was subjected to over 50 generated ground motions in a series of eight tests. The test-bed structure could be constructed into two configurations, one to produce large floor accelerations and the other to produce large inter-story drifts, affecting both acceleration and drift sensitive nonstructural systems. The responses and behaviors of ceiling-piping-partition systems were critically assessed through several design variables, configurations, and materials. The degree of damage observed during testing was used as an evaluation of the performance of nonstructural components.

Post processing of experimental data led to results including acceleration amplification factors, seismic fragility analysis, and overall performance of nonstructural systems. Three significant findings from this experiment are as follows: 1) ceiling systems with pop rivet connections have a lower probability of failure compared to seismic clips, 2) pipe joints with 2.0 in. (50.8 mm) diameter pipes have the greatest

probability of rotation failure compared to other diameter pipes, and 3) acceleration amplification factors for out-of-plane partition walls are comparable with the recommended amplification suggested by the ASCE 7-10 code for flexible components.

ACKNOWLEDGMENTS

The research presented in this study was funded by the National Science Foundation (NSF) under grant number CMMI-0721399, Simulation of the Seismic Performance of Nonstructural Systems. Any opinions, findings, conclusions or recommendations expressed in this document are those of the investigators and do not necessarily reflect the views of the sponsors. The input provided by the Practice Committee of the NEESR-GC Nonstructural Project, composed of W. Holmes (Chair), D. Allen, D. Alvarez, R. Fleming, and P. Malhotra; and its Advisory Board, composed of R. Bachman (Chair), S. Eder, R. Kirchner, E. Miranda, W. Petak, S. Rose and C. Tokas, has been crucial for the completion of this research. The following companies are thanked for providing product donations and technical support: Omboli Interior Inc., Armstrong, Hilti, and CEMCO steel. A word of gratitude goes to Dr. Sherif Elfass, Dr. Patrick Laplace, Dr. Joseph Wiser, Robert Nelson, Chad Lyttle, Todd Lyttle, Mark Lattin and the rest of the University of Nevada, Reno laboratory staff for their assistance with testing.

I would like to thank Dean Manos Maragakis, Dr. Ahmad Itani, and Dr. John Anderson for their time and effort spent as my thesis committee. Dean Manos Maragakis, who is recognized as the committee chair and my advisor, is thanked for providing me with the opportunity to achieve my master's degree under his supervision. A word of gratitude goes to my co-author and fellow colleague, Esmaeel Rahmanishamsi, for his helpful insight and aid throughout the project. A special thank you is expressed to Dr. Siavash Soroushian for providing his knowledge, support, and serving as a mentor for my time as a graduate student.

TABLE OF CONTENTS

Abstract i

Acknowledgments iii

List of Tables vi

List of Figures viii

1. Introduction 1

    Motivation 1

    Project Overview 2

    Background 3

    Literature Review 8

    Objectives and Scope 19

    Report Organization 20

2. Suspended Ceiling Systems 22

    Abstract 22

    Introduction 23

    Experimental Setup 25

    Loading Protocol 30

    Damage Observation 32

    Experimental Results 34

    Summary 50

    Acknowledgements 52

3. Fire Sprinkler Piping Systems 53

    Abstract 53

Introduction 54

Background of Fire Sprinkler Piping Systems 57

Experimental Setup 58

Loading Protocol 66

Damage Observation 67

Experimental Results 69

Summary 80

Acknowledgements 82

4. Partition Wall Systems 83

Abstract 83

Keywords 84

1. Introduction 84

2. Experimental Setup 86

3. Loading Protocol 93

4. Damage Observation 94

5. Experimental Results 97

Summary 106

Acknowledgements 108

5. Summary and Conclusions 109

Summary 109

Findings and Conclusions 110

References 116

LIST OF TABLES

Suspended Ceiling Systems

Table 1. Configuration Properties 26

Table 2. Ceiling Assembly Variables 28

Table 3. Test-bed Responses during Linear and Nonlinear Configurations 32

Table 4. Damage Descriptions 32

Table 5. Damage Observed with Corresponding Minimum Peak Floor Acceleration 33

Table 6. Ceiling Design Variables 35

Table 7. Acceleration Amplification Factors 37

Table 8. Displacement Demand, Capacity, and Fragility Parameters (19.1 mm Pounding Gap) 40

Table 9. Perimeter Displacement Demand, Capacity, and Fragility Parameters (Unseating Gap) 41

Table 10. Support Axial Force Demand Parameters 43

Table 11. Support Axial Force Fragility Parameters 45

Table 12. Damage State Descriptions 46

Table 13. Percentage of Fallen Ceiling Area Determination Process 46

Table 14. Overall Performance Demand Parameters 48

Table 15. Overall Performance Fragility Parameters 50

Fire Sprinkler Piping Systems

Table 1. Configuration Properties 60

Table 2. Test-bed Responses during Linear and Nonlinear Configurations 67

Table 3. Tabulated Examples of Damage Observed 68

Table 4. Acceleration Amplification Factors 70

Table 5. Pipe Joint Rotation Demand and Capacity Parameters 74

Table 6. Comparison of Experimental and Analytical Fragility Parameters 75

Table 7. Support Axial Force Demand and Capacity Parameters 77

Table 8. Support Axial Force Fragility Parameters 78

Table 9. Comparison of Displacement Fragility Parameters 80

Partition Wall Systems

Table 1. Partition Wall Configurations 88

Table 2. Test-bed Responses during Linear and Nonlinear Configurations 94

Table 3. Partition Wall Damage Observed 96

Table 4. Partition Acceleration Amplification Factors 99

Table 5. Damage State Definitions 100

Table 6. Minimum Triggering Drift Ratio (First Floor Partition Walls) 103

Table 6 Continued. Minimum Triggering Drift Ratio (Second Floor Partition Walls) 104

Table 7. Summary of Fragility Parameters 105

Table 8. Comparison of Drift Ratios (Correlating to Partition Damage) Reported from Various Experimental Studies (%) 106

LIST OF FIGURES

Introduction

Figure 1: Typical Suspended Ceiling System Schematic 5

Figure 2: Fire Sprinkler Piping System Schematic 6

Figure 3: Interior Partition Wall Schematic and Example Connections 8

Figure 4: Yao (2000) Ceiling Experiment 10

Figure 5: Badillo et al. (2007) Ceiling Experiment 11

Figure 6: UB and E-Defense Ceiling Experiments 13

Figure 7: UCSD Piping Experiment 14

Figure 8: UB Piping Experiment 15

Figure 9: E-Defense Piping Experiment 16

Figure 10: UCSD Partition Experiment 17

Figure 11: UB Partition Experiment 18

Figure 12: E-Defense Partition Experiment 19

Suspended Ceiling Systems

Fig. 1. Elevation View of Test-bed Structure 26

Fig. 2. Test-bed Structure 26

Fig. 3. Continuous and Separate Ceiling Systems 29

Fig. 4. Examples of Attached and Free Boundary Conditions 29

Fig. 5. Ceiling Instrument Location for Assemblies #1, #9, and #10 30

Fig. 6. Comparison between Achieved and Target 50% IM Spectrum 31

Fig. 7. Examples of Damage Observed 34

Fig. 8. Graphical Representation of Amplification Factors 37

Fig. 9. Regression Plot for Braced/Unbraced Assemblies 40

Fig. 10. Perimeter Displacement Fragility Curves (19.1 mm Pounding Gap)..... 41

Fig. 11. Perimeter Displacement Fragility Curves (Unseating Gap) 42

Fig. 12. Comparison of Demand Axial Force to Capacity Limit..... 44

Fig. 13. Fragility Curves for Hangers and Wire Restrainers 44

Fig. 14. Example of Cumulative Ceiling Area Loss in Terms of Percentage..... 46

Fig. 15. Separate Regression Analysis for Assemblies with Pop Rivets or Seismic Clips 47

Fig. 16. Segmental and Combined Fragility Curves for Assemblies with Seismic Clips 49

Fig. 17. Overall Performance Fragility Curves..... 49

Fire Sprinkler Piping Systems

Figure 1. Fire Sprinkler Piping System Schematic 58

Figure 2. Elevation View of Test-bed Structure 59

Figure 3. Test-bed Structure Design Variables..... 60

Figure 4. Plan View of Piping Configurations..... 62

Figure 5. Elevation View of Separate Piping Configuration 62

Figure 6. Examples of Drop Design Variables 64

Figure 7. Typical Structural Instrument Location..... 64

Figure 8. Typical Piping Instrument Location 65

Figure 9. Example Pictures of Piping Instrumentation..... 65

Figure 10. Comparison between Achieved and Target 50% IM Spectrum 67

Figure 11. Examples of Observed Damage 69

Figure 12. Joint Rotation Parameters 73

Figure 13. Rotation Demand vs Leakage Capacity 73

Figure 14. Example of Regression Fitting 74

Figure 15. Pipe Joint Limit States 74

Figure 16. Pipe Joint Fragility Curves 75

Figure 17. Example Regression Parameters for Hangers and Wire Restrainers 76

Figure 18. Comparison of Demand and Capacity Limit for Support Elements 77

Figure 19. Support Axial Force Fragility Curves 78

Figure 20. Regression Fitting for Large and Small Diameter Pipes 79

Figure 21. Displacement Fragilities for Large and Small Diameter Pipes 80

Partition Wall Systems

Fig. 1. Test-bed Structure 87

Fig. 2. Sample Test-bed Pictures 87

Fig. 3. Partition Wall Layout 90

Fig. 4. Examples of Partition Wall Connections 91

Fig. 5. Typical Structural Instrument Location 92

Fig. 6. Examples of Partition Wall Instrumentation 93

Fig. 7. Comparison between Achieved and Target 50% IM Spectrum 94

Fig. 8. Examples of Observed Damage in Partition Walls 97

Fig. 9. Performance of Top Connections 98

Fig. 10. Experimental Fragility Functions 105

1. INTRODUCTION

Motivation

Structural and nonstructural building components play critical roles during and after an earthquake in terms of life safety, functionality, and economic expense. Extensive research has been conducted on the seismic effects of structural integrity of buildings. Engineers currently follow design guidelines to ensure buildings remain intact and in the immediate occupancy category when subjected to a range of earthquake ground motion excitations. However, the seismic performance of nonstructural components could be considered equally crucial during earthquake motions. Nonstructural components make up 75%-85% of the initial construction cost (FEMA E-74, 2012) and are more prone to damage because their shaking intensity thresholds are lower than structural component thresholds. Damaged nonstructural components can result in high replacement costs. Functionality plays a major role in critical buildings, such as hospitals, because the loss of equipment function could render the ability to save lives. The performance of nonstructural components and systems during an earthquake is currently under research. Experimental results are being used to advance the technical knowledge regarding seismic performance, damage mechanisms, and fragility development. More information and an enhanced understanding of the responses of nonstructural components could lead to better detailing and perhaps reduce the amount of damage.

Project Overview

The research described in this report was conducted as part of the project titled, "NEES Nonstructural Grand Challenge Project (NEESR-GC): Simulation of the Seismic Performance of Nonstructural Systems". The subsequent information may be found on the Network for Earthquake Engineering Simulation (NEES) nonstructural website (NEES Nonstructural, 2015).

"The vision of this Grand Challenge research project is to enhance significantly the seismic resilience of buildings and communities, by providing practicing engineers and architects with verified tools and guidelines for the understanding, prediction and improvement of the seismic response of the ceiling-piping-partition nonstructural system (NEES Nonstructural Proposal, 2007)." Therefore, one of the objectives of the project was to evaluate experimental data that could be used to enhance the seismic performance of the integrated ceiling-piping-partition nonstructural system through multidisciplinary system-level studies. Ceiling-piping-partition systems are complex systems made up several components and subsystems. The response of these systems is difficult to capture because of the three-dimensional geometries, several types of boundary conditions, and large number of design variables. The lack of system-level experiments has led to poor or an insufficient amount of data to define damage levels, fragility functions, or reliable analytical models.

Experimental programs were conducted at the University of Nevada, Reno (UNR) and University at Buffalo (UB) NEES Equipment Sites to evaluate system-level and subsystem-level experiments. Additionally, in coordination with Japanese researchers, the E-Defense facility in Japan was used to carry out a payload project. The experiments

used shake tables or nonstructural component simulators (NCS) to induce artificial ground motions to the test-bed structure in which the nonstructural systems were housed. A large number of design variables including materials, connection detailing, component size, boundary conditions, and more, were tested through several component assembly configurations. Experimental data then led to the development of subsystem-level and system-level fragility functions and the development of analytical models.

The project was funded by the National Science Foundation (NSF) under grant number CMMI-0721399. The project was led by Manos Maragakis, who served as the Principal Investigator (PI). Co-Principal Investigators (Co-PI) include André Filiatrault, Steven French, Tara Hutchinson, and Robert Reitherman. William Holmes is recognized as head of the committee. More information regarding the project can be found on the NEESR-GC website (NEES Nonstructural, 2015).

Background

Suspended Ceiling Systems

The following information was borrowed from the works completed by Soroushian et al. (2015) and should be referred to if more information is needed.

In many U.S. commercial buildings, installed suspended ceiling systems act as an aesthetic barrier between the nonstructural systems above (electrical, mechanical, and piping) and the common workspace below. Typical ceiling systems consist of acoustic tiles, grid members, boundary wall molding (otherwise known as perimeter angles), support elements, and compression posts (see Figure 1). Acoustic ceiling tiles are typically composed of a compressed, high-density mineral fiber material that lay in the ceiling grid system. Many sizes are available; however, the most common is a 2.0 ft. x

2.0 ft. (0.6 m x 0.6 m) with a thickness ranging from 1/2 in. to 3/4 in. (12.7 mm to 19.1 mm). The ceiling grid system is made of interlocking inverted main tee beams and inverted cross tee beams that hold the ceiling tiles. The boundary wall molding is a light gauged L-shaped wall angle, screwed to the surrounding partition walls, in which the perimeter grid members rest. The load carrying capacity of the grid members is categorized into light-duty (5.0 lb/ft or 7.4 kg/m), intermediate-duty (12.0 lb/ft or 17.9 kg/m), and heavy-duty (16.0 lb/ft or 23.8 kg/m) grid systems, following ASTM C635/C635M-13a (2013). The perimeter conditions (molding size and connection) depend on the seismic zone and seismic design category (C or D-E-F) (ASCE 7-10, 2010). In low seismic zones, seismic design category C, a 7/8 in. (22.2 mm) boundary wall molding with a minimum of 3/8 in. (9.5 mm) clearance between the grid and wall molding is specified on all boundaries. For high seismic zones, seismic design category D-E-F, a 2.0 in. (50.8 mm) boundary wall molding with a minimum of 3/4 in. (19.1 mm) clearance is specified on two adjacent boundaries (named “Free”) while the two remaining boundaries are connected via pop rivets or seismic clips (named “Attached”). It should be noted that if seismic clips are used on the attached perimeter, the boundary wall molding can be reduced to 7/8 in. (22.2 mm). The grid assembly is suspended from the above structural system by 12 gauge hanger wires that are spaced at 4 ft. (1.2 m) intervals around the ceiling perimeter and a maximum 8 in. (203.2 mm) from the wall. Braced ceiling systems consist of compression posts and 12 gauge wire restrainers (oriented at 45-degree angles) placed at grid intersections to limit vertical displacement. Alternatively, unbraced ceiling systems only consist of hangers located at grid intersections.

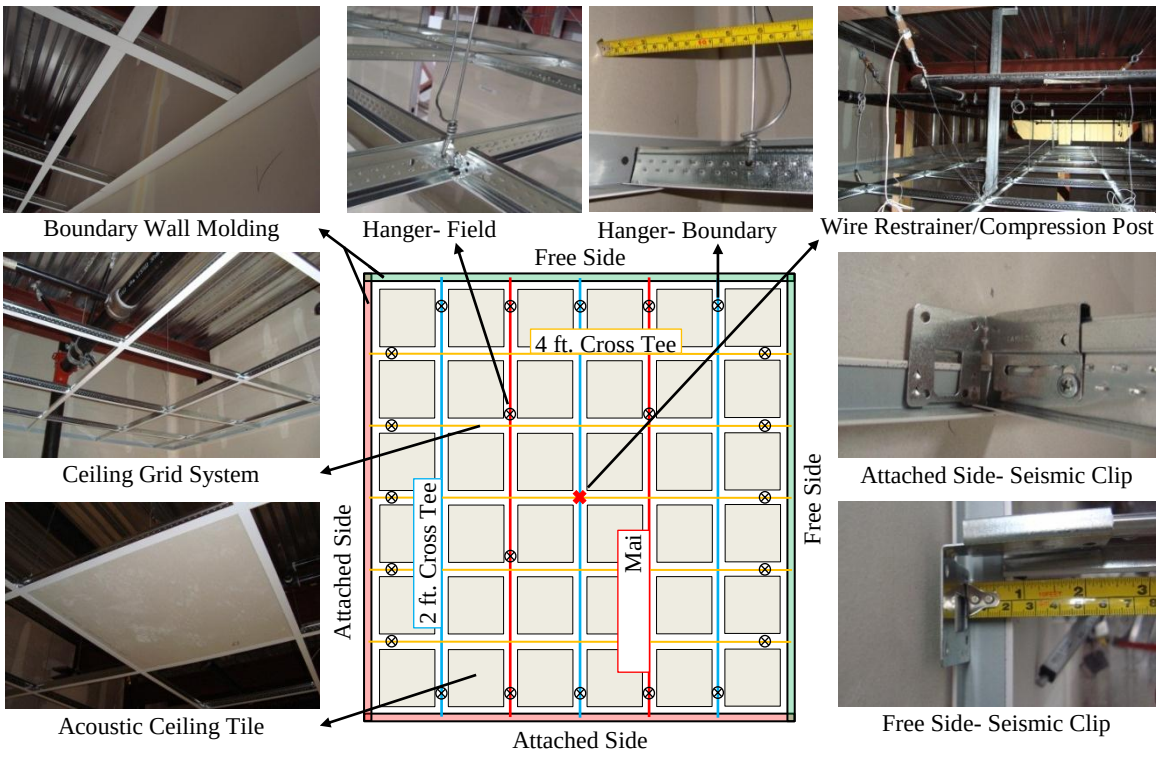

Figure 1: Typical Suspended Ceiling System Schematic

Fire Sprinkler Piping Systems

Fire sprinkler piping systems are common in critical facilities (hospitals and power-plants), residential homes, and commercial buildings. These piping systems are typically made of pressurized water tanks, pipe segments, sprinkler heads, and support components (see Figure 2). The pressurized tank provides water to all areas of the system through pipe segments. There are four pipe segment types: 1) vertical riser pipe, 2) main pipe, 3) branch line, and 4) drops or armovers. Water travels from the tank, up the riser pipe, and to the horizontal assembly which is made of the main pipe run and branch lines. The main pipe run typically extends the length of the floor while branch lines extend off the main pipe to other areas of the floor. Branch lines supply water to drops and armovers

in which the sprinkler heads are attached. The sprinkler heads will automatically activate when smoke or a fire is detected. The last component of the fire sprinkler piping system is the support elements. Hangers, attached to an adjustable band around the pipe, support the dead weight of the system (including water). Wire restrainers (oriented at 45-degrees) limit displacement of branch lines. Braces, also oriented at 45-degrees, resist the lateral and longitudinal sway through solid tubing (compression and tension) or wires (tension only).

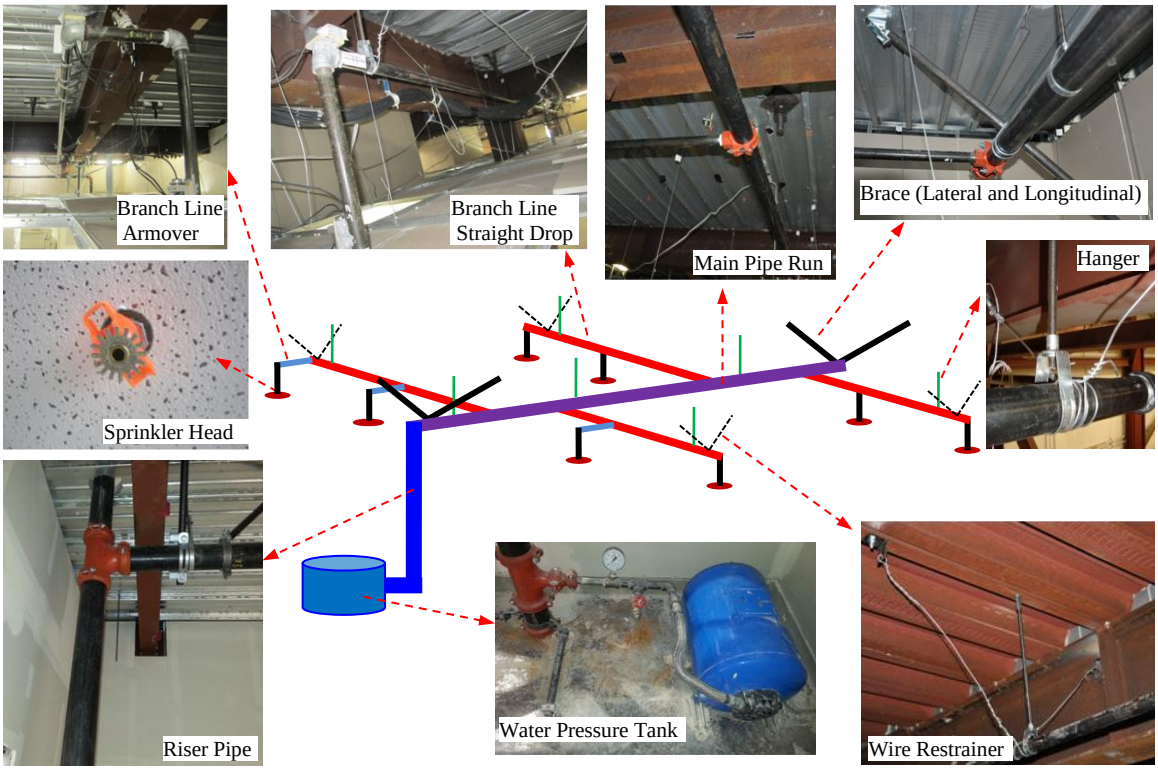

Figure 2: Fire Sprinkler Piping System Schematic, Source: (Soroushian et al., 2014b)

Partition Wall Systems

In commercial and residential buildings, nonstructural interior partition walls are typically used to separate large areas into smaller areas (i.e. offices, rooms). These

nonstructural partition walls are non-load bearing elements and can only withstand self weight and minor gravity or lateral loads. The two main types of framing systems used for partition wall construction are comprised of light-gauged steel or wood, however, the most common framing system is steel. Light-gauged cold-formed steel is preferred because it is light, easy to work with, fast to install, and non-combustible.

Steel-framed partition walls consist of a top and bottom track, vertical studs, and gypsum wall boards (drywall) as shown in Figure 3. The tracks are usually in a U-shape formation and are connected to the concrete decks via powder actuated fasteners. Vertical studs are placed in between the top and bottom tracks, spaced at 12.0 in. (304.8 mm), 16.0 in. (406.4 mm), or 24.0 in. (609.6 mm), and attached using self-drill screws. The cross sectional shape of the studs are similar to the track, however, the studs have returns on the flanges and pre-punched holes to allow electrical wires, plumbing pipes, and bridging elements to pass through. In most cases, the bottom stud-to-track connected is fixed while the top stud-to-track connection is varied depending on the building location. Possible top stud-to-track connections are full connection, slip track, and the newly proposed sliding/frictional connection from Araya-Letelier and Miranda (2012). The steel framing system is then covered with gypsum wallboard panels, ranging in thickness from 1/2 in. (12.7 mm) to 5/8 in. (15.9 mm), or other sheathing materials. The wallboards are connected to the flanges of the studs via Type S drywall screws. The two types of corner connections, in which longitudinal and lateral walls intersect, depend on the thickness and number of steel studs, called commercial or institutional connections.


Steel Framing


Top: Sliding/Frictional

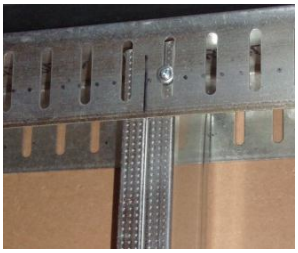
Top: Sliding/Frictional

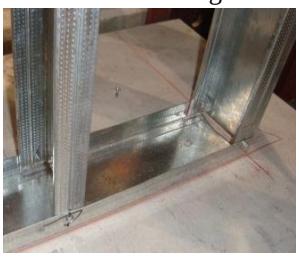
Bottom Stud-to-Track

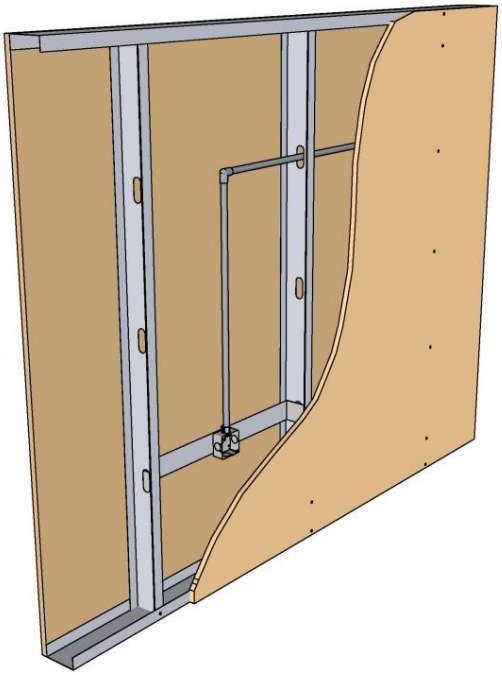

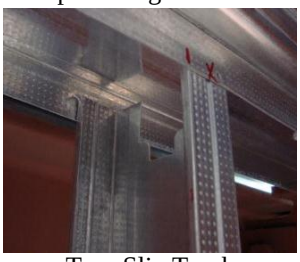
Top: Slip Track


Institutional Corner

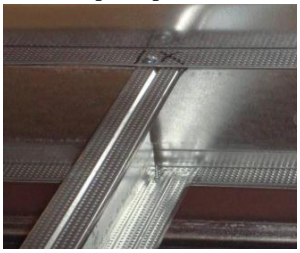
Top: Full

Figure 3: Interior Partition Wall Schematic and Example Connections

Literature Review

The following section describes a few key studies conducted in order to evaluate the performance of suspended ceiling systems, fire sprinkler piping systems, and partition wall systems.

Suspended Ceiling Systems

ANCO Engineers Inc. (1983) and Rihal and Granneman (1984)

In the 1980's, two shake table tests were conducted to assess the performance of suspended ceiling systems. The first was performed by ANCO Engineers Inc. (1983). The ceiling system measured approximately 12.0 ft. (3.7 m) by 30.0 ft. (9.1 m) and

consisted of intermediate-duty runners and lay-in tiles. The table motion was generated from the 1952 Taft earthquake ground motion. Results showed the effectiveness of pop rivets and safety wires on drop-in light fixtures in seismic mitigation. The second experiment, conducted by Rihal and Granneman (1984), aimed to evaluate the dynamic behavior of suspended ceiling systems. The 12.0 ft. (3.7 m) by 16.0 ft. (4.9 m) ceiling system was installed in a test structure that simulated a structural horizontal diaphragm. The loading protocol was a sinusoidal motion. Experimental results determined that bracing, including splay wires and vertical struts, helped reduce dynamic response.

Yao (2000)

Yao (2000) investigated the dynamic behavior and capacity of direct-hung suspended ceiling systems with lay-in panels. The ceiling specimens were 4.0 ft. (1.2 m) by 13.0 ft. (4.0 m) and were composed of runners and lay-in panels that measured 2.0 ft. (0.6 m) by 2.0 ft. (0.6 m). A test sample configuration is shown in Figure 4. One specimen consisted of 45-degree sway wire to evaluate the effects of sway bracing. The input motion was a series of uni-axial horizontal sine waves. Results showed sway bracing was ineffective; however, pop rivet connections and edge hanger wires provided significant seismic capacity.

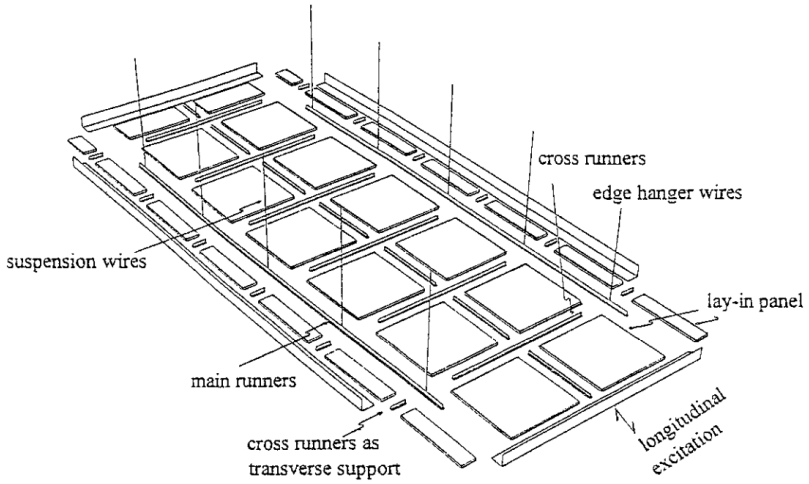

Figure 4: Yao (2000) Ceiling Experiment: Test Sample Configuration, Source: (Yao, 2000)

Badillo et al. (2007) and additional University at Buffalo experiments

As reported by Reinhorn (2010), a number of tests have been conducted on the performance of suspended ceiling systems at the Structural Engineering and Earthquake Simulation Laboratory (SEESL) at the State University of New York at Buffalo (UB) (e.g., Badillo et al. (2002), Kusumastuti et al. (2002), Badillo et al. (2003a), Badillo et al. (2003b), Badillo et al. (2003c), Badillo et al. (2003d), Repp et al. (2003a), Repp et al. (2003b), Lavan et al. (2006), Badillo et al. (2007), and Roh et al. (2008)). The ceiling systems from the experiments were housed in a 16.0 ft. (4.9 m) by 16.0 ft. (4.9 m) test structure that simulated a typical story (Figure 5a). In the experiment conducted by Badillo et al. (2007), fragility curves were developed for suspended ceiling systems to help enable performance-based assessment and design. The ceiling specimens were constructed with Armstrong PRELUDE XL 15/16 in. (23.8 mm) exposed tee systems. The input excitations included a series of unidirectional and bidirectional earthquake motions. In order to develop fragilities, four limit states were defined based on the

percentage loss of ceiling tiles (Figure 5b shows an example of damage observed). A few major findings from this experiment are that failed pop rivet connections lead to a greater number of fallen ceiling tiles and that compression posts help mitigate damage for minor to moderate intensity levels.

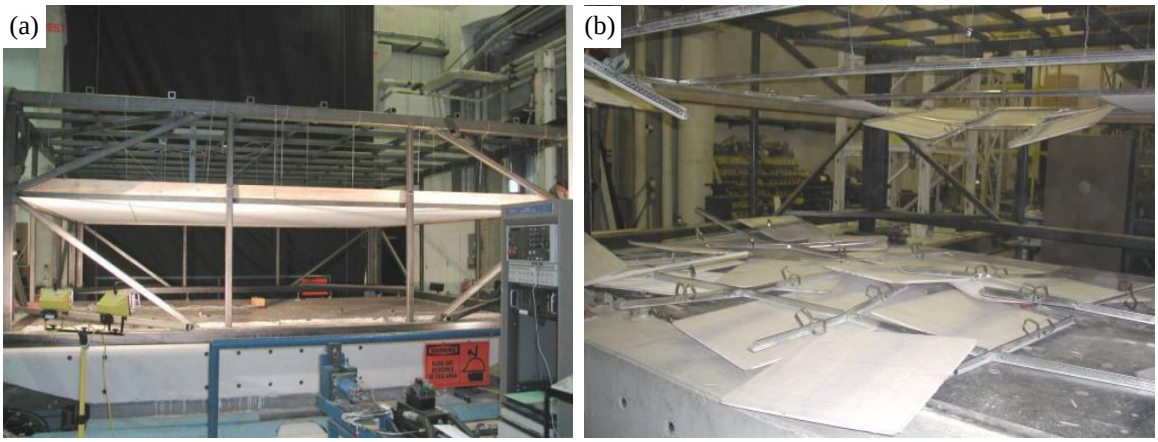

Figure 5: Badillo et al. (2007) Ceiling Experiment: (a) test frame, (b) example of damage observed, Source: (Badillo et al., 2007) and (Reinhorn et al., 2010)

Soroushian et al. (2015)

In the most recent years, two series of studies have been carried out as part of the NEESR-GC: Simulation of the Seismic Performance of Nonstructural Systems project. The first series of experiments were studied at UB to evaluate the performance of ceiling, piping, and partition subsystems through three separate experiments. The component-level performance of ceiling systems was assessed through 15 assemblies that were tested on a tandem of shake tables (Figure 6a). The assemblies were constructed of Armstrong Prelude 15/16 in. (23.8 mm) exposed tee systems and subjected to incremental test motions. Damage observed during this experiment included: failed pop rivets, damaged seismic clips, failed grid connections, and complete ceiling system failure. The second series of experiments (system-level) were performed at the E-Defense test facility in

Japan as a payload project. The seismic response of ceiling-piping-partition systems was evaluated in a full-scale, five-story, steel moment frame building (Figure 6b). Two ceiling assemblies, composed of USG DONN 15/16 in. (23.8 mm) exposed tee systems, were installed in the 4^{th} and 5^{th} floors. The loading protocol included 41 shake table excitations which included triaxial and biaxial motions. This study experienced similar damage as the ones observed during the UB experiment. However, additional damage including failed hangers and braces were recorded. Soroushian et al. (2015) produced fragility functions for ceiling perimeter displacement, axial and inertial forces in hangers and wire restrainers, and overall ceiling performance based on the data from both experiments. A few major findings were: 1) ceiling systems with rigid boundary, with bracing, with seismic clips, and with two sides fixed have a lower failure probability at their floating (Free) perimeter sides, 2) unseating failure of ceiling grid systems with 7/8 in. (22.2 mm) wall angles is probable to occur at low shake intensities, and 3) the code connection capacity for ceiling hangers and diagonal wires should be increased. For more information on the two studies, please refer to the following: Soroushian et al. (2012), Dao and Ryan (2013), Ryu et al. (2013), or Soroushian et al. (2015).

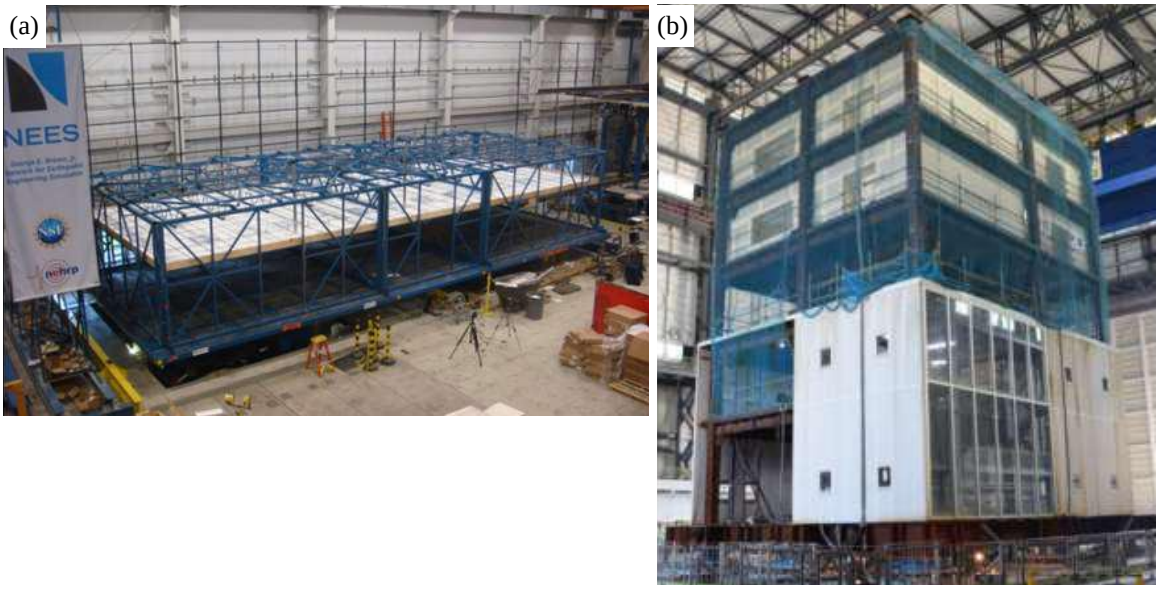

Figure 6: UB and E-Defense Ceiling Experiments: (a) UB test frame, (b) E-Defense test frame, Source: (Soroushian et al., 2015)

Fire Sprinkler Piping Systems

Hoehler et al. (2009)

The University of California at San Diego (UCSD) conducted an experiment to evaluate the performance of post-installed anchors from forces applied to the pipe system during an earthquake. The test structure, shown in Figure 7a, was seven-stories high and had horizontal pipe runs supported on trapeze hangers on three of the stories. The piping systems were constructed from six, 6.0 in. (152.4 mm) cast-iron pipes and the trapezes were made from 1 5/8 in. (41.3 mm) square steel channel struts placed back-to-back. Figure 7b-c shows the pipe assembly and the typical trapeze connection detail. The test structure was subjected to four uniaxial input ground motions. Results from this experiment conclude that measured pipe accelerations were larger than those predicted by the ASCE 7-05 (2005) equation 1.3. In addition, the maximum axial loads in the anchors were relatively low, less than 38% utilization of the ultimate anchor tension capacity.

Hoehler et al. (2009) also showed that although the current ACI 355.2 (2004) seismic anchor loading protocol suggests 140 load cycles before rupture, the mean cumulative number of cycles attributed with a high confidence to earthquake induced forces was about 30.

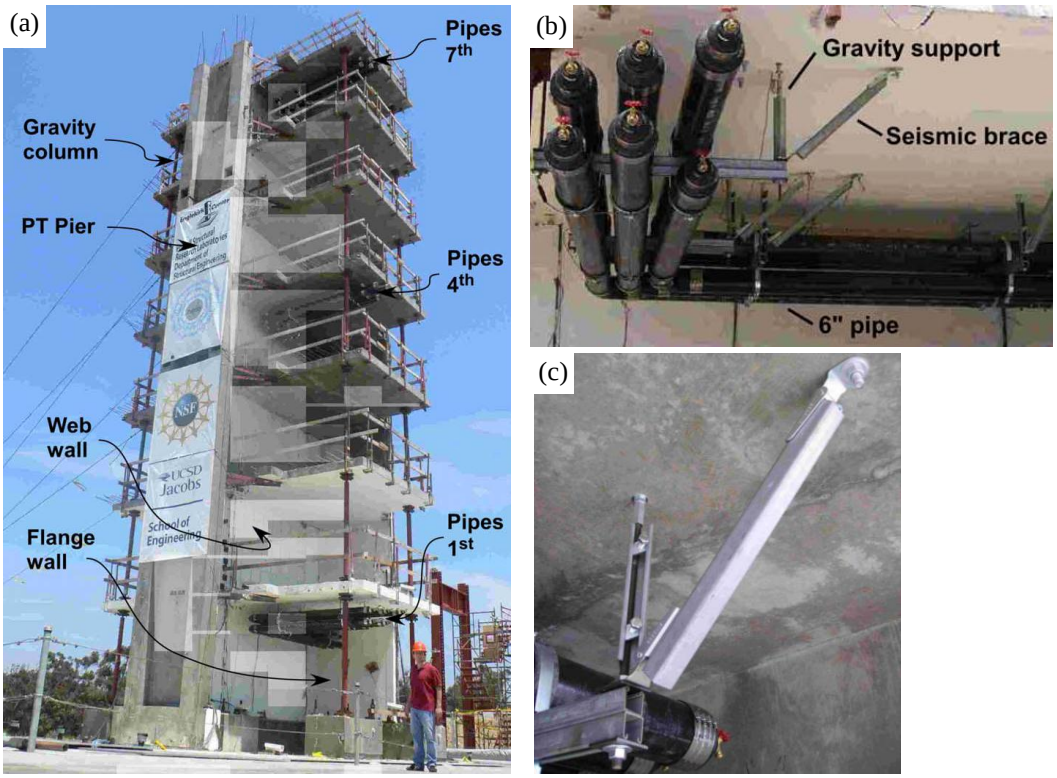

Figure 7: UCSD Piping Experiment: (a) test structure, (b) piping assembly, (c) trapeze connection, Source: (Hoehler et al., 2009)

Tian et al. (2013)

A subsystem-level fire sprinkler piping system experiment was conducted at UB as part of the NEESR-GC: Simulation of the Seismic Performance of Nonstructural Systems project. This experiment investigated the behavior of tee joint connections and fire sprinkler piping systems under seismic loading. Two test series were carried out for this experiment. The first tested 48 piping tee joints under cyclic loading to determine the

rotational capacity at which leakage and/or fracture would occur (Figure 8a). Results show that the rotational capacities at first leakage for all joint types ranged from 0.005 rad. to 0.405 rad. From the observed failure mechanisms, component fragility curves were developed for sprinkler piping joints. The second test series evaluated the overall performance of a piping subsystem by testing three specimens with varying materials, joint arrangements, and bracing systems. Common damage observed during this series was failure of vertical hangers, branch line failure, and sprinkler head damage (Figure 8b). Results conclude that the unbraced specimens experienced extensive damage to vertical hangers, ceiling tiles, sprinkler heads, and pipe joints; however, braced systems suffered no damage. In addition, it was observed that for a number of fire sprinkler piping systems, there was little damage to the supporting elements, but some sprinkler heads were activated due to the interaction between ceiling tiles (Figure 8c).

Figure 8: UB Piping Experiment: (a) tee joint rupture, (b) ceiling-piping damage, (c) activated sprinkler head, Source: (Tian et al., 2013)

Soroushian et al. (2014)

As part of the previously mentioned system-level experiment conducted at the E-Defense facility in Japan, the performance of standard schedule 40 piping systems were assessed. The piping systems consisted of one main run and three branch lines that were suspended from the 5th and roof slabs. Damage observed during the experiment included

permanent rotation of armover drops and damage to ceiling tiles near sprinkler heads (Figure 9a). Soroushian et al. (2014a) calculated acceleration amplification factors and results show an increasing trend in amplification from the main pipe run to branch line and then to the sprinkler heads. Furthermore, fragility functions were developed based on ceiling-piping interaction. Results show that the ceiling-piping interaction damage can be reduced by using a flexible hose drop (Figure 9b) and/or decreasing the spacing of lateral sway braces.

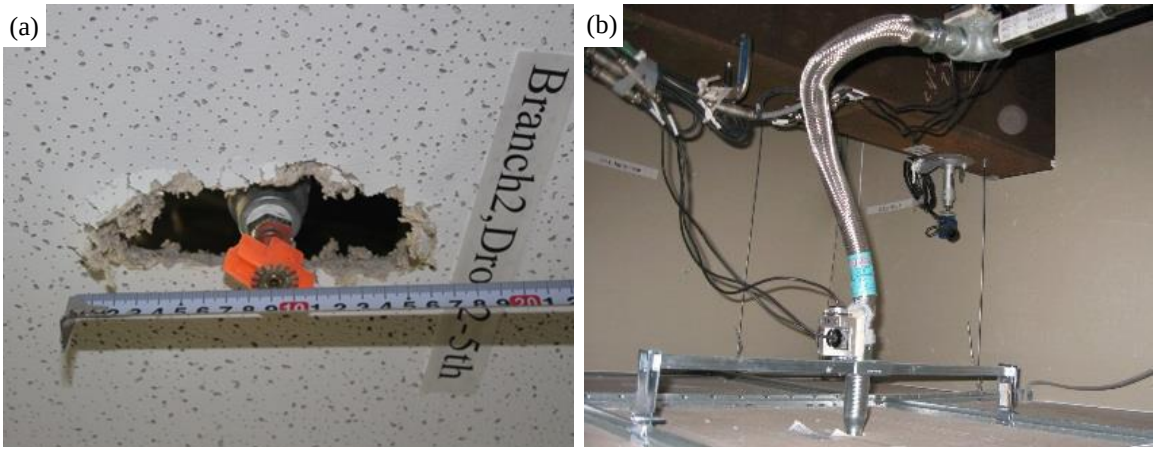

Figure 9: E-Defense Piping Experiment: (a) ceiling-piping interaction damage, (b) flexible hose drop, Source: (Soroushian et al., 2014a)

Partition Wall Systems

Bersofsky (2004)

A number of experiments were conducted at the UCSD Powell Laboratory to evaluate the cyclic performance of light-gauge steel-framed partition walls and gypsum wallboard. In this study, a total of eight tests were conducted using 16 specimens. The specimens were comprised of one main wall (16.0 ft. (4.9 m) long by 8.0 ft. (2.4 m) tall) and two return walls oriented perpendicular to the main wall (4.0 ft. (1.2 m) long by 8 ft. (2.4 m) tall) as shown in Figure 10a. The loading protocol consisted of in-plane quasi-

static reversed cyclic loading patterns. Common damage observed during the test included: screw pop out, gypsum board cracking, buckling of studs, and shear failure of the bottom track. An example of studs buckling at 3% drift ratio is shown in Figure 10b. Three damage states were defined (DS1: Slight, DS2: Moderate, and DS3: Severe) based on level of repair and incremental drift ratios to develop fragility functions. Ranges of recorded drifts for each damage state were 0.1-2.0% (DS1), 1.5-3.0% (DS2), and 1.5-3.5% (DS3).

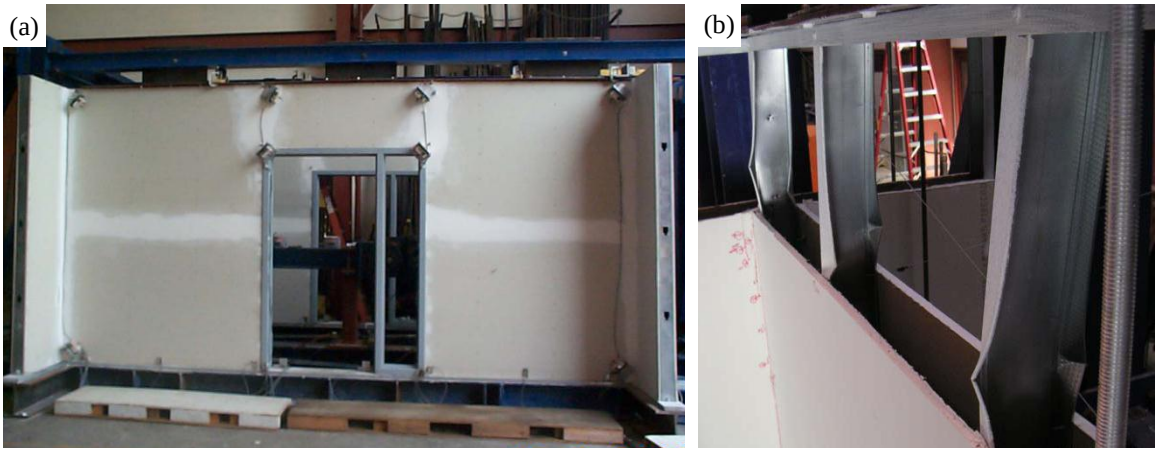

Figure 10: UCSD Partition Experiment: (a) example specimen, (b) buckling of studs (3% drift ratio), Source: (Bersofsky, 2004)

Retamales et al. (2013)

A full-scale subsystem-level experimental program (under NEESR-GC) was conducted at the UB-NEES site that aimed to evaluate the seismic responses, failure mechanisms, and fragilities for steel-framed partition walls with intent to populate a comprehensive seismic fragility database. A total of 50 specimens were tested under dynamic and quasi-static loading protocols. Wall specimens were oriented in an I-shape formation as shown in Figure 11a. The main wall was approximately 12.0 ft. (3.7 m) long by 11.5 ft. (3.5 m) tall and the return walls were 2.0 ft. (0.6 m) or 4.0 ft. (1.2 m) long and

11.5 ft. (3.5 m) tall. Examples of damage recorded during the experiments include: crushing of gypsum wall corners, failure of top (Figure 11b) and bottom tracks for transverse (return) walls, and buckling of studs. Three damage states were defined to produce fragility functions. Results show that excessive corner damage can be reduced by incorporating gaps between the top edge of the gypsum board and concrete slab. In addition, it was observed that the performances of partition walls were different even though identical construction techniques, materials, and personnel were used to construct multiple specimens.

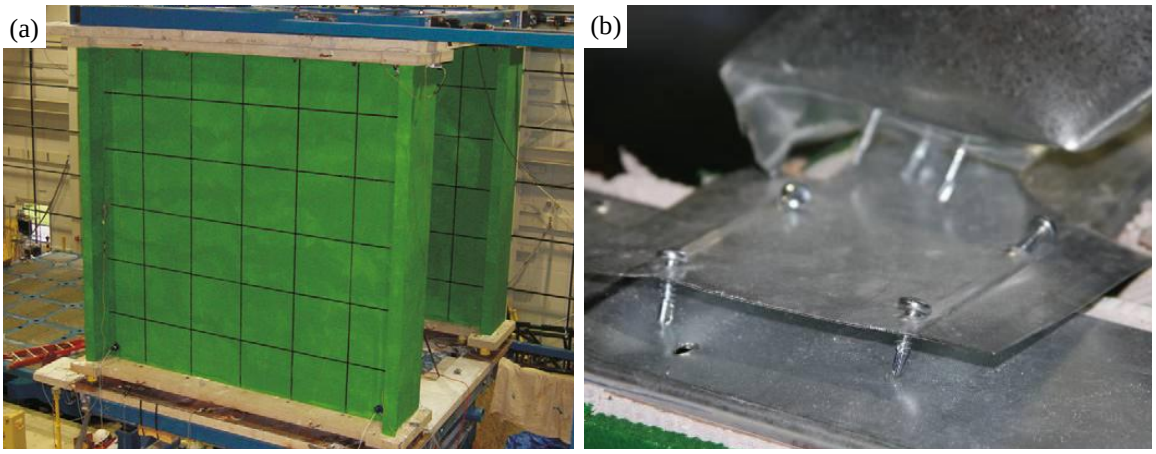

Figure 11: UB Partition Experiment: (a) specimen, (b) top track damage, Source: (Davies et al., 2011) and (Retamales et al., 2013)

Soroushian et al. (2014)

In conjunction with the experiment conducted at the E-Defense Facility in Japan (under NEESR-GC: Simulation of the Seismic Performance of Nonstructural Systems), light-gauge steel studded gypsum partition walls were placed on the 4th and 5th floors of the test-bed structure. The walls were 9.0 ft. (2.7 m) tall and the lengths ranged from 5.0 ft. (1.5 m) to 32.0 ft. (9.8 m) (Figure 12a). Excessive drift-related damage to partition walls was not observe during testing, but the 4th and 5th floors experienced 0.78% and

0.62% drifts, respectively. Due to low inter-story drift, the observed damage was caused by vertical excitation. Figure 12b shows a large crack that formed in a partition wall. Soroushian et al. (2014a) evaluated the acceleration amplification factors for the horizontal and vertical directions. Results show that the amplifications for the horizontal direction were similar to the recommended amplification given by the ASCE 7-10 (2010); however, the vertical amplifications were higher due to an additional amplification produced by slab vibration.

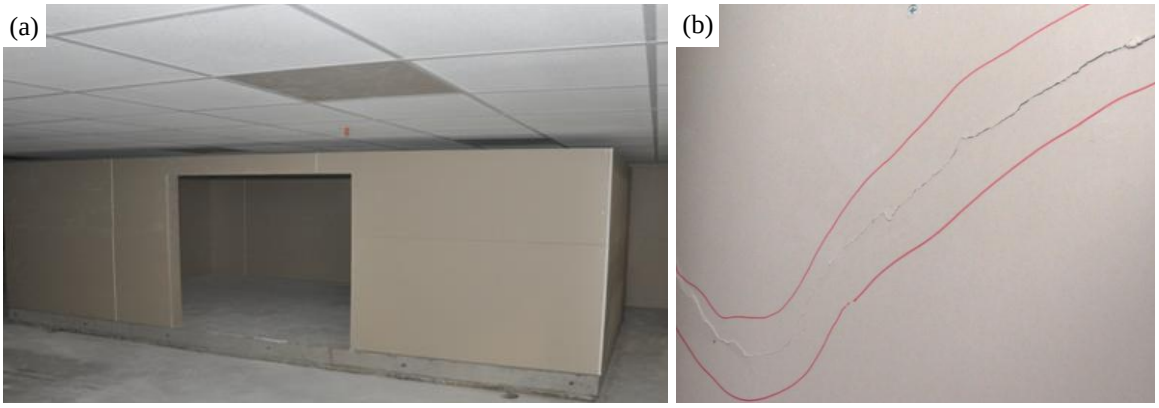

Figure 12: E-Defense Partition Experiment: (a) specimen, (b) partition wall crack, Source: (Soroushian et al., 2014a)

Objectives and Scope

The primary objective of this study was to assess the seismic performance of integrated ceiling-piping-partition systems through full-scale shake table testing in order to enhance the seismic resilience of nonstructural systems. The following goals were developed to better understand the performance of nonstructural systems:

1) Observe the damage experienced from each nonstructural component and compare the performance effects of different assemblies or configurations.

2) Enhance the knowledge of system-level response versus subsystem-level response and understand the roles of additional components or adjacent objects.
3) Determine the acceleration amplification factors for each of the nonstructural components and compare the calculated values to the recommended values prescribed by ASCE 7-10 (2010).
4) Generate fragility curves for suspended ceiling systems based on ceiling perimeter displacement, support axial force, and overall performance.
5) Generate fragility curves for fire sprinkler piping systems based on pipe joint rotation, support axial force, and pipe displacement.
6) Evaluate the performance of different top stud-to-track partition connections including full, slip track, and sliding/frictional connections.
7) Generate fragility curves for steel-framed partition walls based on overall performance.
8) Compare experimental fragility results to previous analytical and experimental studies.

Report Organization

The main structure of this report is composed of three separate papers written for ceiling, piping, and partition systems, respectively. The papers have been submitted to various engineering journals and their status is stated in their respected sections. The outline for each paper includes: 1) experimental setup, which discusses the test-bed structure used to house the nonstructural components, the different nonstructural system

configurations, and the instrumentation used to record the response of structural and nonstructural components, 2) loading protocol, 3) damage observation, and 4) experimental results. The following sections are summarized below.

Section 2 presents the post processing of experimental data for the suspended ceiling systems. The provided information is taken from a paper titled, "Fragility Analysis of Suspended Ceiling Systems in a Full-Scale Experiment," submitted to the ASCE *Journal of Structural Engineering*. The status of the paper is currently under review (Jenkins et. al, 2015d). In this section, fragility functions were developed for ceiling perimeter displacement, support axial force, and the overall performance of the ceiling system.

Section 3 presents the experimental results for the tested fire sprinkler piping systems. The information given in this section is borrowed from a fire sprinkler piping system paper submitted to the *Journal of Earthquake Engineering* titled, "Experimental Fragility Analysis of Pressurized Fire Sprinkler Piping Systems," which is currently under review (Jenkins et. al, 2015c). Fragility curves were developed for pipe joint rotation, support axial force, and pipe displacement.

Section 4 presents the experimental results for cold-formed steel-framed partition wall systems borrowed from the paper, "Experimental Fragility Analysis of Cold-Formed Steel-Framed Partition Wall Systems". This paper is under review with the *Thin-Walled Structures* journal (Jenkins et. al, 2015b). Results from this paper include the performance comparison of different top stud-to-track connections, acceleration amplifications, and a seismic fragility analysis.

Section 5 gives a summary of the project followed by the main conclusions.

2. SUSPENDED CEILING SYSTEMS

The following section is borrowed from a paper submitted to the *Journal of Structural Engineering* (Jenkins et. al, 2015d).

Fragility Analysis of Suspended Ceiling Systems in a Full-Scale Experiment

Craig Jenkins, S.M.ASCE[1], Siavash Soroushian, M.ASCE[2], Esmaeel Rahmanishamsi, S.M.ASCE[3], and E. "Manos" Maragakis, A.M.ASCE[4]

ABSTRACT

The seismic performance of nonstructural components, including suspended ceiling systems, plays a significant role during and after an earthquake. Damage to these systems can leave buildings inoperable, causing economic losses and extensive downtime. Therefore, it is necessary to better understand the response of these systems in order to enhance the seismic resilience of buildings. A series of full-scale system-level experiments conducted at the University of Nevada, Reno Network for Earthquake Engineering Simulation site aimed to investigate the seismic performance of integrated ceiling-piping-partition systems. In this paper, the seismic behavior of suspended ceiling systems is discussed. Experimental results include acceleration amplification factors for different ceiling configurations. In addition, fragility curves are presented for perimeter displacement, support axial force, and overall ceiling performance. Some major findings

1 Graduate Research Assistant, Department of Civil and Environmental Engineering, University of Nevada, Reno, Reno, NV, 89557, email: cjenkins@unr.edu

2 Structural Analyst, Advanced Technology and Research, Arup, San Francisco, CA, 94105, email: siavash.soroushian@arup.com

3 Ph.D. Candidate, Department of Civil and Environmental Engineering, University of Nevada, Reno, Reno, NV, 89557, email: erahmanishamsi@unr.edu

4 Professor, Dean of College of Engineering, University of Nevada, Reno, Reno, NV, 89557, email: maragaki@unr.edu

from this experiment show that the acceleration amplification is most effected by additional ceiling attachments to partition walls and that unseating of grid members in 22.2 mm (7/8 in.) wall angle configurations was one of the dominate failure modes.

INTRODUCTION

The performance of structural and nonstructural systems during and after an earthquake is of great concern when regarding life safety, functionality, and economic impact. Today, seismic design codes have guided engineers to design buildings so that the structural systems remain in the immediate occupancy category after an earthquake (FEMA E-74, 2012). However, many reports show that damage to nonstructural systems have a severe economic impact (Takahashi and Shiohara (2004); Yu and Gonzalez (2008); Miranda et al. (2012)). As a critical component of nonstructural elements, the seismic performance of suspended ceiling systems is evaluated in this paper.

Records from past historical earthquakes show that damage to suspended ceiling systems include falling of panels, grid member disengagement, failure at perimeter locations, and complete system collapse. Different combinations of the described damage has been observed in the following earthquakes: 1989 Loma Prieta earthquake (Ding et al., 1990), 2001 Nisqually (Seattle) earthquake (Filiatrault et al., 2001), 2010 Chile earthquake (Miranda et al., 2012), and 2011 Tohoku earthquake (Motosaka and Mitsuji, 2012). Additional damage during the 1994 Northridge earthquake, as reported from (Reitherman and Sabol, 1995), included the ends of grid members colliding with gypsum boards resulting in a punching effect.

The seismic performance of suspended ceiling systems has been evaluated in several past experimental studies. A few major conclusions have been drawn from the results: 1) pop rivets play an important role in seismic hazard mitigation (ANCO, 1983), 2) bracing, including splay wires and vertical struts, help reduce dynamic response (Rihal and Granneman, 1984), 3) failed pop rivet connections lead to a greater number of fallen ceiling tiles (Badillo et al., 2007), and 4) compression posts help mitigate damage for minor to moderate intensity levels (Badillo et al., 2007). In the most recent years, experiments have been conducted at the University at Buffalo (UB) and the E-Defense test facility in Japan. The goal of these experiments was to evaluate the component-level (assessed at UB) and system-level (assessed at E-Defense) performance of ceiling systems. In the works completed by Soroushian et al. (2015), fragility curves from these experiments were combined and compared showing that 22.2 mm (7/8 in.) wall angles are of insufficient length, the capacity observed for supporting elements was greater than the design capacity suggested by the code, and early damage of ceiling systems can occur due to ceiling-piping interaction. If more information is requested, please refer to Soroushian et al. (2015).

In order to further enhance the seismic performance understanding of ceiling-piping-partition systems, a series of experimental studies have been conducted at the University of Nevada, Reno Network for Earthquake Engineering Simulation (UNR-NEES) site. The integrated nonstructural systems were housed in a full-scale, two-story steel braced-frame structure that spanned over three shake tables. The performance of suspended ceiling systems was evaluated through the observed failure modes. The processing of experimental results included the calculation of acceleration amplification

factors for different ceiling configurations and the development of fragility functions for perimeter displacement, support axial force, and overall ceiling performance.

EXPERIMENTAL SETUP

Test-bed Structure

The integrated nonstructural systems were installed in a full-scale, two-story, two-by-one bay steel braced-frame test-bed structure that spanned over three biaxial shake tables at the UNR-NEES site. The approximate dimensions of the test-bed structure are shown in Fig. 1.

In order to assess both acceleration and drift sensitive components, two test-bed configurations were designed, named “Linear” and “Nonlinear”. Both configurations incorporated two design variables: 1) yielding force of braces and 2) amount of additional attached floor masses. The linear configuration used buckling restrained braces (BRB) with a high yield capacity and a lower amount of attached mass to the floor decks in order to achieve large floor accelerations. Alternatively, the nonlinear configuration used BRB’s with a low yielding capacity and an increased amount of attached mass to achieve large inter-story drift by yielding of the BRB’s (Soroushian et al., 2014c). The test-bed structure and two design variables are shown in Fig. 2 while the configuration properties including BRB yielding force, amount of attached mass, and natural period for the two configurations are shown in Table 1.

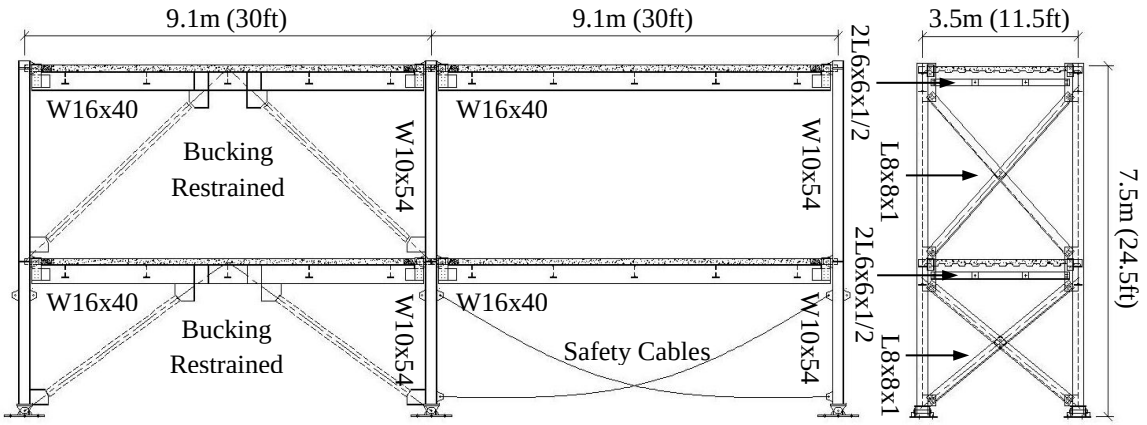

Fig. 1. Elevation View of Test-bed Structure, Source: (Jenkins et al., 2015a)

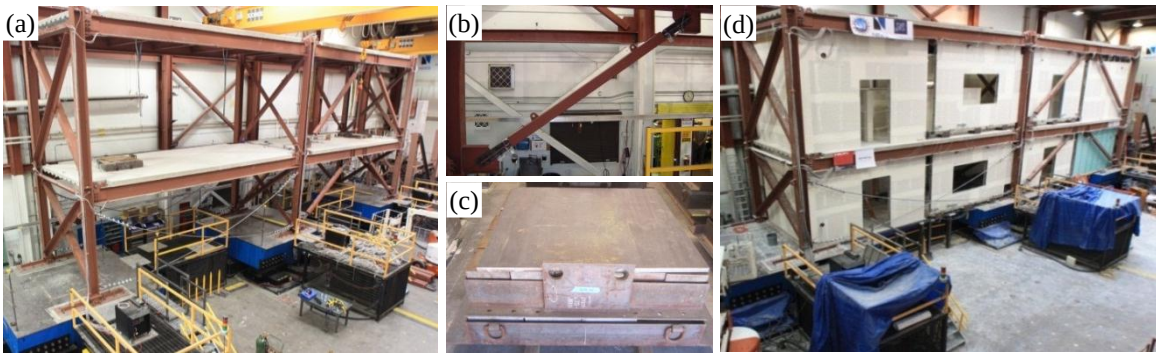

Fig. 2. Test-bed Structure: (a) test-bed frame, (b) BRB, (c) additional mass, (d) test-bed structure with nonstructural components

Table 1. Configuration Properties

Floor	Linear Configuration			Nonlinear Configuration		
	BRB Yielding Force	Attached Mass	Natural Period	BRB Yielding Force	Attached Mass	Natural Period
First	283.0 kN (64.0 Kips)	30.7 kN (6.9 Kips)	0.2 sec	89.0 kN (20.0 Kips)	62.5 kN (14.0 Kips)	0.34 sec
Second	283.0 kN (64.0 Kips)	17.6 kN (4.0 Kips)		89.0 kN (20.0 Kips)	279.1 kN (62.8 Kips)	

Suspended Ceiling System Assembly

The behavior and response of ceiling systems were evaluated through 22 assemblies with 15 configurations (Rahmanishamsi et al., 2014). The considered design

variables of the ceiling system include: area, bracing, boundary conditions, number of attached walls, seismic separation joints, panel weight, and interaction effect from other nonstructural systems (see Table 2). The ceiling assemblies consisted of Armstrong Prelude 23.8 mm (15/16 in.) exposed tee systems including 3.7 m (12 ft.) main runners, 1.2 m (4 ft.) cross tees, 0.6 m (2 ft.) cross tees, and 609.6x609.6x19.1 mm (24x24x3/4 in.) tiles that were installed per ASTM E580/E580M (2011) guidelines. The ceiling systems were suspended 0.9 m (3 ft.) below the concrete deck by 12 gauge Hilti X-CW wire hangers. Hanger spacing was no more than 203.2 mm (8 in.) from perimeter walls and 1.2 m (4 ft.) elsewhere.

Two ceiling areas were considered in this study, labeled “Continuous” and “Separate”. The continuous ceiling measured 17.7x3.0 m (58x10 ft.) and spanned the entire length of the test-bed structure while the separate ceiling measured 8.5x3.0 m (28x10 ft.) and only spanned one bay at a time (Fig. 3). Ceiling assemblies were either braced (9 out of 22) or unbraced (13 out of 22). Braced assemblies used steel stud compression posts and four 12 gauge wire restrainers (oriented at 45-degree angles) to limit displacement in the vertical and lateral/longitudinal directions, respectively. The boundary or perimeter conditions followed the criteria outlined by ASCE 7-10 (2010). The connections were either pop riveted with 50.8 mm (2 in.) perimeter angles or used Armstrong BREC2 seismic clips (Fig. 4a-b) with 22.2 mm (7/8 in.) perimeter angles. All but one of the assemblies had two adjacent walls that were attached and two that were free (see Fig. 3 and Fig. 4). The free sides used a clearance gap of 19.1 mm (3/4 in.) between the ceiling grid and the perimeter angle (Fig. 4c-d). However, four free walls were tested with 50.8 mm (2 in.) perimeter angles in Assembly #11. The performance of

Table 2. Ceiling Assembly Variables

Assembly - Config. No.	Floor	Ceiling Size (m)	Braced	Perimeter Angle (mm)	Connection Type	No. of Attached/ Unattached Walls	Panel Weight (kPa)	Comments
1-1	1	17.7 x 3.0	No	50.8	Pop Rivet	2/2	0.06	
2-2	2	17.7 x 3.0	Yes	50.8	Pop Rivet	2/2	0.06	
3-3	1	17.7 x 3.0	No	22.2	Seismic Clip	2/2	0.06	
4-4	2	17.7 x 3.0	Yes	22.2	Seismic Clip	2/2	0.06	
5-5	1	17.7 x 3.0	No	22.2	Seismic Clip	2/2	0.06	Seismic Separation Joint
6-6	2	17.7 x 3.0	Yes	22.2	Seismic Clip	2/2	0.06	Seismic Separation Joint
7-7	1	8.5 x 10	No	50.8	Pop Rivet	2/2	0.06	
8-8	1	8.5 x 10	No	22.2	Seismic Clip	2/2	0.06	
9-9	2	8.5 x 10	Yes	50.8	Pop Rivet	2/2	0.06	
10-10	2	8.5 x 10	Yes	22.2	Seismic Clip	2/2	0.06	
11-11	1	8.5 x 10	No	50.8	-	0/4	0.06	Four Free Walls
12-12	1	8.5 x 10	No	50.8	Seismic Clip	2/2	0.06	
13-13	2	8.5 x 10	No	50.8	Pop Rivet	2/2	0.06	
14-14	2	8.5 x 10	No	22.2	Seismic Clip	2/2	0.12	Heavy Panel
15-7	1	8.5 x 10	No	50.8	Pop Rivet	2/2	0.06	
16-8	1	8.5 x 10	No	22.2	Seismic Clip	2/2	0.06	
17-9	2	8.5 x 10	Yes	50.8	Pop Rivet	2/2	0.06	
18-10	2	8.5 x 10	Yes	22.2	Seismic Clip	2/2	0.06	
19-1	1	17.7 x 3.0	No	50.8	Pop Rivet	2/2	0.06	
20-2	2	17.7 x 3.0	Yes	50.8	Pop Rivet	2/2	0.06	
21-15	1	17.7 x 3.0	No	22.2	Seismic Clip	2/2	0.12	Heavy Panel
22-4	2	17.7 x 3.0	Yes	22.2	Seismic Clip	2/2	0.06	

seismic separation (expansion) joints were evaluated in Assemblies #5 and #6 (see Table 2) at four cross tee intersections and four main runner lap splices. The separation joints at the main runner locations utilized a 38.1 mm (3/2 in.) gap between the two ends of the main runners. Acoustic ceiling tiles, or panels, were made of high-density mineral fiber and weighed 0.06 kPa (1.31 psf) (labeled “Normal”) or 0.12 kPa (2.62 psf) (labeled “Heavy”), respectively. In addition to panel weight, a few metal tiles were placed at

various locations in order to evaluate effects of fire sprinkler piping interaction. In this study, the light fixtures were represented by gypsum board panels.

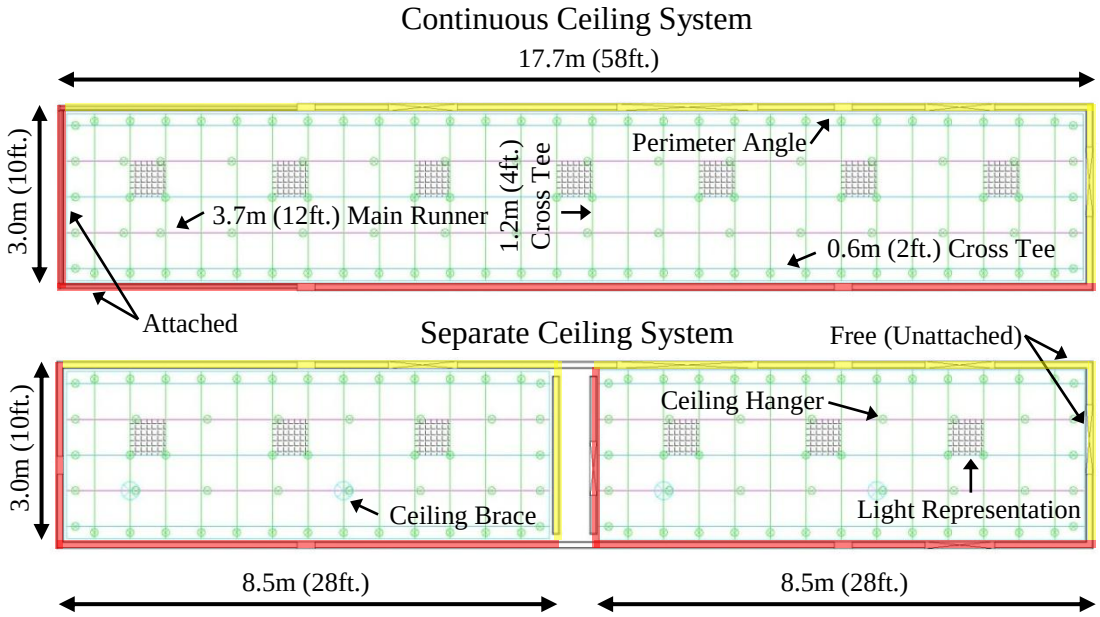

Fig. 3. Continuous and Separate Ceiling Systems

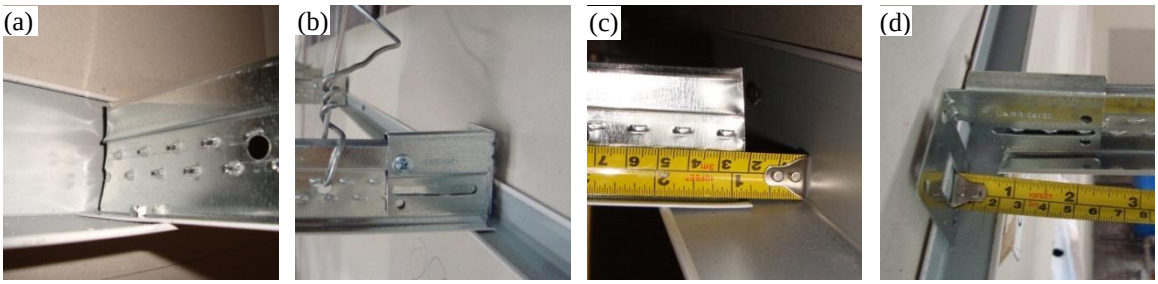

Attached: Pop Rivet | Attached: Seismic Clip | Free: 50.8mm Angle | Free: Seismic Clip

Fig. 4. Examples of Attached and Free Boundary Conditions

Instrumentation

The responses of structural and nonstructural components were monitored through nearly 400 sensor channels with a sampling frequency of 256 Hz. All recorded responses used a 4-pole low-pass Butterworth filter with a cutoff frequency of 50 Hz (Soroushian et al., 2014c). A combination of accelerometers and string potentiometers,

placed at column locations and the middle of floor slabs, were used to record the responses of structural components.

The ceiling system response was measured by string potentiometers, displacement transducers, accelerometers, and load cells. The number and orientation/layout of these instruments were dependent on the assembly configuration. An example of instrument location for Assembly #1 and Assembly #9-10 is show in Fig. 5.

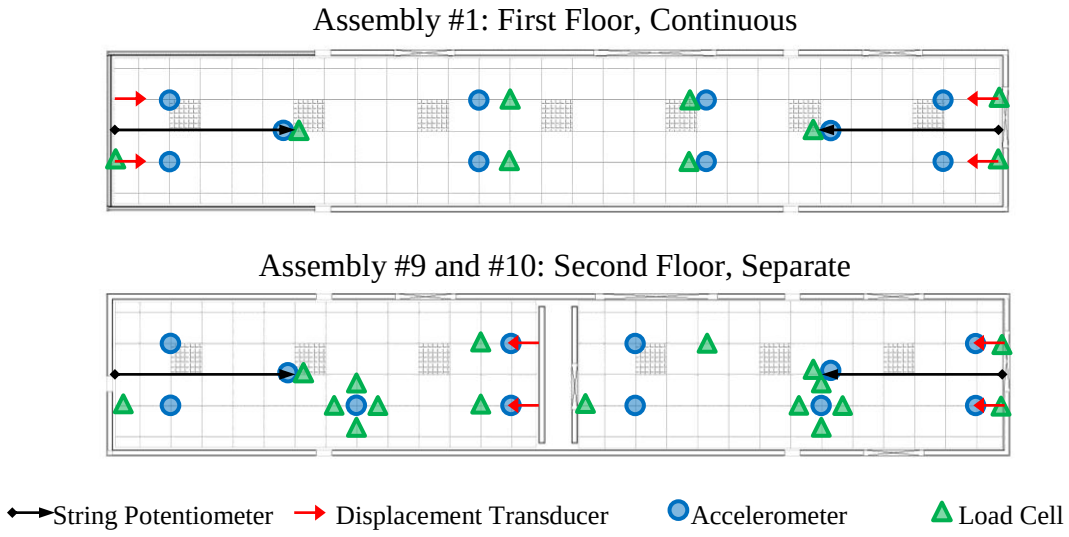

Fig. 5. Ceiling Instrument Location for Assemblies #1, #9, and #10

LOADING PROTOCOL

Three shake tables induced 59 artificially generated ground motions to the test-bed structure from a spectrum-matching procedure. Two targeted acceleration spectra were developed. The first target spectrum was designed at the shake table level and was developed from the AC 156 (ICC, 2010) parameters, story height ratio (z/h = 0.5) and the design spectral response acceleration at short periods (S_{DS} = 2.5g). The second used

algorithms defined by Soroushian et al. (2011) to design the target spectrum at the second floor level.

The number of ground motions subjected to the linear and nonlinear test-bed configurations were 42 and 17, respectively (Soroushian et al., 2014c). The linear configuration encompassed two types of motions, "Unmodified Linear" and "Modified Linear", both with durations of 30 sec. The Unmodified Linear motions (12 out of 42) were set to represent the target spectrum at the shake table level while the Modified Linear motions (30 out of 42) were set to represent the target spectrum at the second floor level. The nonlinear configuration was subjected to motions named "Nonlinear" which were set to represent the target spectrum at the shake table level. It should be noted that the motion durations during this portion of testing were reduced to 10 sec. due to ductility capacity limitation of the bracing systems. A comparison of 5% damped spectra achieved on the shake table and the second floor during 50% of full scale motions (50% IM) is shown in Fig. 6. Table 3 shows a summary of the peak floor accelerations and inter-story drift ratios for the Unmodified Linear, Modified Linear, and Nonlinear motions.

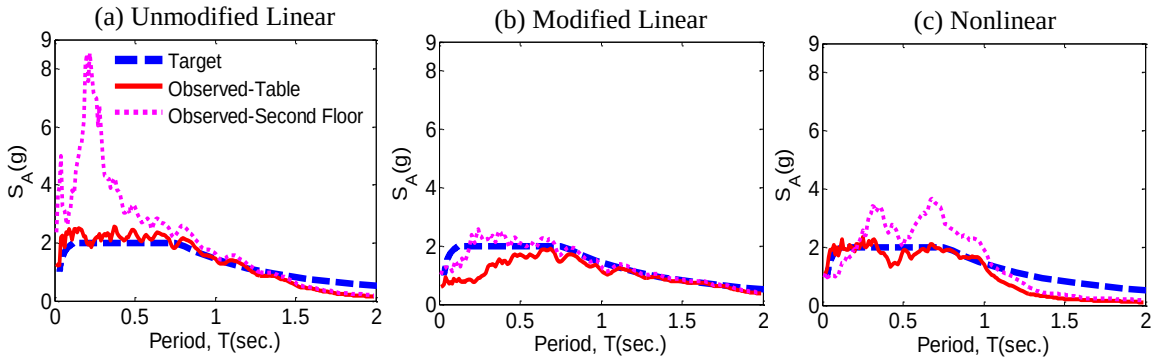

Fig. 6. Comparison between Achieved and Target 50% IM Spectrum
Source: (Soroushian et al., 2014c)

Table 3. Test-bed Responses during Linear and Nonlinear Configurations
Source: (Jenkins et al., 2015a)

Floor	Maximum Peak Floor Acceleration (g)			Maximum Story Drift Ratio (%)		
	Unmodified Linear	Modified Linear	Nonlinear	Unmodified Linear	Modified Linear	Nonlinear
First	1.59	1.16	1.22	0.75	0.66	2.79
Second	2.47	1.65	1.41	0.27	0.18	2.09

DAMAGE OBSERVATION

The performance of the suspended ceiling system configurations can be evaluated through the damage observed during testing. Detailed descriptions of the damage experienced were recorded for every ground motion through inspection sheets, pictures, and videos. The recorded damage was then categorized into different damage types, as shown in Table 4. The damage observed and corresponding minimum peak floor accelerations for each of the different assemblies are summarized in Table 5. A few of the main damage seen during testing is highlighted in Fig. 7.

Table 4. Damage Descriptions

	Ceiling Tile Damage
D1	Misalignment of ceiling tiles
D2	Falling of ceiling tiles
D3	Damage (tearing) of ceiling tiles due to fire sprinkler piping interaction
	Boundary Conditions
D4	Failure of pop rivet connections (attached side)
D5	Damage to 22.2mm (7/8in.) seismic clip (attached side)
D6	Permanent displacement from wall angle and end of grid member
D7	Unseating of grid members from 50.8mm (2in.) perimeter angle
D8	Unseating of grid members from 22.2mm (7/8in.) perimeter angle (seismic clip)
D9	Damage to wall angles (crushing, bending)
	Ceiling Grid Systems
D10	Damage to grid latches (bending)
D11	Buckling of grid members (bending)
D12	Failure of grid connections (falling down of grids)
	Seismic Separation Joint
D13	Damage to separation joint, permanent displacement

Table 5. Damage Observed with Corresponding Minimum Peak Floor Acceleration

Assembly	D1	D2	D3	D4	D5	D6	D7	D8	D9	D10	D11	D12	D13
1	-	-	0.99	0.89	-	-	-	-	-	0.99	-	-	-
2	-	-	1.52	1.24	-	-	-	-	1.52	1.24	1.52	-	-
3	0.83	-	-	-	-	-	-	0.76	-	1.10	0.58	-	-
4	1.48	1.00	1.48	-	1.23	-	-	0.48	2.35	1.23	-	2.35	-
5	-	-	-	-	0.93	1.16	-	0.42	0.79	0.93	-	-	-
6	2.27	1.04	1.91	-	2.27	-	-	1.04	-	1.04	-	2.27	1.65
7	-	-	1.40	1.40	-	-	-	-	-	1.40	-	-	-
8	-	-	1.40	-	1.40	-	-	0.54	-	0.88	-	-	-
9	-	-	2.39	-	-	-	-	-	-	-	-	-	-
10	-	1.65	1.65	-	1.65	-	-	1.87	1.87	1.03	-	2.39	-
11	-	-	0.93	-	-	-	-	-	-	0.93	-	-	-
12	-	1.12	0.93	-	-	-	1.12***	-	-	-	-	-	-
13	-	-	1.25	1.60	-	-	1.60	-	-	-	-	-	-
14	-	1.60	1.25	-	1.60	1.60	-	0.71	1.60	1.60	-	2.47	-
15	-	-	-	-	-	1.03	1.03	-	1.03	-	-	1.03	-
16	-	1.03	-	-	1.22	-	-	0.75	-	1.22	-	-	-
17	-	-	1.41	-	-	-	1.27	-	-	1.27	-	1.41	-
18	-	-	-	-	-	-	-	0.93	1.41	-	-	-	-
19	-	-	0.87	0.92	-	-	0.92	-	0.87	0.92	-	-	-
20	-	-	1.04	1.21	-	-	-	-	-	-	1.21	-	-
21	-	0.89	-	-	0.81	-	-	0.44	0.44	0.81	-	0.84	-
22	-	0.92*	1.01**	-	-	-	-	1.01	1.06	1.01	-	1.01	-

Note: * Falling of metal ceiling tile
** Tearing of metal ceiling tile
*** Specimen includes seismic clip

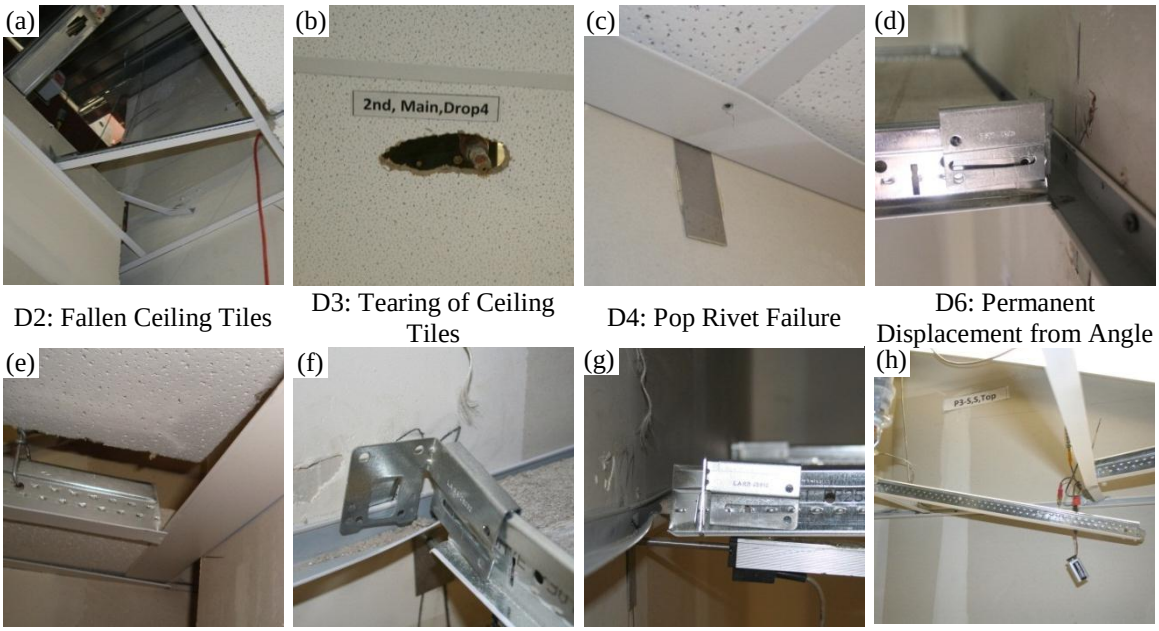

Fig. 7. Examples of Damage Observed

EXPERIMENTAL RESULTS

The following section addresses the processing of experimental results in terms of acceleration amplification factors and fragility curves (ceiling perimeter displacement, support axial force, and overall ceiling performance). In order to best compare the results, the 22 assemblies were categorized into different design variables: 1) bracing, 2) boundary condition, 3) number of attached walls, 4) seismic separation joint, 5) panel weight, and 6) partition wall height. It should be mentioned that not every design variable is compared to one another in the following sections. Specific variables were chosen to be compared for each experimental result sub section and will be highlighted as such.

The ceiling design variable test matrix is shown in Table 6, however, only a few variables are shown for brevity. The effect of partition wall height is considered because

in three assemblies the partition walls that were used to simulate content rooms on the second floor (Jenkins et al., 2015a) extended to the ceiling elevation. In these assemblies, the partition walls were connected to the ceiling system via steel track (350T125) and #8 self-drill screws (labeled "connected" in Table 6). Alternatively, eight assemblies consisted of partition walls (content rooms) that did not extend to the ceiling elevation and were labeled "not connected". The remaining 11 assemblies were not applicable for this effect because content rooms were not placed on the first floor.

Table 6. Ceiling Design Variables

Assembly	Braced /Unbraced		Boundary Condition		Panel Weight		Partition Wall Height (Content Room)	
	Braced	Unbraced	Pop Rivet	Seismic Clip	Heavy	Normal	Connected	Not Connected
1		X	X			X		N/A
2	X		X			X		X
3		X		X		X		N/A
4	X			X		X		X
5		X		X		X		N/A
6	X			X		X		X
7		X	X			X		N/A
8		X		X		X		N/A
9	X		X			X	X	
10	X			X		X		X
11		X	* Free	* Free		X		N/A
12		X		X		X		N/A
13		X	X			X	X	
14		X		X	X			X
15		X	X			X		N/A
16		X		X		X		N/A
17	X		X			X	X	
18	X			X		X		X
19		X	X			X		N/A
20	X		X			X		X
21		X		X	X			N/A
22	X			X		X		X

Note: * Free = All perimeter connections are unattached
N/A = Not applicable because there were no content rooms on the first floor

Acceleration Amplification Factors

Acceleration amplification (a_p) factors for suspended ceiling systems were calculated by taking the ratio of the peak ceiling acceleration over the peak floor acceleration (PFA). The ceiling design variables chosen to be compared were braced/unbraced, number of attached walls, panel weight, and partition wall height. The statistical parameters (max, min, and median) for the different design variables are shown in Table 7. The ASCE 7-10 (2010) recommends an amplification of 2.5 for flexible components. A graphical representation of the max, min, median, and ranges of amplifications calculated for each design variable along with the prescribed value from ASCE 7-10 is shown in Fig. 8. As shown, the maximum and minimum amplifications are 1.03 and 7.61, respectively, while the median amplifications range from 1.57 to 3.56. The two design variables that have the most effect on ceiling amplification are number of attached walls and partition wall height. The lowest median (1.57) occurred in assemblies that had ceilings connected to additional partition walls (content rooms). The additional connection increased the rigidity, causing the amplification to be more comparable to the rigid amplification value (1.0) suggested by ASCE 7-10. The highest median (3.56) was observed when the four ceiling perimeters were free (unattached). Due to the added flexibility from the unattached perimeters, the amplification exceeded the prescribed limit.

Table 7. Acceleration Amplification Factors

Amplification Parameters	Braced vs Unbraced		Number of Attached Walls		Panel Weight		Partition Wall Height (Content Rooms)		All Data
	Braced	Unbraced	2 Attached / 2 Free	4 Free	Heavy	Normal	Connected	Not Connected	
Max	5.30	7.61	7.61	4.60	4.92	7.61	3.13	5.30	7.61
Min	1.03	1.06	1.03	2.02	1.41	1.03	1.03	1.24	1.03
Median	2.44	2.92	2.68	3.56	2.99	2.69	1.57	2.75	2.71

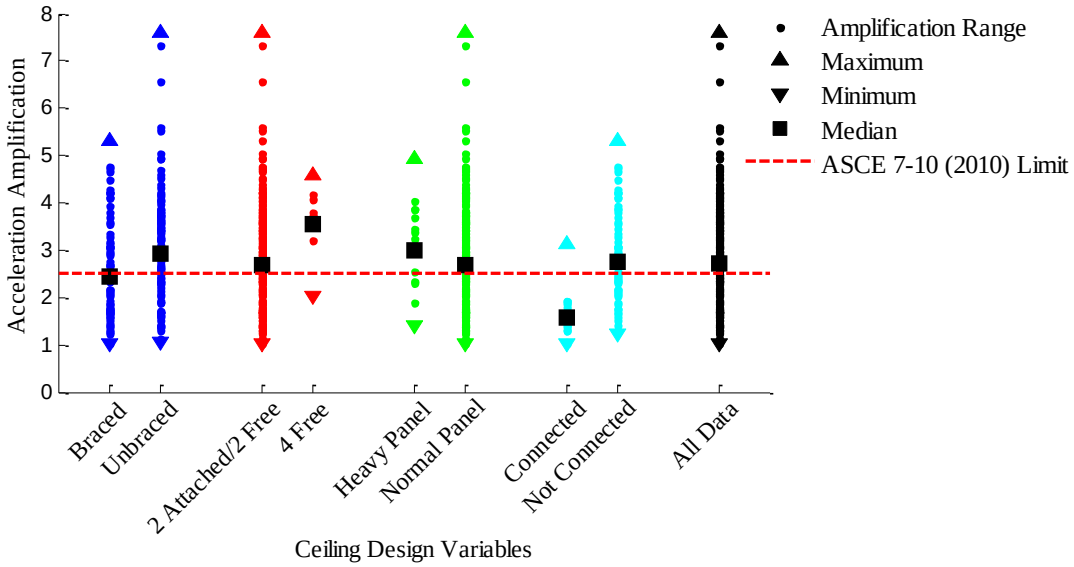

Fig. 8. Graphical Representation of Amplification Factors

Seismic Fragility Analysis

Experimental results of suspended ceiling systems were used to develop fragility functions for perimeter displacement, support axial force, and overall ceiling performance. A fragility function is a conditional probability statement used to assess the seismic vulnerability of a system. The vulnerability can be expressed as the probability of an engineering demand parameter (EDP) exceeding the capacity limit (C) that is associated with a damage state (DS). The capacity limit and associated damage states are dependent the required repair action, repair time, and system functionality. In this study,

the intensity measure (IM) is peak floor acceleration (PFA) because ceiling systems are prone to damage when subjected to large accelerations.

By following the works of Nielson and DesRoches (2007), the relationship between EDP, C, and IM, can be approximately represented with a cumulative normal distribution function, as shown in Eq. (1).

$$P(EDP \geq C|IM) = \Phi\left(\frac{\ln\left(\frac{S_d}{S_c}\right)}{\sqrt{\beta_{d|IM}{}^2 + \beta_c{}^2}}\right) \quad (1)$$

where S_d is the median of the demand estimate as a function of IM, $\beta_{d|IM}$ is the logarithmic standard deviation of the demand with respect to the IM, S_c is the median estimate of the capacity, β_c is the logarithmic standard deviation of component capacities, and $\Phi[\cdot]$ is the normal cumulative distribution. It should be mentioned that for this study, β_c is considered to be zero (β_c=0).

A power-law regression analysis of the local (i.e. perimeter displacement) and global (PFA) seismic demands was used to estimate the demand parameters, S_d (Eq. (2) and $\beta_{d|IM}$ (Eq. (3) (Cornell et al., 2002).

$$S_d = aIM^b \quad (2)$$

$$\beta_{d|IM} \cong \sqrt{\frac{\sum_{i=1}^{N}[\ln(d_i) - \ln(aIM^b)]^2}{N-2}} \quad (3)$$

where a and b are unknown regression coefficients, d_i is the peak local demand corresponding to the i^{th} floor motion, and N is the total number of data points.

Ceiling Perimeter Displacement

The first set of fragility functions developed for this study is based on the ceiling perimeter displacement EDP. Two types of displacements, otherwise known as damage states, were considered to evaluate the performance of ceiling perimeters. The first, named "pounding gap", is the distance between the ends of grid members and the partition wall. The second, named "unseating gap", is the distance that the grid member may travel before falling off or unseating from the wall angle. The demand, capacity, and fragility parameters for both damage states are described below.

In this study, a pounding gap of 19.1 mm (3/4 in.) was installed at all free sides of ceiling configurations. The effects of the pounding gap were compared through six design variables: bracing, boundary condition, number of attached walls, seismic separation joint, panel weight, and partition wall height. The recorded maximum perimeter displacements at the free ends from each ground motion were plotted against the corresponding PFA on a log-log scale to attain the regression plots for each design variable (example shown in Fig. 9). Then, from the regression line coefficients the demand parameters (S_d and $\beta_{d|PFA}$) were determined using Eq. (2) and Eq. (3) above for each of the design variables. The fragility curves shown in Fig. 10 were developed (using Eq. (1) from the demand and capacity parameters (Table 8). As previously mentioned, β_c is considered to be zero. From the median and dispersion fragility parameters, also shown in Table 8, the design variable with the highest probability of failure is four free perimeter walls. On the other hand, the smallest probability of failure is when the ceiling is connected to additional partition walls (content rooms).

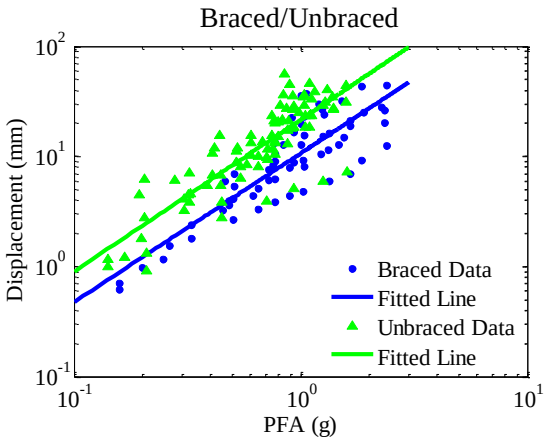

Fig. 9. Regression Plot for Braced/Unbraced Assemblies

Table 8. Displacement Demand, Capacity, and Fragility Parameters (19.1 mm Pounding Gap)

Ceiling Design Variable	Demand			Capacity		Fragility	
	a	b	$\beta_{d\|PFA}$	S_d	β_c	x_m	β
Braced	10.646	1.349	0.514			1.539	0.514
Unbraced	21.512	1.378	0.505			0.916	0.505
Pop Rivet	12.219	1.180	0.639			1.457	0.639
Seismic Clip	17.111	1.283	0.547			1.087	0.547
2 Attached / 2 Free	14.993	1.255	0.602			1.210	0.602
4 Free	27.121	0.997	0.119			0.702	0.119
With Seismic Separation Joint	16.237	1.107	0.676	19.1	0	1.155	0.676
Without Seismic Separation Joint	15.320	1.254	0.602			1.190	0.602
Heavy Panel	35.669	1.909	0.661			0.720	0.661
Normal Panel	14.706	1.218	0.580			1.237	0.580
Connected	5.716	0.928	0.385			3.659	0.385
Not Connected	12.615	1.477	0.412			1.322	0.412
All Data	15.380	1.237	0.607			1.189	0.607

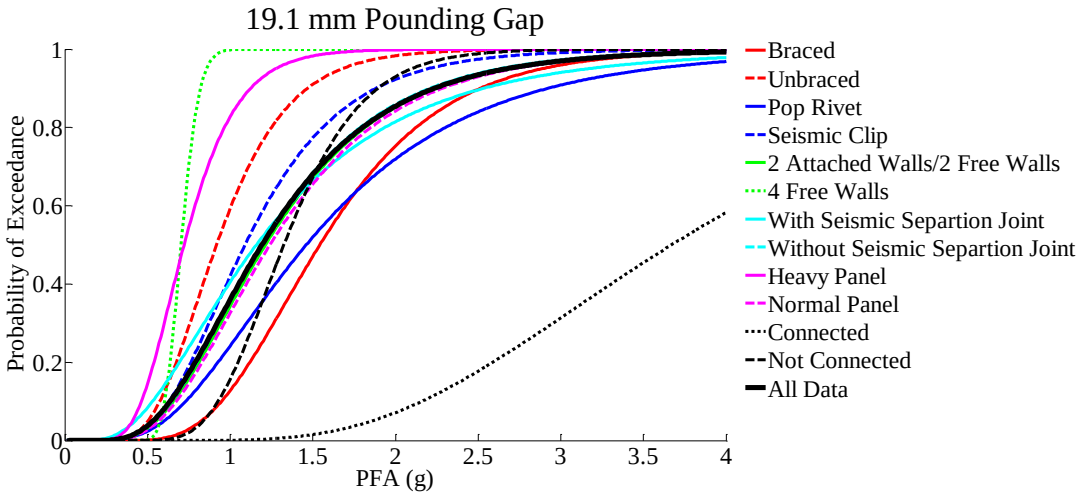

Fig. 10. Perimeter Displacement Fragility Curves (19.1 mm Pounding Gap)

A similar process was used to determine the demand and capacity parameters for the unseating gap damage state (Table 9). However, the only design variable considered was the number of attached walls. The capacity limit is dependent on the seismic design category and the size of wall angle. The recommended unseating displacements, per ASTM E580/E580M (2011), are shown in Table 9. Similarly, fragilities based on the unseating gap (Fig. 11) for each seismic design category were determined from Eq. (1). The seismic design category D-E-F governs the failure probability compared to category C. The probability is highest for the unseating of 22.2 mm (7/8 in.) wall angles and the lowest for unseating of 50.8 mm (2 in.) wall angles. A summary of the unseating fragility parameters is presented in Table 9.

Table 9. Perimeter Displacement Demand, Capacity, and Fragility Parameters (Unseating Gap)

Seismic Design Category (Wall Angle Size)	Design Variable	Demand			Capacity		Fragility	
		a	b	$\beta_{d\|PFA}$	S_d	β_c	x_m	β
D-E-F (50.8mm)	2 Attached / 2 Free	14.993	1.255	0.602	31.750	0	1.818	0.602
D-E-F (22.2mm)		14.993	1.255	0.602	3.175	0	0.290	0.602
C (22.2mm)	4 Free	27.121	0.997	0.119	12.700	0	0.467	0.119

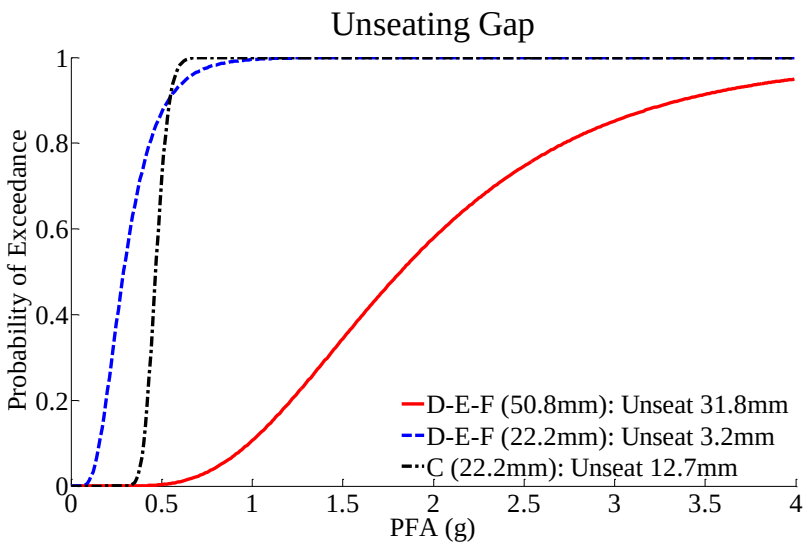

Fig. 11. Perimeter Displacement Fragility Curves (Unseating Gap)

Support Axial Force

The second set of fragility functions are based on the axial force observed in hangers and wire restrainers. The total axial force includes the dead weight of the suspended ceiling system and the applied force caused from the generated earthquake excitations. Three design variables were selected in order to observe different effects on support elements: 1) bracing, 2) panel weight, and 3) partition wall height. It should be noted that the data for assemblies 7, 8, 9, and 10 was disregarded due to an error in the load cell readings. The power-law regression analysis outlined above was used to determine the parameters: a, b, and $\beta_{d|PFA}$ for each design variable as well as a combination of all the data (Table 10).

Table 10. Support Axial Force Demand Parameters

Demand Parameters	Braced/Unbraced		Panel Weight		Partition Wall Height (Content Rooms)		All Data
	Braced	Unbraced	Heavy	Normal	Connected	Not Connected	
				Hangers			
a	0.189	0.186	0.342	0.174	0.115	0.219	0.187
b	0.489	0.489	0.479	0.501	0.573	0.475	0.492
$\beta_{d\|PFA}$	0.328	0.468	0.215	0.372	0.188	0.358	0.417
				Wire Restrainers			
a	0.639	0.151	N/A	0.517	0.246	0.644	0.517
b	0.820	0.768	N/A	0.842	0.741	0.823	0.842
$\beta_{d\|PFA}$	0.364	0.136	N/A	0.622	0.734	0.383	0.622

The capacity limits for hangers and wire restrainers were taken from ASTM E580/E580M (2011) as 0.40 kN (0.09 kips) and 1.11 kN (0.25 kips), respectively. The demand axial force observed during testing was higher than the capacity limit suggested by ASTM in hangers and wire restrainer specimens. However, there were no occurrences of complete hanger or wire restrainer failure. A graphical representation of the demand axial force compared to the suggested capacity limit for all the data is shown in Fig. 12. As shown, axial forces recorded in hangers and wire restrainers were 0.91 kN (0.21 kips) and 1.43 kN (0.32 kips), respectively. These values suggest that the ASTM capacity limit underestimates the actual capacity limits. Nevertheless, the damage state considered for this study is the capacity (failure) limit of 0.40 kN (0.09 kips) for hangers and 1.11 kN (0.25 kips) for wire restrainers. The fragility curves (Fig. 13) were developed from the demand and capacity parameters by using Eq. (1). The median and dispersion fragility parameters are presented in Table 11. As shown from the fragility curves, hangers supporting heavy panels, 0.12 kPa (2.62 psf), have the highest failure probability. Wire restrainers in braced and with additional partition connection configurations also have the

highest failure probability. However, when including all the data, wire restrainers have a higher probability of failure compared to hangers.

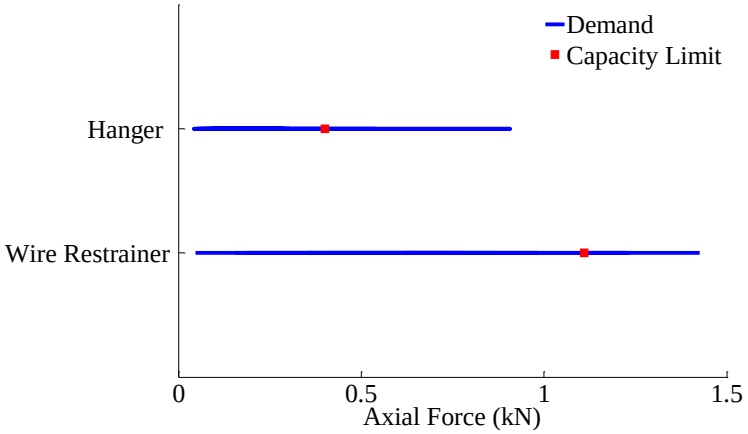

Fig. 12. Comparison of Demand Axial Force to Capacity Limit

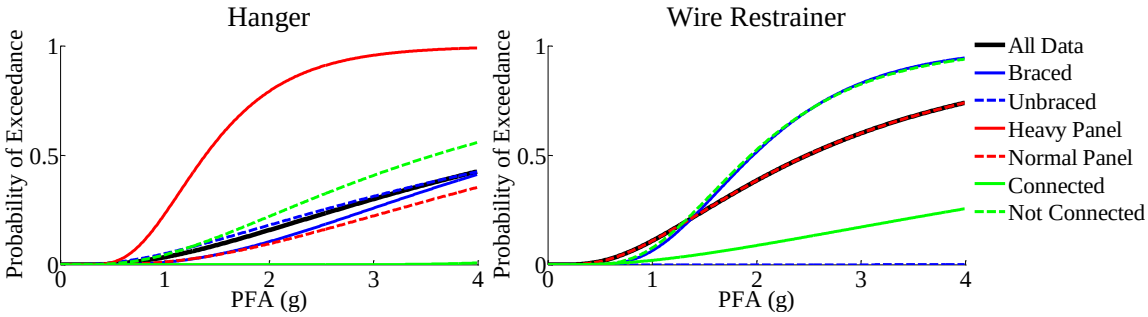

Fig. 13. Fragility Curves for Hangers and Wire Restrainers

Table 11. Support Axial Force Fragility Parameters

Fragility Parameters	Braced/Unbraced		Panel Weight		Partition Wall Height (Content Rooms)		All Data
	Braced	Unbraced	Heavy	Normal	Connected	Not Connected	
				Hangers			
x_m	N/A*	N/A*	1.388	N/A*	N/A*	3.575	N/A*
β	N/A*	N/A*	0.215	N/A*	N/A*	0.358	N/A*
				Wire Restrainers			
x_m	1.966	N/A*	N/A	2.483	N/A*	1.942	2.483
β	0.364	N/A*	N/A	0.622	N/A*	0.383	0.622
Note:	N/A = Wire restrainers did not support heavy panels N/A* = Median values greater than 4g						

Overall Ceiling Performance

The last set of fragility functions were developed for the overall performance of ceiling systems. From the specifications outlined by FEMA P-58 (2011), three damage states were defined for this study (Table 12). The damage states were developed based on the percentage of fallen ceiling panels to the total ceiling panel area. As shown in Table 12, the thresholds of fallen ceiling panel percentages of the total ceiling area for the three damage states are 5%, 30%, and 50%, respectively. In order to find the percentage of fallen area, a determination process (as shown in Table 13) was used to equate the damage observed to an amount of fallen panels. This process was used to determine the cumulative percentage of ceiling area loss for each of the ground motions. A visual representation of the cumulative damage (with respect to percentage loss) that occurred in one of the ceiling assemblies is shown in Fig. 14. For brevity, only a few of the ground motions are shown. The percentages of ceiling loss and the PFA at which the loss occurred for each ground motion, was used as the data to formulate fragility curves.

Table 12. Damage State Descriptions

Damage State	Description	Repair	Percentage of Fallen Ceiling Area
DS1	Ceiling tiles dislodge and fall	Reinstall tiles	5%
DS2	Ceiling grid and tile damage	Replacement for grid and tile	30%
DS3	Major ceiling damage and some grid collapse	Total replacement of grid and tile	50%

Table 13. Percentage of Fallen Ceiling Area Determination Process

Damage Type	Description	Equivalent Number of Panels
Perimeter Damage	Pop rivet failure	2
	Seismic clip failure or crushing	2
	Unseating of grid members from wall angle	2
Grid Damage	0.6 m (2 ft.) grid member joint damage, buckling	2
	1.2 m (4 ft.) grid member joint damage, buckling	4
	Main Run joint damage, buckling	48
Tile Damage	Excessive tile damage from sprinkler heads	1
	Misaligned tiles	0

a) Ground Motion 7: Measured PFA= 1.56g, 28.3% Failed Area

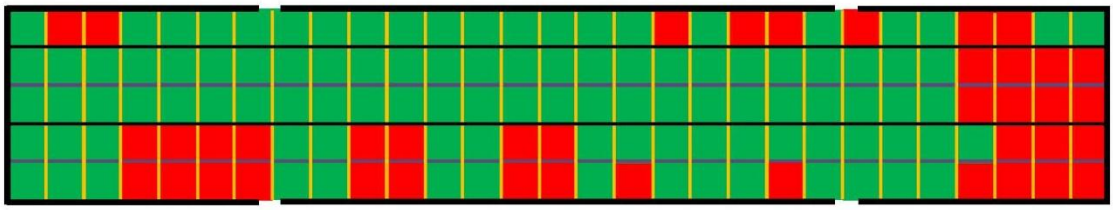

b) Ground Motion 9: Measured PFA= 2.35g, 41.4% Failed Area

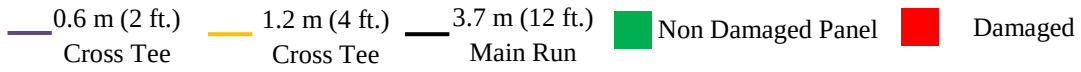

(Assembly #4, Test L-2, Second Floor, Config. #4, Ceiling Size 17.7 x 3.0 m, $PFA_{achieved}$ 2.35g, Panel Weight 0.06 kPa, Braced, 22.2 mm wall angle and seismic clip)

Fig. 14. Example of Cumulative Ceiling Area Loss in Terms of Percentage

Three design variables were selected in order to compare the performance of ceiling assemblies: 1) bracing, 2) boundary condition, and 3) partition wall height. The demand parameters were determined through the power-law regression analysis (as previously described). However, a segmental analysis approach was used to fit the data because at low intensity ground motions, the ceiling systems may not have encountered any damage (zero percent ceiling area loss). An example of separate regression lines used to fit the data for assemblies with pop rivet or seismic clip connections are shown in Fig. 15. Table 14 shows the demand parameters for the selected design variables and all the data, labeled "All Data". It should be mentioned that only the parameters for the data with a percentage area loss are given because the parameters for the data with zero percent area loss are zero.

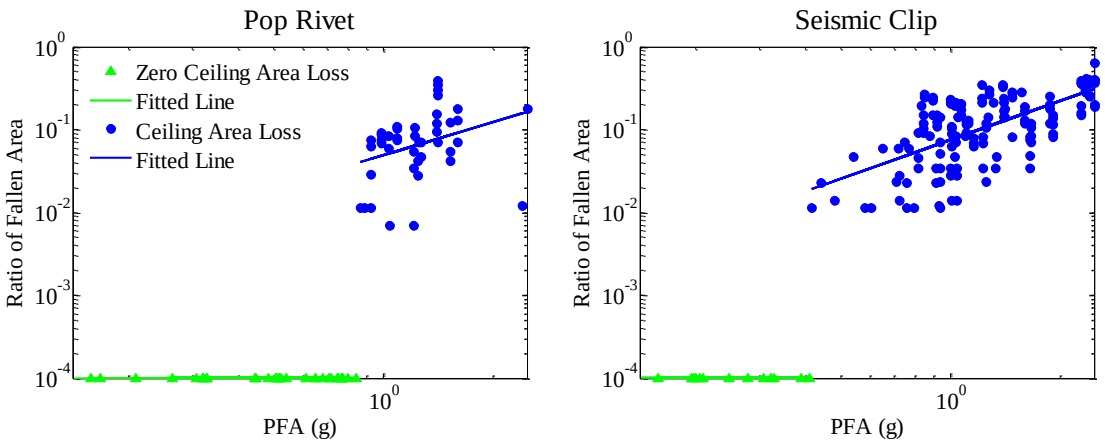

Fig. 15. Separate Regression Analysis for Assemblies with Pop Rivets or Seismic Clips

Table 14. Overall Performance Demand Parameters

Demand Parameters	Braced/Unbraced		Boundary Condition		Partition Wall Height (Content Rooms)		All Data
	Braced	Unbraced	Pop Rivet	Seismic Clip	Connected	Not Connected	
a	0.058	0.077	0.049	0.076	0.096	0.053	0.069
b	1.619	1.804	1.338	1.566	0.941	1.859	1.619
$\beta_{d\|PFA}$	0.857	0.741	0.936	0.745	0.749	0.756	0.778

Note: Only the parameters for the data with percent area loss are shown

From the demand parameters, segmental fragility functions (example shown in Fig. 16) were developed using Eq. (1) above. Then, a least squares curve fitting process was used to combine (or fit) the two separate fragility functions. For clarity, only the segmental and combined fragility curves for the seismic clip design variable that correlate to DS1 are shown (Fig. 16). The combined fragility curves for all three damage states are shown in Fig. 17. As depicted from the fragility curves, design variables under DS1 have a concentrated probability of failure. However, as the damage state increases (to DS2 and DS3), the difference in the performance variation of the design variables also increases. Additionally, there becomes a clear difference in trend between design variables. Assemblies that were unbraced, included seismic clips, or were not connected had a higher failure probability than assemblies that were braced, included pop rivets, or were connected. These results suggest that systems that are more susceptible to movement have a higher chance of exceeding their capacity limits under DS2 or DS3. The fragility curves also show that assemblies that use pop rivets have the lowest probability of failure compared to other design variables for all three damage states. The median and dispersion fragility parameters for each design variable are shown in Table 15. As shown,

the median for all the combined data is 0.82g, 2.47g, 3.39g for the three damage states, respectively.

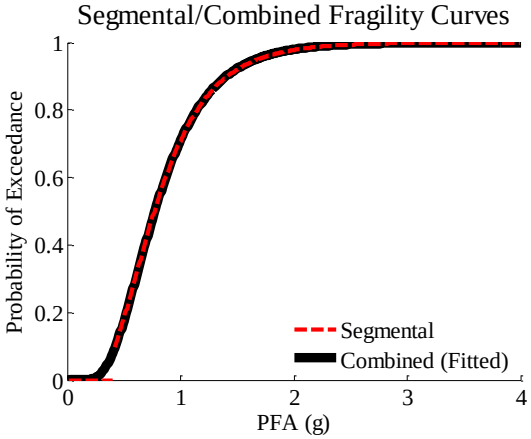

Fig. 16. Segmental and Combined Fragility Curves for Assemblies with Seismic Clips

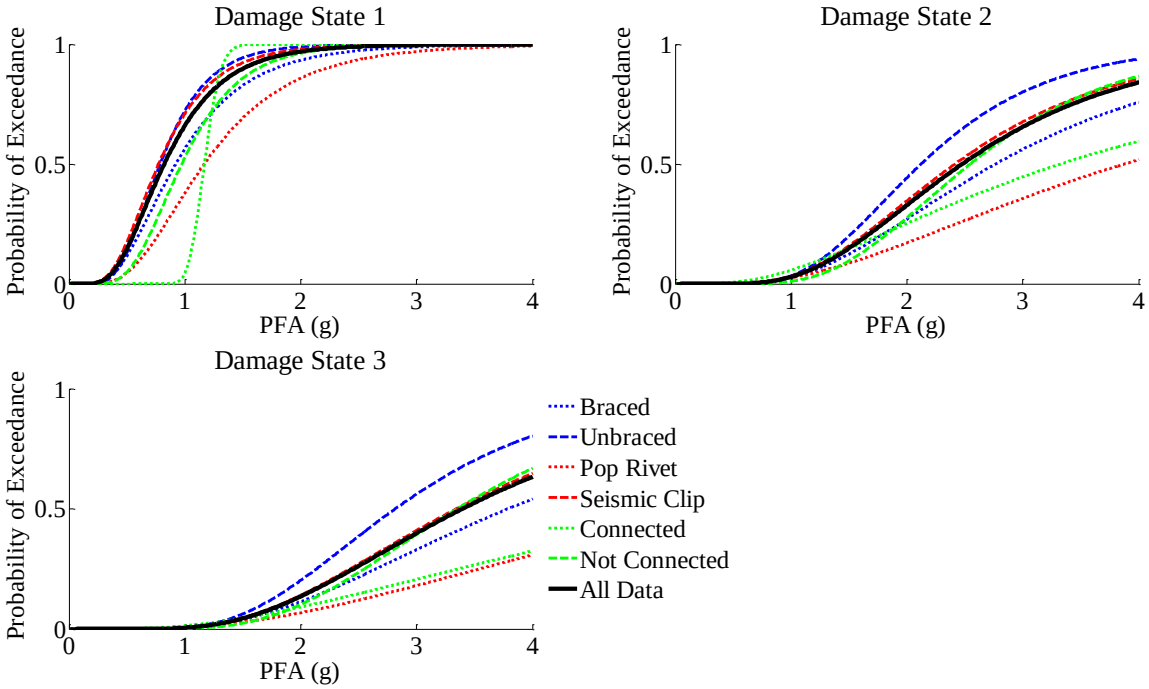

Fig. 17. Overall Performance Fragility Curves

Table 15. Overall Performance Fragility Parameters

Damage State	Braced/Unbraced				Boundary Condition				Partition Wall Height (Content Rooms)				All Data	
	Braced		Unbraced		Pop Rivet		Seismic Clip		Connected		Not Connected			
	x_m	β	x_m	β	x_m	β	x_m	β	x_m	β	x_m	β	x_m	β
DS1	0.92	0.52	0.79	0.41	1.17	0.50	0.77	0.47	1.17	0.09	0.97	0.40	0.82	0.47
DS2	2.76	0.53	2.12	0.41	3.87	0.70	2.41	0.48	3.32	0.76	2.55	0.41	2.47	0.48
DS3	3.79	0.53	2.82	0.41	N/A*	N/A*	3.34	0.48	N/A*	N/A*	3.35	0.41	3.39	0.48
Note:	N/A* = Median values greater than 4g													

SUMMARY

The full-scale, system-level experiments conducted at the University of Nevada, Reno NEES site aimed to evaluate the seismic performance of integrated ceiling-piping-partition systems. A two-story, two-by-one bay steel braced-frame structure that spanned over three biaxial shake tables was used to house the nonstructural components. In this study, the performance of the suspended ceiling systems was assessed through 22 different assemblies. A brief description of the damage observed during testing was presented. Experimental results included the acceleration amplifications for four design variables: bracing, number of attached walls, panel weight, and effects of connections to partition walls. In addition, experimental results also led to the development of fragility functions for ceiling perimeter displacement, support axial force, and overall ceiling performance. The major findings are summarized as follows:

- Ceiling acceleration amplifications are most effected by: 1) additional attachments to partition walls (a_p = 1.57) and 2) four free (unattached) walls (a_p = 3.56).

- Ceiling systems that have all free sides (grids unattached to the wall angle) have the highest failure probability while ceilings with additional partition walls (content rooms) have the lowest failure probability when assessing a pounding gap of 19.1 mm (3/4 in.).
- Fragility functions based on the unseating gap show that the seismic design category D-E-F governs the failure probability (high and low) compared to category C. Unseating of grid members from 22.2 mm (7/8 in.) wall angles have the highest probability of exceedance and unseating of grid members from 50.8 mm (2 in.) wall angles has the lowest exceedance probability.
- From the support element fragility curves, results show that wire restrainers have a higher probability of failure compared to hangers.
- Fragility functions for the overall performance of ceiling systems show that assemblies that were unbraced, included seismic clips, or did not have additional connections to partition walls had a higher failure probability than assemblies that were braced, included pop rivets, or had additional connections.
- Overall fragility results show that systems with pop rivet connections have the lowest probability of failure compared to other ceiling system variables.
- The median fragility parameters based on overall ceiling system performance are 0.82g, 2.47g, and 3.39g for percentage of ceiling area loss of 5% (DS1), 30% (DS2), and 50% (DS3), respectively.

ACKNOWLEDGEMENTS

This material is based upon work supported by the National Science Foundation under Grant No. 0721399. This Grand Challenge (GC) project to study the seismic response of nonstructural systems is under the direction of M. Maragakis from the University of Nevada, Reno and Co-PIs: T. Hutchinson, A. Filiatrault, S. French, and B. Reitherman. Any opinions, findings, conclusions or recommendations expressed in this document are those of the investigators and do not necessarily reflect the views of the sponsors.

3. FIRE SPRINKLER PIPING SYSTEMS

The following section is borrowed from a paper submitted to the *Earthquake Engineering* Journal (Jenkins et. al, 2015c). Currently, this paper has been reviewed and re-submitted for publication.

Experimental Fragility Analysis of Pressurized Fire Sprinkler Piping Systems

Craig Jenkins[1], Siavash Soroushian[2], Esmaeel Rahmanishamsi[3], and E. "Manos" Maragakis[4]

ABSTRACT

The seismic performance of nonstructural components, including pressurized fire sprinkler systems, plays a significant role during and after an earthquake. A series of full-scale system-level experiments was conducted at the University of Nevada, Reno Network for Earthquake Engineering Simulation site in order to evaluate the seismic performance of integrated ceiling-piping-partition systems. In this study, the performance of fire sprinkler piping systems were evaluated through several design variables. Processing of experimental data led to the calculation of acceleration amplification factors and development of fragility functions. Results show that 50 mm (2.0in.) diameter pipes have the greatest failure probability when evaluating pipe joint rotations.

1 Graduate Research Assistant, Department of Civil and Environmental Engineering, University of Nevada, Reno, Reno, NV, 89557, email:cjenkins@unr.edu

2 Structural Analyst, Advanced Technology and Research, Arup, San Francisco, CA, 94105, email: siavash.soroushian@arup.com

3 Ph.D. Candidate, Department of Civil and Environmental Engineering, University of Nevada, Reno, Reno, NV, 89557, email: erahmanishamsi@unr.edu

4 Professor, Dean of College of Engineering, University of Nevada, Reno, Reno, NV, 89557, email: maragaki@unr.edu

INTRODUCTION

The extensive shaking caused from earthquakes can greatly affect the performance of structural and nonstructural components. However, reports show that even when structural damage is low, nonstructural damage can have a significant impact on the overall performance of a building [Miranda et al., 2012]. Nonstructural systems are more prone to damage than structural systems due to their lower capacities [Taghavi and Miranda, 2003]. In order to evaluate the seismic performance of integrated nonstructural components, such as ceiling-piping-partition systems, a study was conducted at the University of Nevada, Reno Network for Earthquake Engineering Simulation (UNR-NEES) site. A key component of the integrated nonstructural systems is the fire sprinkler piping system. This paper aims to evaluate the behavior and responses of fire sprinkler piping systems when subjected to earthquake ground motions.

The seismic response of fire sprinkler piping systems can be evaluated through damage observed during past earthquakes. Common seismic damage includes breaking of sprinkler heads from adjacent nonstructural components, failure of bracing systems, and leaking or complete rupture of pipe joints causing minor to severe water damage. During the 1964 Alaska earthquake, the sprinkler systems came in contact with adjacent objects such as a cross brace from the roof causing a sprinkler head to activate [NRC, 1973]. In addition, damage was observed at threaded pipe fittings joints [Ayres et al., 1973]. Similar piping damage occurred in the 1994 Northridge earthquake, including the rupturing of sprinkler heads due to the collision to the ceiling system. As reported from Fleming [1998], the main damage to the fire sprinkler systems were caused by inadequate bracing. Excessive pipe leakage during the 2010 Chile earthquake left hospitals

inoperable and the airport terminal at Santiago shut-down [Miranda et al., 2012]. The common damage listed above and additional damage to fire sprinkler piping systems has been observed in other past earthquakes such as the 1971 San Fernando [Ayres and Sun, 1973], 1989 Loma Prieta [Arnold, 1991], 2001 Seattle (Nisqually) [Filiatrault et al., 2001], 2006 Hawaii [RMS, 2006], and 2011 Tohoku Pacific [Mizutani et al., 2012] earthquakes.

Several past experimental studies, component and system-level, have been conducted in order to evaluate the seismic performance of fire sprinkler piping systems. The component-level experiments included the study on joint connections and seismic-brace components. Antaki and Guzy [1998] observed the effects of first leakage of threaded and grooved fit joints through bending tests. Observed damage included stripped threads in threaded joints and cracked housing in grooved joints, both leading to joint leakage. In addition, Wittenberghe et al. [2010] conducted a study to evaluate the crack propagation in threaded joints by performing fatigue testing. Tian et al. [2013] tested 48 different piping tee joints, with a variety of pipe material and diameters, to determine their rotational capacities at first leakage. It was determined that typical rotational capacities at first leakage range from 0.005 rad to 0.405 rad. The seismic-brace component test, conducted by Malhotra et al. [2003], assessed the amount of cycles that the component must resist during an earthquake. Results suggest that sway-brace components tested in this experiment can resist for 15 cycles before rupture. Other component-level tests that have been conducted in order to assess the seismic response of piping systems include Larson et al. [1975], Rodabaugh et al. [1978], Gerdeen et al. [1979], Wais [1995], Masri et al. [2002], and Matzen et al. [2002]. The component-level

experiments listed above provide valuable test data that was used to increase the knowledge base of component-level behavior.

In addition to component-level, subsystem and system-level experiments have been conducted on fire sprinkler piping systems. The University of California at San Diego (UCSD) conducted an experiment to evaluate the performance of anchors from loads and forces applied to the pipe system during an earthquake. Results show that the maximum axial loads in the anchors were relatively low, less than 38% utilization of the ultimate anchor tension capacity [Hoehler et al., 2009]. The experiment conducted at the E-Defense facility in Japan assessed the permanent rotation of armover drops and damage to ceiling tiles near sprinkler heads. It was shown that the use of flexible hose drops can reduce damage caused from ceiling-piping interaction [Soroushian et al., 2014a]. Tian et al. [2013] tested three specimens with varying materials, joint arrangements, and bracing systems to evaluate the overall performance of a piping subsystem. Common damage observed during this experiment included failure of vertical hangers, branch line failure, and sprinkler head damage.

Although there is essential data on component-level behavior of fire sprinkler piping systems, there is still a need for more information on their system-level performance. A better understanding of the behavior and responses during earthquake motions could help the design and detailing of components with intent to minimize damage. In order to further analyze the seismic performance of fire sprinkler piping systems, a series of system-level tests were conducted at the UNR-NEES site. A full-scale, two-story steel braced-frame structure was used to house the nonstructural components including fire sprinkler piping systems. Different design variables were used

to evaluate the performance of the schedule 40 piping system: 1) pipe configuration, 2) pipe diameter, 3) branch length, 4) brace detailing, 5) joint type, and 6) sprinkler pipe detailing. Acceleration amplifications were calculated from experimental results and compared against the recommended value given by ASCE 7-10 [2010]. Fragilities were developed based on pipe joint rotation, support anchor capacities, and displacement capacities. The following section addresses typical properties of a fire sprinkler piping system including layout and the different components. Then, the experimental setup section, including the test-bed structure, piping assembly, and instrumentation, is discussed. Next, the loading protocol is presented followed by the damage observed during testing. The final section, experimental results, includes the acceleration amplification factors and the development of fragility curves.

BACKGROUND OF FIRE SPRINKLER PIPING SYSTEMS

Fire sprinkler piping systems are common in critical facilities (hospitals and power-plants), residential homes, and commercial buildings. These piping systems are typically made of pressurized water tanks, pipe segments, sprinkler heads, and support components (see Figure 1). The pressurized tank provides water to all areas of the system through pipe segments. There are four pipe segment types: 1) vertical riser pipe, 2) main pipe, 3) branch line, and 4) drops or armovers. Water travels from the tank, up the riser pipe, and to the horizontal assembly which is made of the main pipe run and branch lines. The main pipe run typically extends the length of the floor while branch lines extend off the main pipe to other areas of the floor. Branch lines supply water to drops and armovers in which the sprinkler heads are attached. The sprinkler heads will automatically activate when smoke or a fire is detected. The last component of the fire sprinkler piping system

is the support elements. Hangers, attached to an adjustable band around the pipe, support the dead weight of the system (including water). Wire restrainers (oriented at 45-degrees) limit displacement of branch lines. Braces, also oriented at 45-degrees, resist the lateral and longitudinal sway through solid tubing (compression and tension) or wires (tension only).

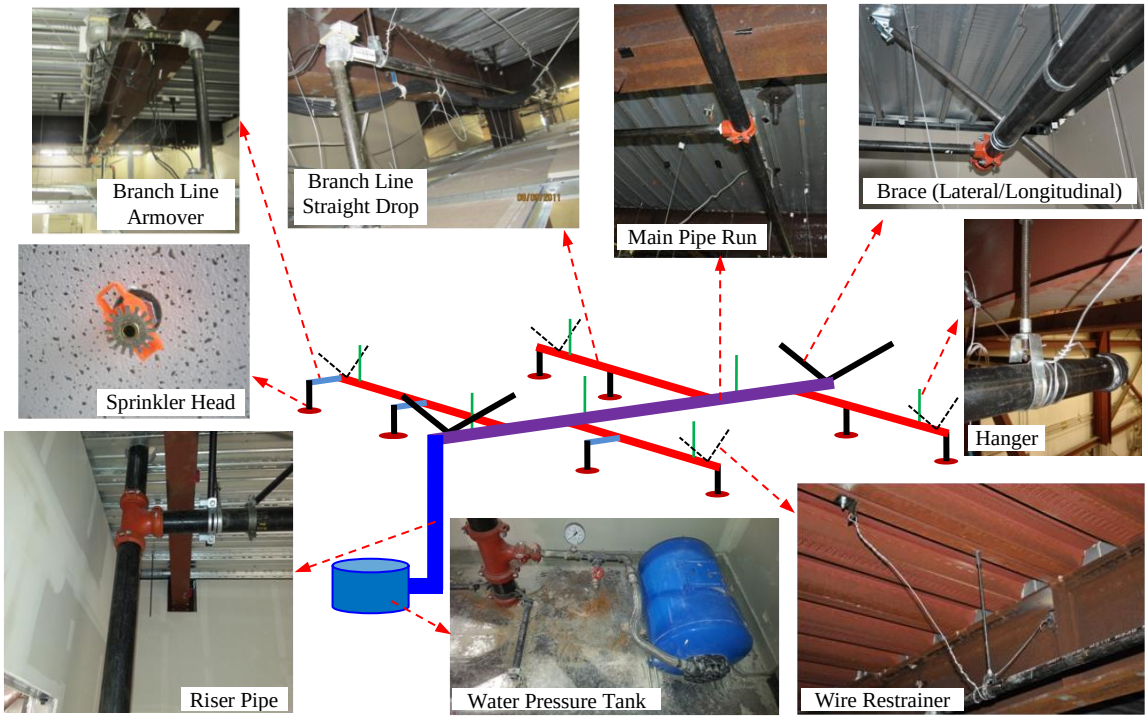

Figure 1. Fire Sprinkler Piping System Schematic [Figure courtesy of Soroushian et al., 2014b]

EXPERIMENTAL SETUP

Test-bed Structure

A full-scale, two-story, two-by-one bay steel braced-frame test-bed structure was designed in order to assess the seismic performance of acceleration and drift sensitive nonstructural systems. The test-bed structure spanned over three biaxial shake tables at

the University of Nevada, Reno NEES site. Figure 2 shows the elevation view of the test-bed structure along with approximate dimensions.

The test-bed structure was designed to be arranged into two configurations in order to evaluate the response of acceleration and drift sensitive components. Design variables of the two configurations include the yielding force of buckling restrained braces (BRB) and amount of additional attached floor masses. The first configuration, named "Linear", was designed to achieve large floor accelerations by using BRB's with a high yield capacity and a lower amount of attached mass to the floor decks. The properties for BRB yielding forces and floor masses are shown in Table 1. The second

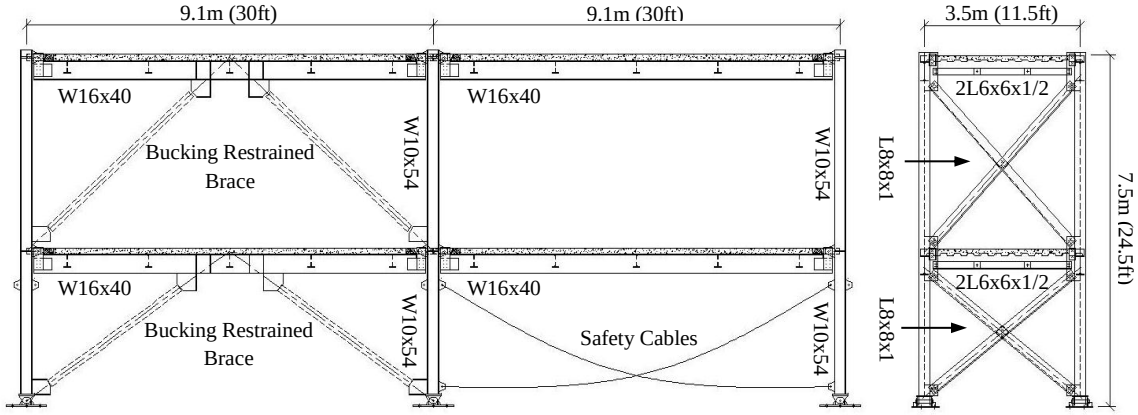

Figure 2. Elevation View of Test-bed Structure [Figure courtesy of Jenkins et al., 2015a]

configuration, named "Nonlinear", used BRB's with a low yielding capacity and an increased amount of attached mass (Table 1). The yielding of BRB's led the structure to experience large inter-story drift. The natural periods for the linear and nonlinear configurations were found to be 0.20 seconds and 0.34 seconds, respectively [Soroushian et al., 2014c]. Figure 3 shows the test-bed structure and the two design variables. The

additional floor masses, located on the first and second floors, as well as an example of a BRB with its connection to the structure are shown in Figure 3b-d.

Table 1. Configuration Properties

Floor	Linear Configuration		Nonlinear Configuration	
	BRB Yielding Force	Attached Mass	BRB Yielding Force	Attached Mass
First	283 kN (64Kips)	30.7 kN (6.9Kips)	89 kN (20.0Kips)	62.5 kN (14.0Kips)
Second	283 kN (64Kips)	17.6 kN (4.0Kips)	89 kN (20.0Kips)	279.1 kN (62.8Kips)
T_n	0.2 sec		0.34 sec	

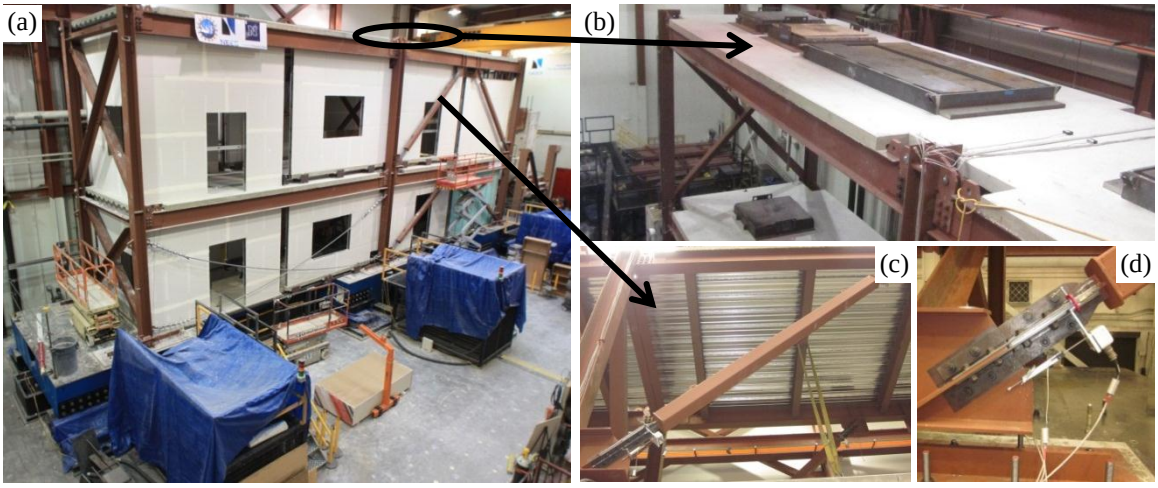

Figure 3. Test-bed Structure Design Variables: (a) 3-D view, (b) additional floor mass, (c) buckling restrained brace (BRB), (d) BRB connection

Fire Sprinkler Piping System Assembly

Fire sprinkler piping system assemblies were installed on the first and second floors of the test-bed structure. A total of 16 assemblies, eight tests with two assemblies each were conducted to evaluate the effects of design variables including: pipe configuration, pipe diameter, branch length, brace detailing, joint type, and sprinkler pipe detailing. Two piping configurations were designed, named “Continuous” and “Separate” [Rahmanishamsi et al., 2014], as shown in Figure 4. The continuous configuration spanned between the north and south bays and used one pressurized water system of 345 kPa (50psi) to detect leakage. Ten out of 16 assemblies utilized the continuous

configuration. The separate configuration (installed in 6 out of 16 assemblies) only spanned one bay at a time and used two pressurized water systems also at 345 kPa (50psi). It should be noted that in the separate configuration, the piping assembly consisted of two elevations, or levels, to account for obstructing structural or nonstructural members (see Figure 5). Throughout testing, all configurations (including systems on the first and second floors) utilized the same piping design variables so that investigators could evaluate the performance of different ceiling systems. Therefore, it is expected that the second floor piping system will experience a more severe loading condition due to the accelerations being larger on the second floor.

The pipe configurations were composed of different pipe segments, varying from 25 to 100 mm (1.0 to 4.0in.) diameter, and were categorized as riser pipes, main pipes, branch lines, armovers, and drops (see Figure 4). The riser pipe, typically 100 mm (4.0in.) diameter, connected the pressurized water tank to the horizontal assembly, made of main pipe runs and branch lines, on the two floors. The horizontal assembly suspended 457 mm (18.0in.) below the floor above. The main pipe run supplied water to the branch lines which expanded to other areas of the floor plan. Due to test-bed limitations, an additional mass 0.08 or 0.09 kN (21.0lb. or 18.0lb.) was attached to the ends of some branch lines to simulate a longer branch length. Branch lines supplied water to armovers and drops with typical diameters of 25 mm (1.0in.).

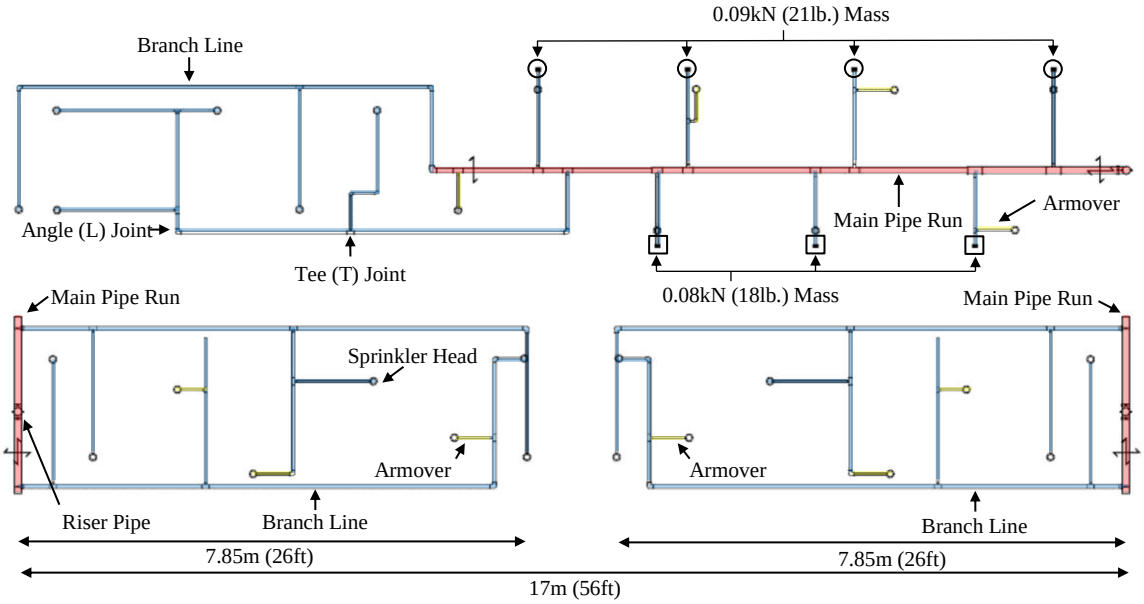

Figure 4. Plan View of Piping Configurations: (top) continuous, (bottom) separate

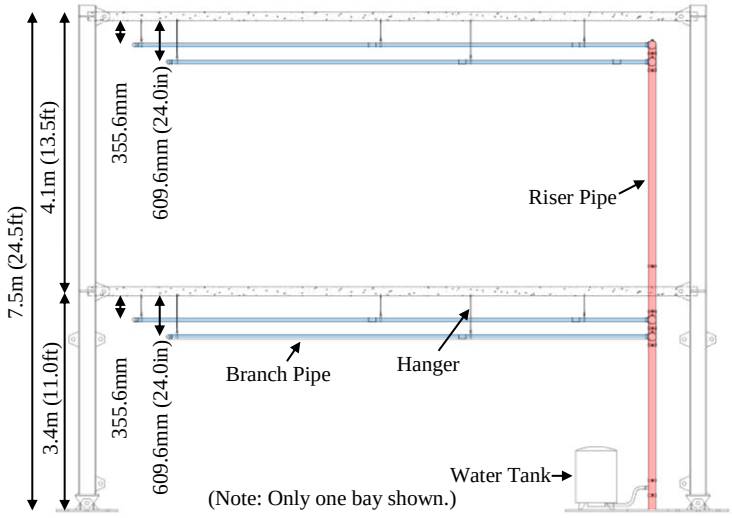

Figure 5. Elevation View of Separate Piping Configuration

The fire sprinkler piping support elements include hangers, braces, and wire restrainers. Hangers supported the dead weight of the piping system (including water) through 10 mm (0.375in.) diameter rods. The hangers were connected to the pipe through an adjustable band around the pipe. Braces resisted lateral and longitudinal sway through 25 mm (1.0in.) schedule 40 pipes oriented at 45-degree angles. Wire restrainers (also

known as splay wires) consisted of two 12 gauge wires, oriented at 45-degrees, to limit the displacement of branch lines. The braces and wire restrainers were connected to the concrete deck through 10 mm (0.375in.) Hilti KB-TZ expansion anchors. In this study, two types of tee (T) and L shape threaded joint assemblies were used. The continuous configurations consisted of 13 tee joints and seven angle joints while the separate configurations included 20 tee and four angle joints (Figure 4). The last set of design variables included drop length, hose type, and gap between the sprinkler head and ceiling tile that were varied through seven different drop configurations. The drop length (Figure 6a) was either 305mm (12in.), 559mm (22in.), or it varied in a way that the sprinkler head elevation was above the ceiling elevation (see the drop on the right in Figure 6b). Although the ceiling elevation remained the same for both floors (0.91m (3.0ft.)), the drop length was varied to account for the different pipe segment elevations in the separate configurations. The hose type was either rigid or flexible, as presented in Figure 6b. The gap between the sprinkler head and ceiling tile (Figure 6c-d) was either 50mm (2.0in.) or there was no gap. It should be noted that the piping assemblies were not altered in between ground motions; however, the damaged parts were replaced at the end of each test. Moreover, all new design variables were installed when transferring from continuous to separate configurations.

The governing boundary condition for the fire sprinkler piping system was the different size gaps between sprinkler heads and ceiling tiles. Additional boundary conditions include the gaps between the riser pipes extending through the floors/ceiling tiles and the gap between the ends of the piping systems and partition walls. In this study,

these gaps were sized in a way that minimized the interaction between the riser pipes and ceiling tiles.

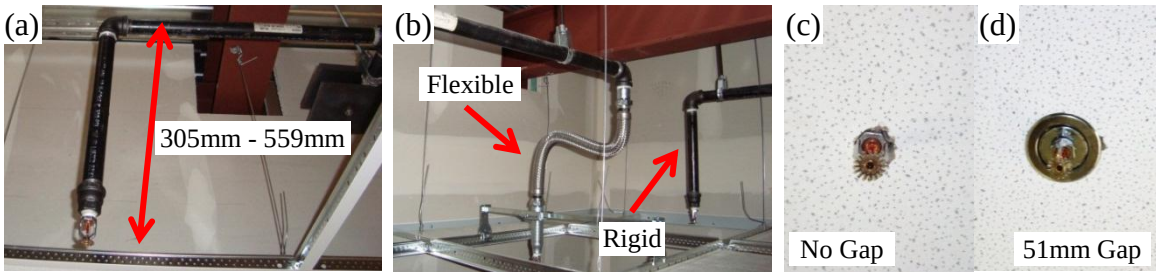

Figure 6. Examples of Drop Design Variables: (a) drop length, (b) hose type, (c-d) gap between sprinkler head and ceiling tile

Instrumentation

Nearly 400 sensor channels with a sampling frequency of 256 Hz were used to monitor the responses of structural and nonstructural components. All recorded responses used a 4-pole low-pass Butterworth filter with a cutoff frequency of 50 Hz [Soroushian et al., 2014c]. The responses of structural components were monitored by a combination of accelerometers and string potentiometers which were placed at column locations and the middle of floor slabs (Figure 7).

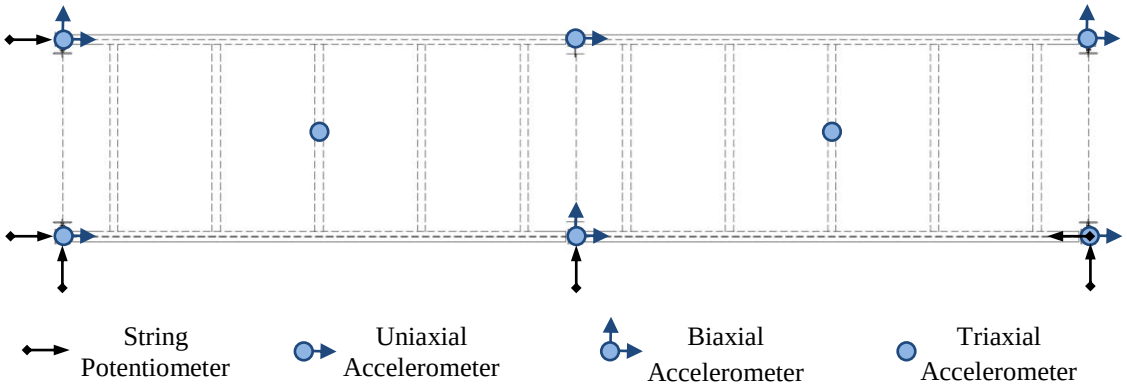

Figure 7. Typical Structural Instrument Location [Figure courtesy of Jenkins et al., 2015a]

The piping system response was measured by string potentiometers, displacement transducers, accelerometers, and load cells. The locations of these instruments for the two piping configurations are shown in Figure 8. String potentiometers extended from structural members to the ends of pipe segments in order to measure pipe displacements (Figure 9a), while displacement transducers were used to measure the rotation of joints (Figure 9b). Accelerometers, located on various pipe segments including main pipe runs, branch lines, and sprinkler heads (Figure 9c), captured accelerations experienced by different pipe segments. Load cells (Figure 9d) were used to record the axial force in hangers and wire restrainers.

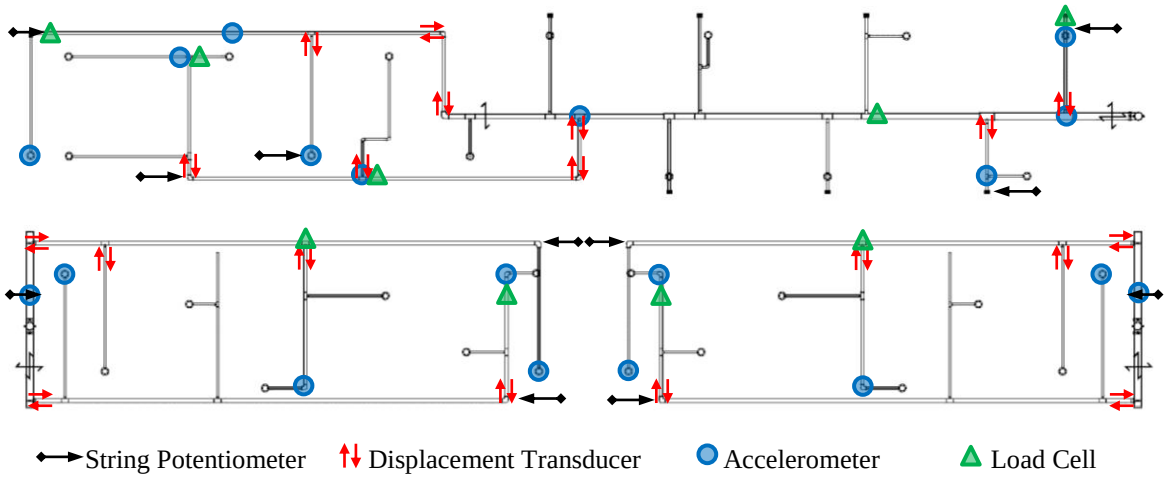

Figure 8. Typical Piping Instrument Location

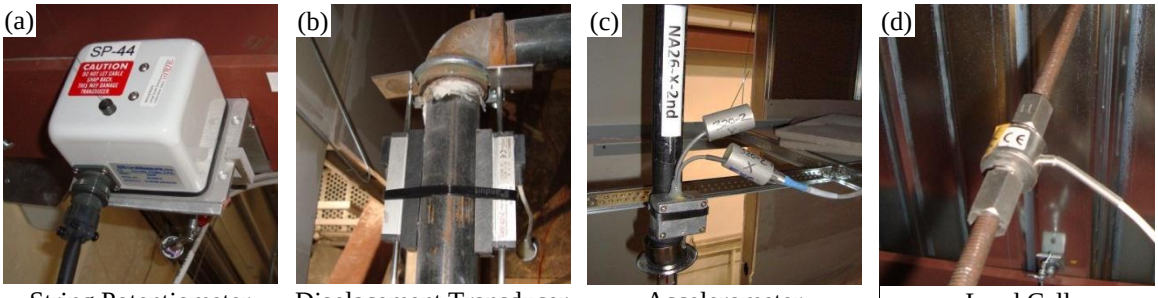

String Potentiometer | Displacement Transducer | Accelerometer | Load Cell

Figure 9. Example Pictures of Piping Instrumentation

LOADING PROTOCOL

The test-bed structure was subjected to a number of uniaxial shake table (ground) motions that were artificially generated by using a spectrum-matching procedure. Parameters from the AC 156 [ICC, 2010] including, a story height ratio (z/h) of 0.5 and the design spectral response acceleration at short periods (S_{DS}) of 2.5g, were used to develop two targeted acceleration spectra. The first target spectrum was designed at the shake table level while the second was designed at the second floor level by using algorithms defined by Soroushian et al. [2011].

The linear structure was subjected to 42 ground motions and the nonlinear structure was subjected to 17 ground motions [Soroushian et al., 2014c]. The 42 motions for the linear structure consisted of two motion types named "Unmodified Linear" (12 out of 42) and "Modified Linear" (30 out of 42). The Unmodified and Modified Linear motions were set to represent the target spectrum at the shake table and second floor levels, respectively. During the linear portion of testing, motion durations were 30 sec. The remaining 17 ground motions applied to the nonlinear structure were named "Nonlinear". During this portion of testing, the shake tables were set to represent the target spectrum at the table level. In addition, the motion durations were reduced to 10 sec. due to the limitation on the ductility capacity of the bracing systems. Figure 10 shows the comparison of 5% damped spectra achieved on the shake table and the second floor during 50% of full scale motions (50% IM) [Soroushian et al., 2014c]. The summary of peak floor accelerations and inter-story drift ratios for the three motions are presented in Table 2 [Jenkins et al., 2015a].

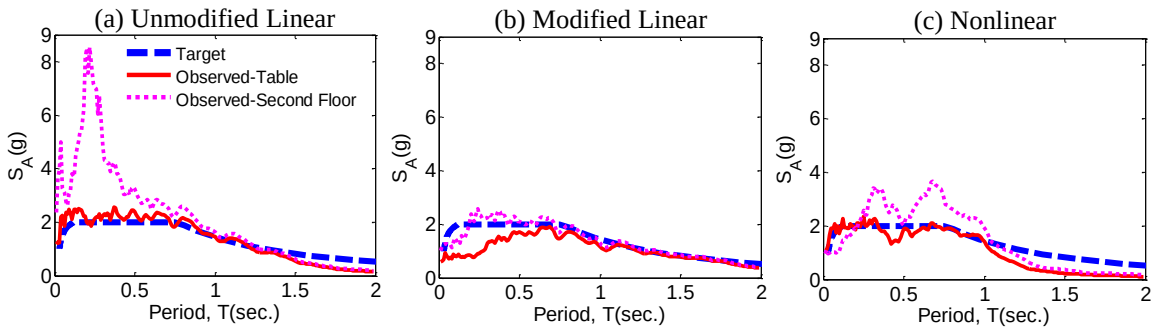

Figure 10. Comparison between Achieved and Target 50% IM Spectrum
[Graphs courtesy of Soroushian et al., 2014c]

This study encompassed eight tests in which five were linear, named "Linear-1" through "Linear-6" (example L-1), and three were nonlinear, named "Nonlinear-1" through "Nonlinear-3" (example NL-1). It should be mentioned that test Linear-4 was removed from testing to ensure a timely project completion. The remaining tests were not updated in terms of nomenclature due to a pre-assignment of scheduling and documentation.

Table 2. Test-bed Responses during Linear and Nonlinear Configurations
[Table courtesy of Jenkins et al., 2015a]

Floor	Maximum Peak Floor Acceleration (g)			Maximum Story Drift Ratio (%)		
	Unmodified Linear	Modified Linear	Nonlinear	Unmodified Linear	Modified Linear	Nonlinear
First	1.59	1.16	1.22	0.75	0.66	2.79
Second	2.47	1.65	1.41	0.27	0.18	2.09

DAMAGE OBSERVATION

The seismic performance of the fire sprinkler piping system can be evaluated through the damage observed during testing. Damage after every motion was recorded using detailed inspection sheets, pictures, and videos. It should be mentioned that minimal damage to the piping system was observed throughout the experiments. Investigators believe possible factors resulting in minimal damage could include (but not limited to): inadequate floor accelerations, uniaxial ground motions, insufficient length of

pipe segments, material properties, or distance between bracing. However, the damage that was observed is summarized into two categories, support system damage and sprinkler head/drop damage, as presented in Table 3. Examples of damage to hangers include: slipping (Figure 11a) or drifting of the adjustable band around the pipe, bending or deforming of the hanger (Figure 11b), and bending of the hanger near anchor locations. Figure 11c shows complete failure of a wire restrainer connection. Longitudinal and lateral sway braces encountered damage such as complete failure of bracing clips (Figure 11d). In addition to support systems, damage was observed near sprinkler heads or at drop locations. A common damage was the tearing of ceiling tiles due to the interaction with the sprinkler heads (Figure 11e). The last (minor) damage was the falling or dislodging (Figure 11f) of sprinkler rings.

One focus of this study was to evaluate the performance of integrated ceiling-piping-partition systems. As described above, the interaction between ceiling and piping systems led to a tearing damage within the ceiling tile. However, there was no direct interaction between the piping systems and the partition walls.

Table 3. Tabulated Examples of Damage Observed

Support System	**Description**
Hanger	Band slip/drift along pipe, bend or deform, surge clip rupture, damage to deck anchor location
Wire Restrainer	Permanent deformation or complete failure of connection
Brace	Complete rupture
Sprinkler Head/Drops	**Description**
Ceiling Tiles	Tearing of ceiling tiles due to interaction between sprinkler heads
Sprinkler Ring	Loose/fallen sprinkler ring

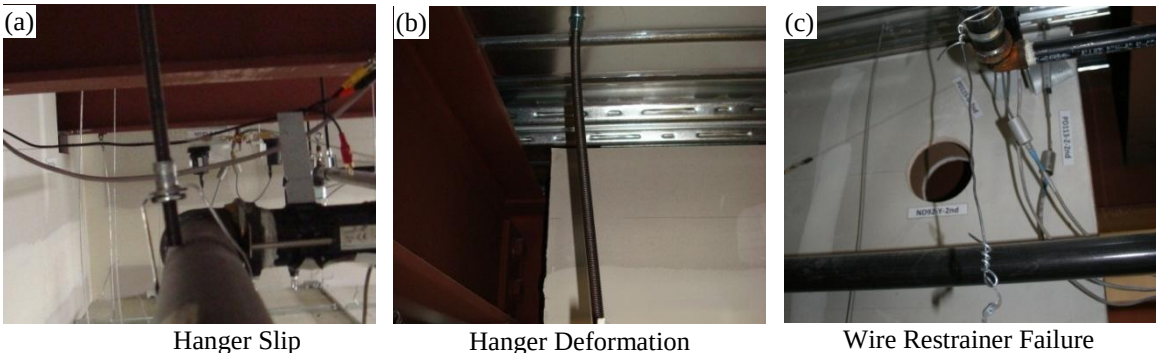

Figure 11. Examples of Observed Damage

EXPERIMENTAL RESULTS

Acceleration Amplifications

The fire sprinkler piping acceleration amplification (a_p) factors were calculated by normalizing the peak piping system acceleration by the peak floor acceleration in which it was supported. This process was applied to the two piping configurations and three pipe segments, as shown in Table 4. The amplifications were compared through the statistical parameters: maximum, minimum, and median. The amplifications have a consistent increasing trend from the main pipe runs to the sprinkler heads. When combining both the continuous and separate configuration (labeled "All" in Table 4), the median values for the main pipe run, branch line/armover, and sprinkler heads are 2.7, 3.5, and 6.1, respectively. The amplification for the main pipe run (a_p = 2.7) is comparable to the ASCE 7-10 [2010] amplification suggestion of 2.5 for flexible

components. However, the branch line/armover and sprinkler head pipe segments have an increased amplification due to the acceleration of the main pipe run acting as an input excitation [Soroushian et al., 2014a]. Therefore, the ASCE 7-10 [2010] value underestimates the amplifications for branch line/armover and sprinkler head pipe segments.

Table 4. Acceleration Amplification Factors

		Continuous	
a_p	**Main Pipe Run**	**Branch Line/Armover**	**Sprinkler Head**
Min	1.2	1.3	1.7
Max	7.7	8.8	32.5
Median	2.5	2.7	5.8
		Separate	
a_p	**Main Pipe Run**	**Branch Line/Armover**	**Sprinkler Head**
Min	1.3	2.4	2.5
Max	9.4	14.0	19.0
Median	3.1	5.5	6.5
		All	
a_p	**Main Pipe Run**	**Branch Line/Armover**	**Sprinkler Head**
Min	1.2	1.3	1.7
Max	9.4	14.0	32.5
Median	2.7	3.5	6.1

Seismic Fragility Analysis

Experimental results were used to develop fragility functions for the fire sprinkler piping system. A fragility function is a conditional statement that relates the probability of an engineering demand parameter (EDP) exceeding the capacity (C) of a component, dependent on a limit state (LS), when subjected to an intensity measure (IM) [after Soroushian et al., 2014d]. In this study, three EDP's were considered: pipe joint rotation, support axial force, and displacement of the piping system. The capacities and associated LS's for each EDP were established based on seismic performance measures including required repair actions. Peak floor acceleration (PFA) was considered as the IM due to the acceleration sensitive nature of fire sprinkler piping systems.

Methodology

The methodology employed for the experimental fragility analysis is outlined by Nielson and DesRoches [2007]. (1 is the cumulative normal distribution function that relates the parameters: EDP, C, and IM.

$$P(EDP \geq C|IM) = \Phi\left(\frac{\ln\left(\frac{S_d}{S_c}\right)}{\sqrt{\beta_{d|IM}{}^2 + \beta_c{}^2}}\right) \quad (1)$$

where S_d is the median of the demand estimate as a function of IM, $\beta_{d|IM}$ is the logarithmic standard deviation of the demand with respect to the IM, S_c is the median estimate of the capacity, β_c is the logarithmic standard deviation of component capacities, and $\Phi[\cdot]$ is the normal cumulative distribution.

Due to a limited amount of damage observed during testing, the demand parameters (S_d and $\beta_{d|IM}$) were determined using a power-law regression analysis and a single value for dispersion. It should be noted that this process is not the only method to represent the seismic demand as a function of IM [Ramanathan, 2012], however, it is often used. Equations (2 and (3 [Cornell et al., 2002] were used to calculate the demand parameters, median and dispersion, respectively.

$$S_d = aIM^b \quad (2)$$

$$\beta_{d|IM} \cong \sqrt{\frac{\sum_{i=1}^{N}[\ln(d_i) - \ln(aIM^b)]^2}{N-2}} \quad (3)$$

where d_i is the peak demand corresponding to the i^{th} floor motion, out of the total N motions. It should be mentioned that the capacities and associated LS's are dependent on the EDP and therefore, described in their respected sections below.

Pipe Joint Rotation

The first EDP to be considered in this study was the rotation of fire sprinkler pipe joints. Instrumented pipe joints were categorized by pipe diameter: 25, 32, 40, and 50 mm (1.0, 1.25, 1.5 and 2.0in.). Then, pipe joint rotations were calculated using (4 shown below.

$$\theta = \frac{2\bar{d}}{e_1 + e_2 + d_o} \tag{4}$$

where $\bar{d}$ is the average measurement of the two displacement transducers, e is the eccentricity from the center line of the instruments to the outside diameter of the pipe, and d_o is the outside pipe diameter. A visual representation of the joint rotation parameters is presented in Figure 12. Median pipe joint rotations for the various pipe diameters ranged from 0.001 to 0.013 rad.

There were no occurrences of pipe leakage throughout the duration of tests conducted in this study. The lack of leakage can be confirmed by comparing the maximum rotation demands observed during the experiments with the leakage rotation capacities defined in the works by the State University of New York at Buffalo (UB) and Soroushian et al. [2013] (see Figure 13). The 50 mm (2.0in.) diameter pipe was the only diameter in which the maximum rotation demand almost met the leakage capacity threshold. Due to a minimal amount of observed damage, the demand parameters were determined by the power-law regression analysis (example shown in Figure 14). Joint rotations were compared with the corresponding PFA's for each of the ground motions and then fitted with a regression line to acquire the regression parameters *a* and *b* (see Table 5).

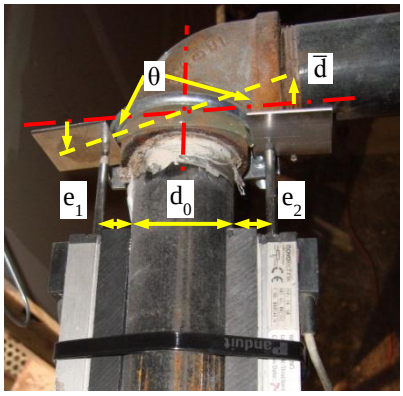

Figure 12. Joint Rotation Parameters

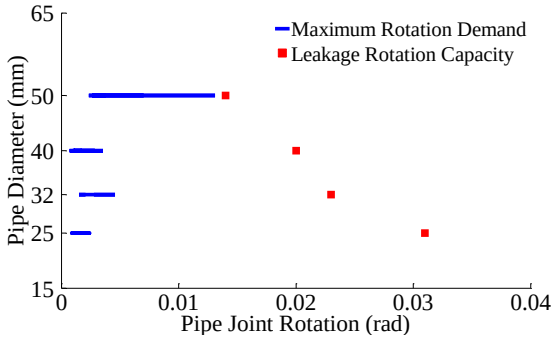

Figure 13. Rotation Demand vs Leakage Capacity

Three limit (damage) states, defined by Soroushian et al. [2013], for fire sprinkler pipe components were used in this study (Figure 15). The first is named "Slight" and is assumed to be the start of nonlinear behavior within the joint. The second, named "Moderate", includes dripping or spraying of the threaded joints. The last limit state, named "Extensive", corresponds to the first significant leakage of the joint. In addition to limit states, Soroushian et al. [2013] produced capacity parameters (median and dispersion) for each limit state based on analytical studies (Table 5). It should be noted that this study borrowed the capacity parameters produced by Soroushian et al. [2013] because specimen capacities were not exceeded in the experiments.

The pipe joint fragility curves (Figure 16) were developed using (1 and the demand and capacity parameters presented in Table 5. It is also noted that pipes with 50 mm (2.0in.) diameters have a higher probability of failure than any other pipe diameter for the three limit states. The experimental fragility parameters, median and dispersion, are compared against the fragility parameters suggested by Soroushian et al. [2013] in Table 6. Results show that the experimental median values occur at a higher PFA

compared to the analytical suggestion (excluding 50mm (2.0in.) diameter pipe). However, this effect may be due to the geometry limitation during this experiment.

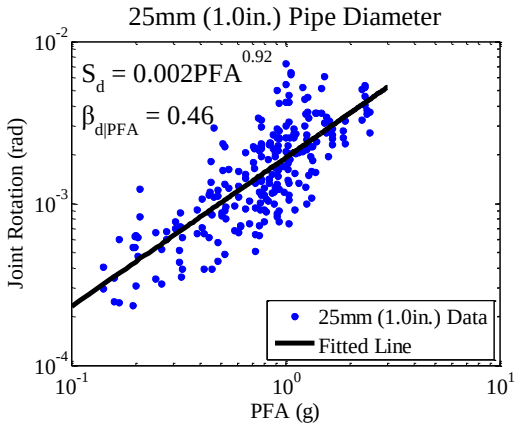

Figure 14. Example of Regression

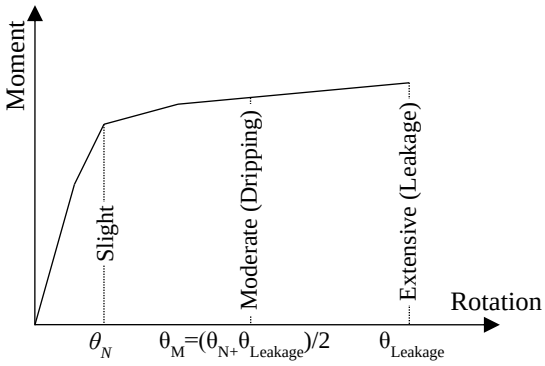

Figure 15. Pipe Joint Limit States [Graph courtesy of Soroushian et al., 2013]

Table 5. Pipe Joint Rotation Demand and Capacity Parameters

Pipe Diameter	Demand Parameters			Capacity Parameters [Soroushian et al., 2013]			
	Median, S_d (rad.)		Dispersion	Median, S_c (rad.)			Dispersion
	Regression Parameters		$\beta_{d\|PFA}$	Slight	Moderate	Extensive	β_c
25 mm (1.0in.)	a	0.002	0.457	0.005	0.018	0.031	0.146
	b	0.917					
32 mm (1.25in.)	a	0.003	0.730	0.005	0.014	0.023	0.133
	b	1.160					
40 mm (1.50in.)	a	0.002	0.564	0.005	0.013	0.020	0.120
	b	0.881					
50 mm (2.0in.)	a	0.007	0.813	0.005	0.009	0.014	0.094
	b	1.276					

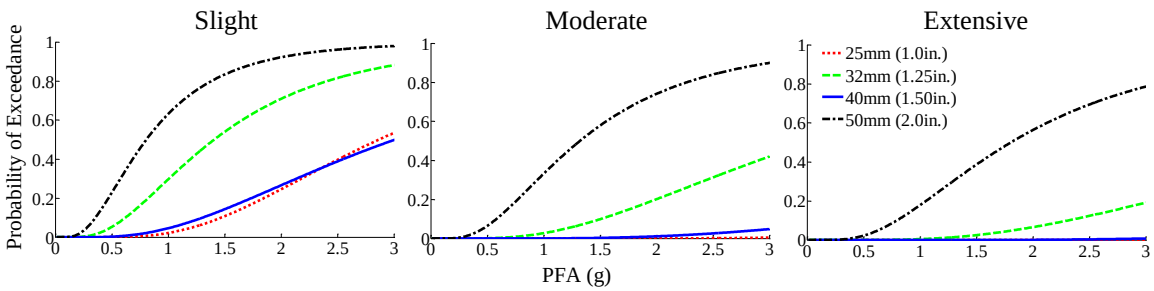

Figure 16. Pipe Joint Fragility Curves

Table 6. Comparison of Experimental and Analytical Fragility Parameters

Pipe Diameter	Experimental				Analytical [Soroushian et al., 2013]			
	Slight	Moderate	Extensive		Slight	Moderate	Extensive	
		x_m		β		x_m		β
25 mm (1.0in.)	2.86	N/A	N/A	0.48	0.68	1.57	2.23	0.55
32 mm (1.25in.)	1.41	3.41	N/A	0.74	0.57	1.17	1.67	0.56
40 mm (1.5in.)	3.01	N/A	N/A	0.58	0.61	1.15	1.59	0.61
50 mm (2.0in.)	0.81	1.32	1.80	0.82	0.99	1.44	1.94	0.67

Support Axial Force

The second set of fragilities developed from experimental results is based on the axial force within support elements, hangers and wire restrainers. The two support elements were categorized by the pipe diameter in which they supported. In this study, hangers supported 25, 32, 40, 50, and 80 mm (1.0, 1.25, 1.50, 2.0, and 3.0in.) diameter pipes while wire restrainers only supported 40 mm (1.50in.) diameter pipes. The axial forces in hangers and wire restrainers were measured by load cells. The total axial load, measured in the load cells, include the dead weight of the piping system (filled with water) plus the applied force caused from earthquake excitations. The maximum measured axial loads for hangers and wire restrainers were 5.6 kN (1.26Kips) and 1.5 kN (0.34Kips), respectively.

Similar to the previously defined methodology, the demand parameters were determined using the regression analysis (Eqs. (2 and (3). Figure 17 presents an example

of the regression parameters for hangers and wire restrainers that supported 40 mm (1.50in.) diameter pipes. The capacity requirements for the hanger and wire restrainer components were taken from the NFPA 13 [2011] and USG [2010], respectively. Hangers shall be designed to carry five times the dead load of the pipe (filled with water) plus an additional 1.11 kN (250lbs.). Wire restrainers shall be designed to carry 1.78 kN (400lbs.). The median capacity calculations for hangers and wire restrainers are shown by Eqs. (5 and (6, respectively. The dispersion capacity parameter, $\beta_{c,}$ was defined as 0.4 as suggested from ATC-58 [2013] as a typical value for nonstructural systems. The demand and capacity parameters for support axial forces are presented in Table 7.

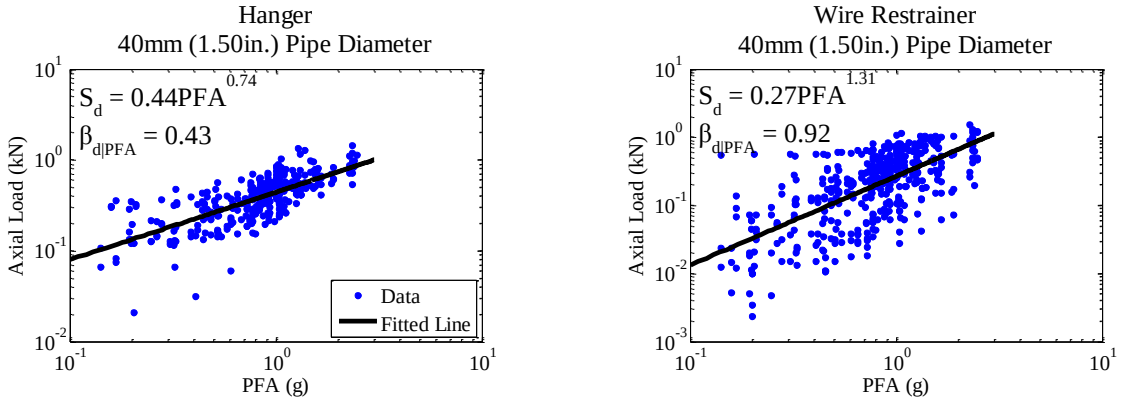

Figure 17. Example Regression Parameters for Hangers and Wire Restrainers

$$S_c(\text{Hanger}) = 5 * \left(x_{m(DL)}\right) + 1.11\text{kN} \quad (5)$$

$$S_c(\text{Wire Restrainer}) = 1.78\text{kN} \quad (6)$$

where $x_{m(DL)}$ is the median dead load of the pipe on the hanger support element.

Figure 18 shows a comparison between the capacity limits suggested by NFPA 13 [2011] and USG [2010] and the demands (total axial load) for hangers and wire restrainers categorized by the pipe diameter in which they supported. The demand exceeded the capacity limit in a hanger supporting a 80 mm (3.0in.) diameter pipe,

however, there were no observed occurrences of complete hanger failure. The damage observed includes deformation of hangers and damage to the anchor location attached to the deck. The support axial force fragility curves, produced using (1, are presented in Figure 19 and Table 8. As shown, a hanger supporting 80 mm (3.0in.) diameter pipes has the highest probability of exceedance compared to other supported diameter pipes.

Table 7. Support Axial Force Demand and Capacity Parameters

	Demand Parameters			Capacity Parameters		
Pipe Diameter	**Variable**	**Hanger**	**Wire Restrainer**	**Variable**	**Hanger**	**Wire Restrainer**
25.0 mm (1.0in.)	a	1.064		$x_{m(DL)}$	0.463	
	b	0.462		S_c	3.428	
	$\beta_{d\|PFA}$	0.181		β_c	0.400	
32.0 mm (1.25in.)	a	0.558		$x_{m(DL)}$	0.253	
	b	0.541		S_c	2.379	
	$\beta_{d\|PFA}$	0.279		β_c	0.400	
40.0 mm (1.5in.)	a	0.441	0.267	$x_{m(DL)}$	0.113	0.007
	b	0.743	1.306	S_c	1.675	1.779
	$\beta_{d\|PFA}$	0.427	0.923	β_c	0.400	0.400
50.0 mm (2.0in.)	a	0.962		$x_{m(DL)}$	0.270	
	b	0.677		S_c	2.463	
	$\beta_{d\|PFA}$	0.275		β_c	0.400	
80.0 mm (3.0in.)	a	1.627		$x_{m(DL)}$	0.246	
	b	1.169		S_c	2.339	
	$\beta_{d\|PFA}$	0.458		β_c	0.400	

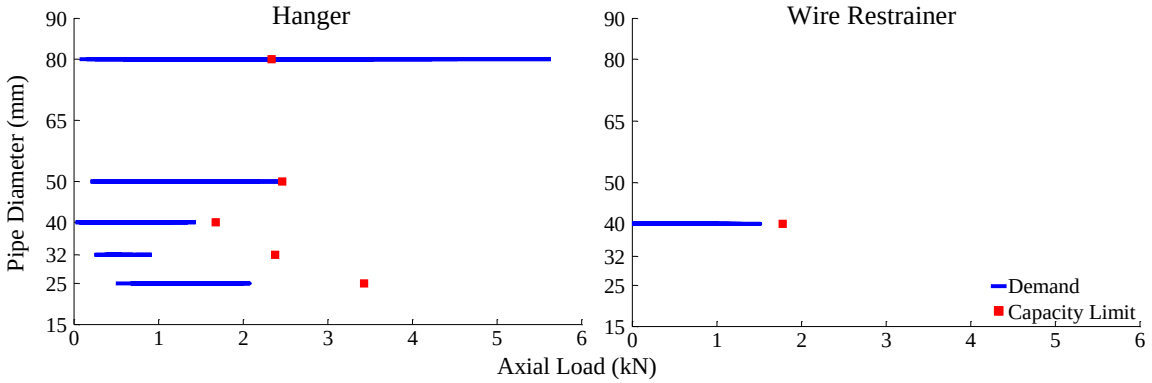

Figure 18. Comparison of Demand and Capacity Limit for Support Elements

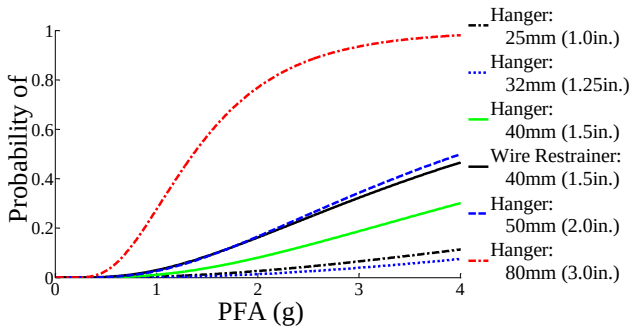

Figure 19. Support Axial Force Fragility Curves

Table 8. Support Axial Force Fragility Parameters

Pipe Diameter	Experimental	
	x_m	β
Hanger		
25.0 mm (1.0in.)	N/A	N/A
32.0 mm (1.25in.)	N/A	N/A
40.0 mm (1.5in.)	N/A	N/A
50.0 mm (2.0in.)	4.01	0.49
80.0 mm (3.0in.)	1.36	0.61
Wire Restrainer		
40.0 mm (1.5in.)	4.28	1.01

Pipe Displacement

The last set of fragility functions developed from the experimental results was the fire sprinkler piping displacement fragilities. The displacement was chosen as an EDP because earthquakes can induce large movements within the piping systems resulting in collisions with adjacent objects such as the stationary frame, walls, or ceiling components [Soroushian et al., 2014d]. String potentiometers were used to capture displacements at critical locations of the pipe assembly (corners of the perimeter, or boundary, pipes) relative to the test-bed structure. Typical measured displacements ranged from 0.92 mm (0.04in.) to 176.8mm (6.96in.). The instrumented pipe segments were categorized into "Large" and "Small" diameter pipes. Large diameter pipes are greater or equal to 50 mm (2.0in.) while small diameter pipes are less than 50 mm (2.0in.). The same regression analysis methodology was used to calculate the demand parameters, median (Eq. (2) and dispersion (Eq. (3). Figure 20 shows the regression analysis parameters for the large and small diameter pipes. The data shown in the large diameter pipe plot has two groups of

data points due to the displacement restriction caused by wire restrainer orientation near some of the string potentiometers.

The capacity parameters for large and small diameter pipes were based on distances between the pipe and adjacent objects, also known as clearance, given by NPFA 13 [2011]. Using the defined clearances from NPFA 13 [2011], Soroushian et al. [2014d] developed four limit states (LS) for each of the pipe diameter categories. Limit states for the large diameter pipe segments include the following clearances: 15, 25, 50, and 80 mm (0.5, 1.0, 2.0, and 3.0in.) while the small diameter pipe segments use clearances of 25, 50, 125, and 200 mm (1.0, 2.0, 5.0, and 8.0in.). Both of these pipe diameter categories involve lower and upper limits that represent a minimum and extreme gap scenario that the pipe segments may encounter. The dispersion, β_c, was set to a constant value of 0.4 which is a typical value for nonstructural systems [ATC-58, 2013].

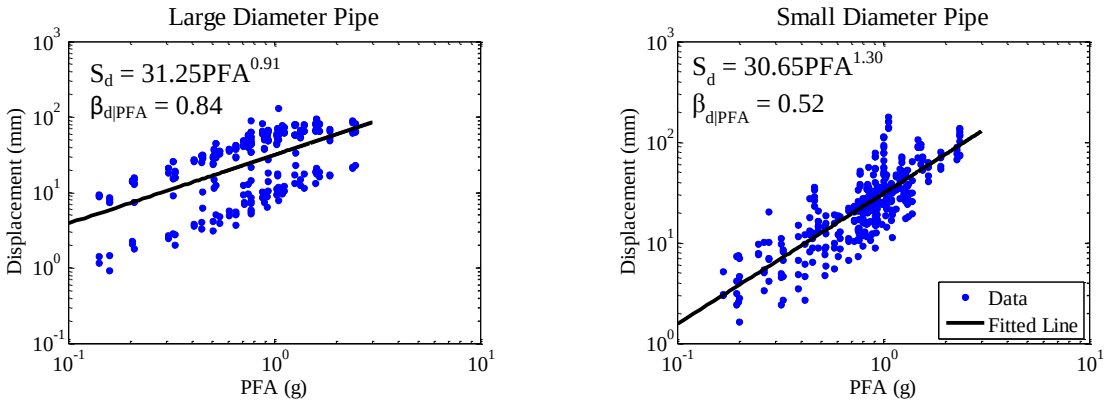

Figure 20. Regression Fitting for Large and Small Diameter Pipes

The demand and capacity parameters were then used in Eq. (1 to calculate the displacement fragilities as presented in Figure 21. The experimental fragility parameters are compared with a combination of analytical and experimental values (Table 9) produced by Soroushian et al. [2014d]. Results show that the experimental median values

are higher than the analytical/experimental for the large and small pipe diameter categories. Experimental fragility parameters from the three EDP's considered show that pipe displacement is the governing EDP and has the greatest probability of failure compared to pipe joint rotation and support axial force. This effect was determined by comparing the minimum median fragility parameters for pipe joint rotation, support axial force, and pipe displacement which are 0.81, 1.36, and 0.37, respectively.

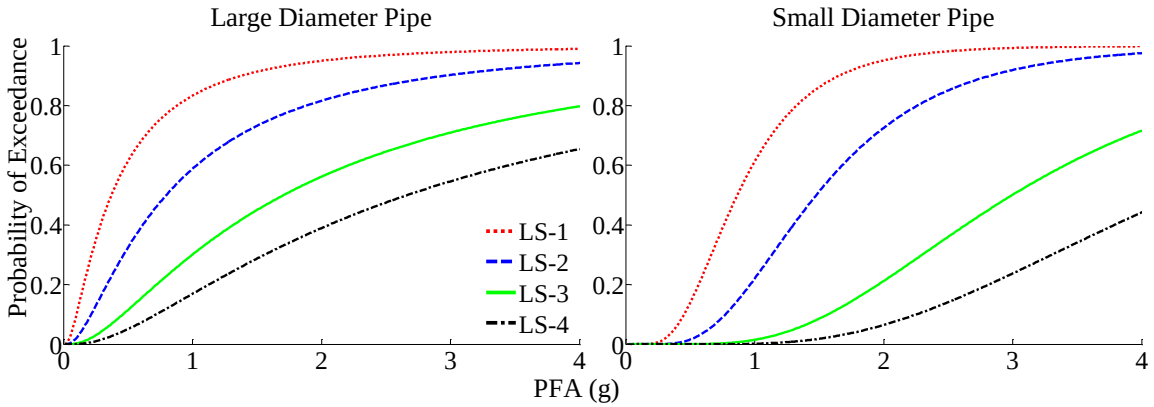

Figure 21. Displacement Fragilities for Large and Small Diameter Pipes

Table 9. Comparison of Displacement Fragility Parameters

LS	Experimental				Analytical/Experimental [Soroushian et al., 2014d]			
	Large Diameter Pipe		Small Diameter Pipe		Large Diameter Pipe		Small Diameter Pipe	
	x_m	β	x_m	β	x_m	β	x_m	β
1	0.37	0.93	0.86	0.66	0.29	0.52	0.24	0.51
2	0.80		1.48		0.50		0.43	
3	1.71		3.00		0.86		0.91	
4	2.66		4.31		1.18		1.34	

SUMMARY

The study conducted at the University of Nevada, Reno NEES site aimed to investigate the seismic performance of nonstructural components through full-scale system-level experiments. The nonstructural components were housed in a two-story, two-by-one bay steel braced-frame structure that spanned over three biaxial shake tables.

As part of the integrated ceiling-piping-partition systems, the performance of a pressurized fire sprinkler piping system was evaluated through several design variables. Experimental results led to the computation of acceleration amplification factors for three pipe segment types: main pipe run, branch line/armover, and sprinkler heads. Experimental results also led to the development of fragility curves for pipe joint rotation, support axial force, and pipe displacement. The major findings are summarized as follows:

- Acceleration amplification factors show an increasing trend (2.7, 3.5 and 6.1) from the main pipe run to branch lines/armovers to the sprinkler heads.
- The main pipe run amplification (2.7) is comparable to the ASCE 7-10 [2010] recommended amplification value for flexible components (a_p = 2.5).
- The ASCE 7-10 [2010] value underestimates the amplifications for branch line/armover and sprinkler head pipe segments.
- Pipe joint rotation fragilities show that 50 mm (2.0in.) diameter pipes have the greatest probability of failure compared to other diameter pipes.
- Support axial force fragilities depict that hangers supporting 80 mm (3.0in.) diameter pipes exceed the suggested capacity value given by NFPA 13 [2011].
- Pipe segments that are 80 mm (3.0in.) in diameter have the highest vulnerability of hanger or wire restrainer failure compared to other supported pipe diameters.

- Pipe displacement fragilities indicate that pipe segments with large diameters have greater displacements and probability of failure compared to small pipe diameters.
- Pipe displacement is the governing fragility function compared to pipe joint rotation and support axial force.

ACKNOWLEDGEMENTS

This material is based upon work supported by the National Science Foundation under Grant No. 0721399. This Grand Challenge (GC) project to study the seismic response of nonstructural systems is under the direction of M. Maragakis from the University of Nevada, Reno and Co-PIs: T. Hutchinson, A. Filiatrault, S. French, and B. Reitherman. Any opinions, findings, conclusions or recommendations expressed in this document are those of the investigators and do not necessarily reflect the views of the sponsors.

4. PARTITION WALL SYSTEMS

It should be noted that the following section is from a paper submitted to the *Thin-Walled Structures* journal (Jenkins et. al, 2015b).

Experimental Fragility Analysis of Cold-Formed Steel-Framed Partition Wall Systems

Craig Jenkins[a], Siavash Soroushian[b], Esmaeel Rahmanishamsi[c], and E. "Manos" Maragakis[d]

[a] Corresponding Author, Graduate Student, Department of Civil and Environmental Engineering, University of Nevada, Reno, Reno, NV, 89557, email: cjenkins@unr.edu

[b] Structural Analyst, Advanced Technology and Research, Arup, San Francisco, CA, 94105, email: siavash.soroushian@arup.com

[c] Ph.D. Candidate, Department of Civil and Environmental Engineering, University of Nevada, Reno, Reno, NV, 89557, email: erahmanishamsi@unr.edu

[d] Professor, Dean of College of Engineering, University of Nevada, Reno, Reno, NV, 89557, email: maragaki@unr.edu

ABSTRACT

A series of full-scale system-level experiments using a two-story steel braced-frame structure was conducted at the University of Nevada, Reno Network for Earthquake Engineering Simulation site in order to better understand the seismic performance of integrated ceiling-piping-partition systems. In this study, responses and behaviors of cold-formed steel-framed partition wall systems were critically assessed through several design variables. Experimental results led to the calculation of out-of-plane acceleration amplification factors and the development of fragility functions.

Results show that the acceleration amplification factors for out-of-plane partition walls are comparable with the recommended amplification suggested by the code for flexible components.

KEYWORDS

Nonstructural Systems, Experimental Study, Fragility Analysis, Shake Table Simulation, Partition Wall System, Steel-Framed

1. Introduction

Structural and nonstructural components of critical facilities play key performance roles during an earthquake. However, failures of nonstructural components make up the majority of earthquake damage [FEMA E-74, 2012]. Nonstructural components, such as partition wall systems, are more susceptible to damage because the shake intensities that trigger damage in these systems are much lower than those for structural components [Taghavi and Miranda, 2003]. Partition walls are prone to several forms of damage such as cracking of gypsum boards, rocking of partial height partitions, and complete collapse of full/partial height partitions. Nearly all of these damage mechanisms were observed during past earthquakes including the 1994 Northridge earthquake [Reitherman and Sabol, 1995], the 2010 Darfield (Canterbury) earthquake [Dhakal, 2010], and the 2010 Chile earthquake [Miranda et al., 2012]. Several experimental studies were conducted to evaluate the performance of light-gauge steel-stud partition wall systems. Damage reported from these experiments included cracking of gypsum boards, bending of studs, out-of-plane damage of partition walls, popping out of studs from top tracks, gypsum screw connection damage, track-to-slab connection damage (or failure) and collapse of partition walls [Bersofsky, 2004; Retamales et al.,

2013; Soroushian et al., 2014a; Rahmanishamsi et al., 2015a; Rahmanishamsi et al., 2015b; Wang et al., 2015].These experiments provided valuable data that was employed to help understand the performance characteristics of component-level and system-level partition walls. However, there is still a demand for more informational data regarding seismic responses of partition walls.

In attempt to provide additional resources about the seismic performance of partition walls, a series of system-level tests were conducted at the University of Nevada, Reno as part of the Grand Challenge Project (NEESR-GC: Simulation of the Seismic Performance of Nonstructural Systems). This study investigated the response and failure mechanism of integrated ceiling-piping-partition systems installed in a full-scale, two-story steel braced-frame structure that spanned over three biaxial shake tables. Light-gauged steel-framed partition walls were evaluated through different design variables including: 1) framing systems, 2) partition wall heights, 3) partition wall geometries, 4) openings in partition walls, and 5) top connections. Experimental results were used to evaluate the performance of different top connections. In addition, out-of-plane acceleration amplification factors were computed and compared against the recommended amplification prescribed by ASCE 7-10 [2010]. Experiemental fragilities were developed based on damage caused by inter-story drift. In the following sections, a description of the test-bed structure and the partition wall variables is given. Then, the instrumentation and loading protocol are described followed by a summary of the observed damage. Next, the performance of top connections is evaluated. Acceleration amplification factor and experimental fragility curve results are also discussed. Finally,

ranges of inter-story drift ratios that represent certain levels of damage in partition walls observed from this study and past experimental studies are compared.

2. Experimental Setup

2.1. Test-bed Structure

A test-bed structure was designed in order to assess the seismic performance of acceleration and drift sensitive nonstructural systems. This full-scale, two-story, two-by-one bay steel braced-frame structure spanned over three biaxial shake tables at the University of Nevada, Reno Network for Earthquake Engineering Simulation (UNR-NEES) site. The overall dimensions were approximately 7.5m (24.5 ft.) high, 3.5m (11.5 ft.) wide, and 18.3m (60.0 ft.) long (Fig. 1).

Investigators were able to evaluate the response of acceleration and drift sensitive components by designing two test-bed configurations. While the primary elements of the structure (beams, columns, transverse bracing) were the same, the longitudinal brace properties and amount of additional attached floor masses were different. The first configuration, named "linear", used buckling restrained braces (BRB) with a high yield capacity, 283kN (64 kip), to achieve large floor accelerations. Additional attached floor masses were 30.7kN (6.9 kip) and 17.6kN (4 kip) for the first and second floors, respectively. The natural period for the linear configuration was found to be 0.20 sec. The second configuration, named "nonlinear", incorporated BRBs with a lower yielding capacity of 89kN (20 kip), to produce large inter-story drifts through the yielding of BRBs. The amount of additional mass was increased in this structure to 62.5kN (14 kip) for the first floor and 279.1kN (62.8 kip) for the second floor. The natural period for the nonlinear configuration was calculated as 0.34 sec. Fig. 2(a-b) shows the north and south

bays of the first floor while Fig. 2c shows the entire test-bed structure. Fig. 2(d-e) shows an example of a content room on the second floor.

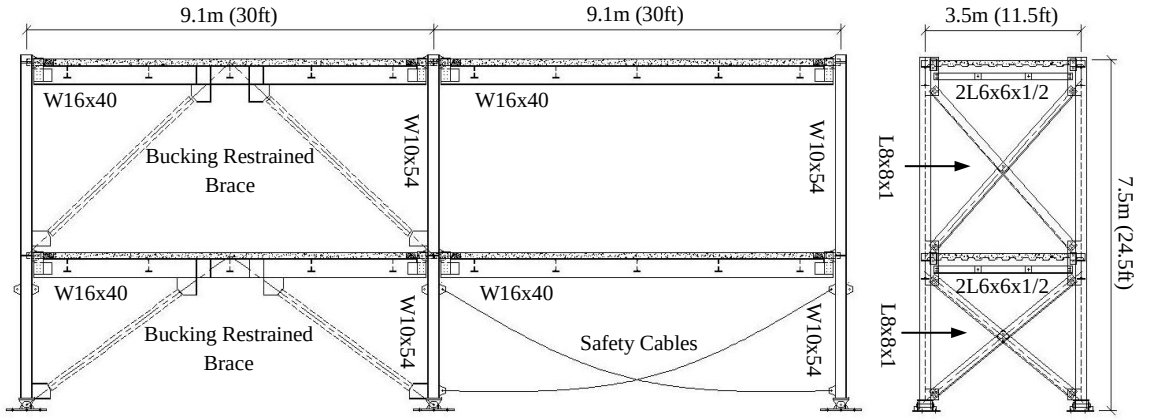

Fig. 1. Test-bed Structure: (left) longitudinal view, (right) transverse view

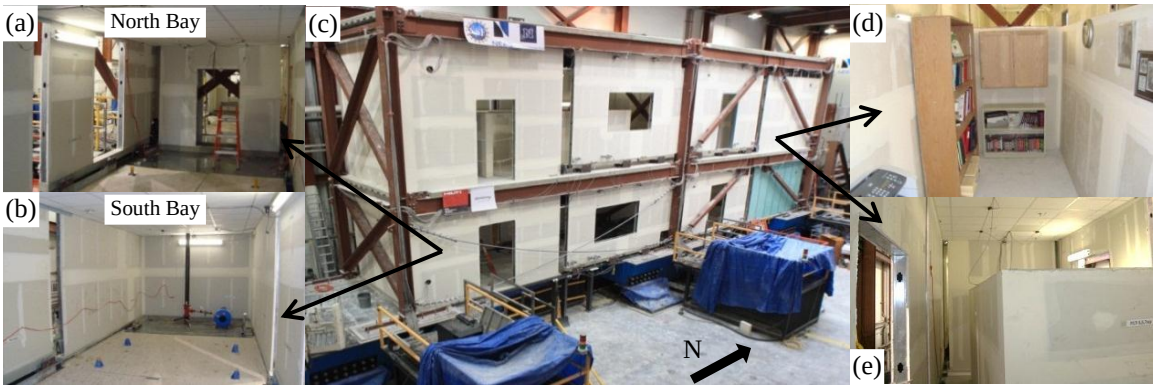

Fig. 2. Sample Test-bed Pictures: (a-b) north and south bay rooms, (c) full structure, (d) content room, (e) free standing partition walls formulating content room

2.2. Partition Wall Specimen

Over 100 light-gauged steel-framed partition walls were tested and evaluated during this study. Responses and behaviors were critically assessed through several design variables including: 1) framing systems, 2) partition wall heights, 3) partition wall geometries, 4) openings in partition walls, and 5) top connections. Table 1 tabulates the different partition variations and the partition wall layout is shown in Fig. 3. The nomenclature used is PX_i-X_j where P standings for partition, X_i is the specimen number,

and X_j is the floor location (F: first, S: second). For additional resources on partition walls, please refer to Rahmanishamsi et al. [2014].

Table 1. Partition Wall Configurations

Partition Label	Commercial/ Institutional Detail	Wall Height/Stud Height	Return Wall	Wall Shape Config.	Opening	Top Connection
P1-F	-	Full/Full	No	C	-	Shaft Wall1/Shaft Wall2
P2-F	Commercial	Full/Full	No	S	Door and Window	Full
P3-F	Institutional	Full/Full	No	C	Door	Sliding/Frictional
P4-F	Institutional	Full/Full	Yes	C	Window	Sliding/Frictional
P5-F	Institutional	Full/Full	No	C	-	Sliding/Frictional
P6-F	Institutional	Full/Full	No	S	-	Sliding/Frictional
P7-F	-	Full/Full	No	C	-	Shaft Wall1/Shaft Wall2
P8-F	-	Full/Full	Yes	C	-	Shaft Wall1/Shaft Wall2
P10-F	Commercial	Partial/Partial Braced	No	-	-	-
P11-F	Commercial	Partial/Partial Braced	No	-	Door	-
P1-S	Institutional	Partial/Full	No	L	-	Full
P2-S	Institutional	Full/Full	No	S	Door and Window	Slip Track
P3-S	Commercial	Full/Full	No	C	Door	Slip Track
P4-S	Institutional	Full/Full	Yes	C	Window	Slip Track
P5-S	Institutional	Full/Full	No	C	Door	Slip Track
P6-S	Institutional	Full/Full	No	S	-	Slip Track
P7-S	Institutional	Partial/Full	No	L	-	Slip Track
P8-S	Institutional	Partial/Full	Yes	L	-	Slip Track
P9-S	Institutional	Partial/Full	Yes	L	-	Full
P10-S	Institutional	Partial/Partial Braced	No	-	-	-
P11-S	Institutional	Partial/Partial Braced	No	-	Door	-
P12-S	Commercial	Partial/Partial Braced	No	-	-	-
P13-S	Commercial	Partial/Partial Braced	No	-	Door	-
P14-S	Commercial	Partial/Partial Braced	No	-	-	-
P15-S	Commercial	Partial/Partial Free	No	-	-	-
P16-S	Commercial	Partial/Partial Free	No	-	Door	-
P17-S	Commercial	Partial/Partial Free	No	-	-	-

Typical partition walls were constructed from steel framing systems (studs and tracks) and gypsum boards. The web and flange dimensions of the studs and tracks were

88.9mm (3.5 in.) and 31.8mm (1.25 in.), respectively, while the thickness was either 18mil (0.02 in.) or 30mil (0.03 in.). The naming designation, that will be used to describe stud and track properties herein, for a 18mil (0.02 in.) stud is 350S125-18. The gypsum board thickness was 15.5mm (5/8 in.). Thinner framing systems (350S125-18 studs and 350T125-18 tracks) and corner detailing, as shown in Fig. 4a, were considered as the commercial construction. Thicker studs (350S125-30) and tracks (350T125-30) along with a more robust corner connection represented the institutional construction. While #8 self-drill screws were used for stud-track connections, #6 self-drill screws were used for gypsum-stud and gypsum-track attachments. Also, shot pins (Hilti X-u27) were utilized for the track to concrete connections.

Full height partition walls considered in the test program consisted of full height studs paired with full or partial height gypsum boards. Partial height partition walls were either free standing or braced. Braced partial height walls utilized either 45 degree steel studs or two 45 degree steel wires (connecting the tops of partition walls to the above deck) as the bracing mechanism. Studs and gypsum boards stopped 152.4mm (6.0 in.) above the ceiling elevation for specimens that included steel studs as the bracing. In the specimen that involved wire bracing, the studs and gypsum walls stopped at the ceiling elevation. The south and north content rooms (shown in Fig. 3) were made from free standing and braced partial height partitions, respectively. Moreover, three types of wall shapes were considered in this study: 1) single walls (no return wall) named ‘S’, 2) one return (transverse) wall with one longitudinal wall named ‘L’, and 3) one return wall with two longitudinal walls named ‘C’. Besides shape variations, several doors and windows were built in partitions to investigate the effect of openings in partition walls.

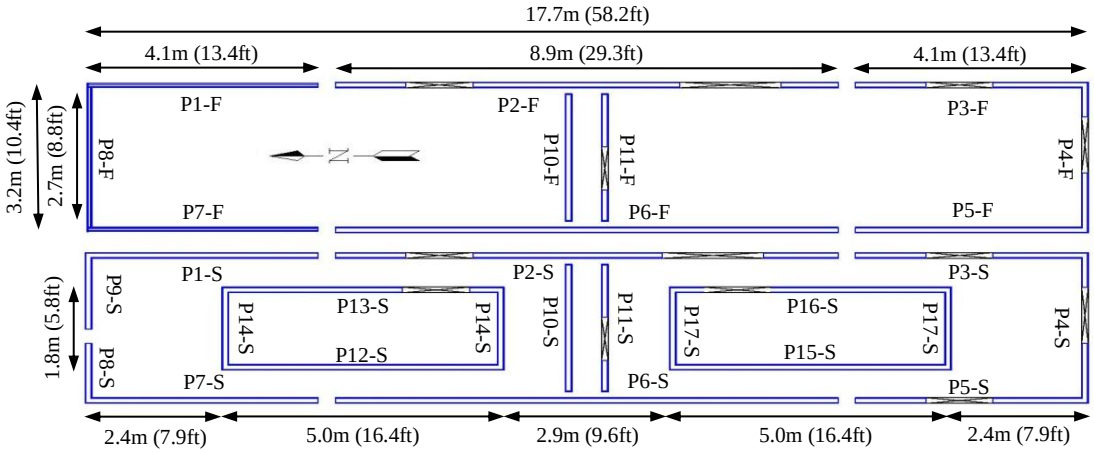

Fig. 3. Partition Wall Layout: (top) first floor, (bottom) second floor

The response of different partition connections was critically assessed during this experiment. The bottom connection of all partition walls were composed of track-to-deck attachments with shot pins, track-to-stud and gypsum-to-track connections using mentioned self-drilling screws. However, three types of detailing named slip track, full, and sliding/frictional were used for top connections. In the slip track connection detail, the track was only connected to the deck through Hilti X-u27 shot pins. The connection from track-to-stud was omitted to allow the studs to slide within the track. Similar to the slip track connection detail, the full connection detail used Hilti X-u27 shot pins to connect the track to the deck. However, a track-to-stud connection with self-drilling screws was included in the full connection detail (Fig. 4b). In the sliding/frictional connection (Fig. 4c) a thin 6mm by 25mm steel plate (0.25 by 1.0 in.) was attached to the concrete deck by shot pins (Hilti X-U32S15). The top track was then sandwiched between the plate and 19mm by 25mm (0.75 by 1.0 in.) rectangular tubing. It should be

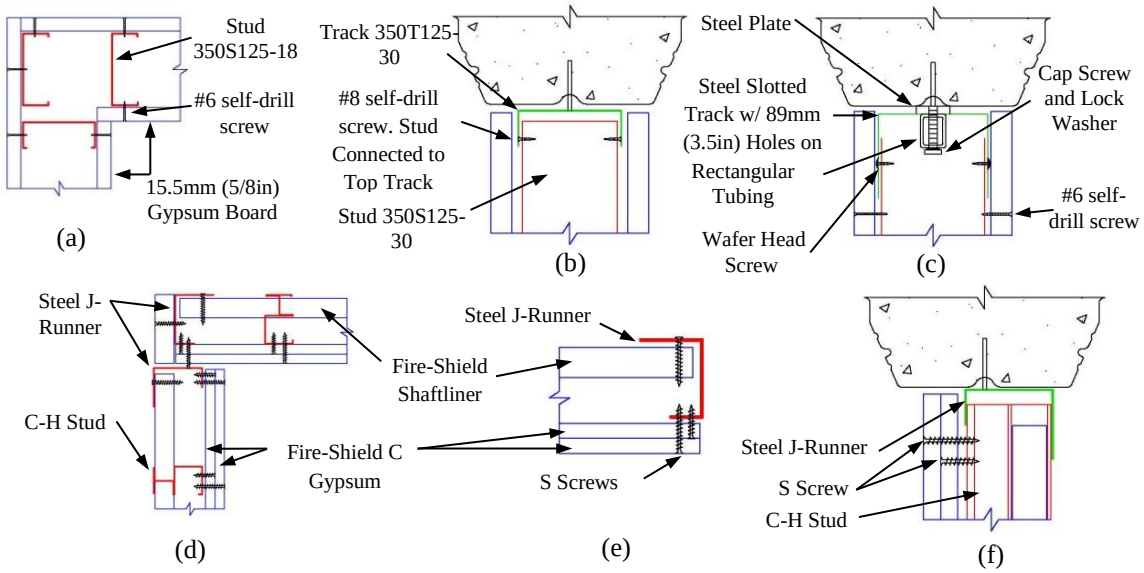

Fig. 4. Examples of Partition Wall Connections: (a) commercial corner, (b) full top connection, (c) sliding/frictional top connection, (d) shaft wall corner, (e) shaft wall end, and (f) shaft wall 1 top connection

mentioned that pre-drilled holes with diameters equal to the track width (88.9mm (3.5 in.)) allowed for the tubing to be connected to the steel plate without connecting the track. The studs were connected to the 18 gage slotted track using the 12.7mm (0.5 in.) wafer head screws. Additional information about the details and performance of the sliding/frictional connection can be found in Araya-Letelier and Miranda [2012].

In addition to the described partition walls, the performance of shaft walls was also evaluated during the test program. These walls were constructed from one layer of 25.4mm (1.0 in.) thick Fire-Shield Shaftliner board on one side and two layers of 12.7mm (0.5 in.) Fire-Shield C gypsum boards on the other. The gypsum boards were attached to 50.8-12.7mm (2-0.5 in.) steel C-H studs by S (drywall) screws (Fig. 4d-e). The top and bottom track was connected to their corresponding deck by shot pins. While their bottom attachment was similar to the previously discussed partition walls (Hilti X-u27 shot pins), two types of details were used for their top connection. During all the linear and the first

nonlinear tests, neither the studs nor gypsum boards were connected to the top track (named “Shaft Wall 1”), shown in Fig. 4f. During the remaining tests, the studs and gypsum boards were connected to the top track via #8 and #6 self-drill screws, respectively (named “Shaft Wall 2”).

2.3. Instrumentation

The responses of structural and nonstructural components were monitored by nearly 400 sensor channels with a sampling frequency of 256 Hz. A 4-pole low-pass Butterworth filter with a cutoff frequency of 50 Hz was applied to all recorded responses [Soroushian et al., 2014c]. The structure movement was measured by a combination of accelerometers and string potentiometers. These instruments were placed at column locations and the middle of floor slabs (see Fig. 5).

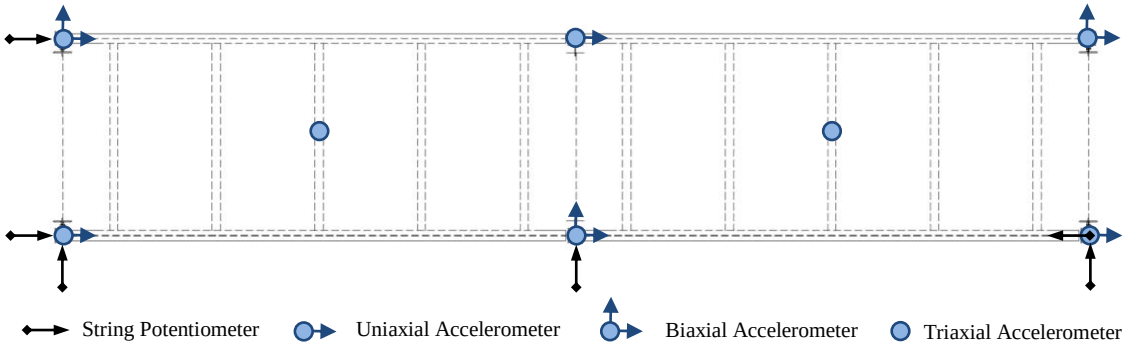

Fig. 5. Typical Structural Instrument Location [Source: Jenkins et al., 2015a]

The responses of nonstructural components were recorded by displacement transducers, string potentiometers, and accelerometers. Displacement transducers were placed at the top and bottom of partition specimens with vertical or horizontal orientations (Fig. 6a-c). Diagonal string potentiometers were also attached as shown in Fig. 6d. Uniaxial accelerometers were located at the center of some partition walls at the ceiling elevation (Fig. 6e).

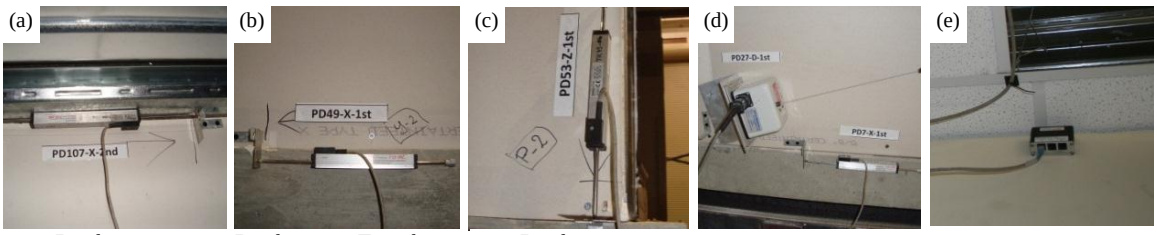

Displacement Transducer (top, horizontal) | Displacement Transducer (bottom, horizontal) | Displacement Transducer (bottom, vertical) | String Potentiometer (diagonal) | Accelerometer (near ceiling elevation)

Fig. 6. Examples of Partition Wall Instrumentation

3. Loading Protocol

A total of 59 ground motions were applied to the test-bed structure. A spectrum-matching procedure was adopted to artificially generate shake table motions. The AC 156 [ICC, 2010] parameters, used to develop the targeted acceleration spectrum, were defined based on a story height ratio (z/h) of 0.5, and the design spectral response acceleration at short periods (S_{ds}) of 2.5g [Soroushian et al., 2014c]. In addition to the target spectrum at the shake table, it was a goal to attain the target spectrum at the second floor. This goal was accomplished using the algorithms defined by Soroushian et al. [2011].

Forty-two of the 59 motions were applied to the linear test-bed structure; 12 were titled “Unmodified Linear”, and 30 were titled “Modified Linear”. The shake tables for the Unmodified Linear and Modified Linear motions were set to represent the target spectrum at the table and at the second floor levels, respectively. Motion durations during the linear portion of testing were 30 sec. The remaining (17 out of 59) motions were applied to the nonlinear test-bed configuration. Motions during this portion of testing were titled “Nonlinear” and the shake tables were set to represent the target spectrum at the table level. Durations for nonlinear motions were reduced to 10 sec. Fig. 7 shows the comparison of 5% damped spectra achieved on the shake table and the second floor during 50% of full scale motions (50% IM) [Soroushian et al., 2014c].

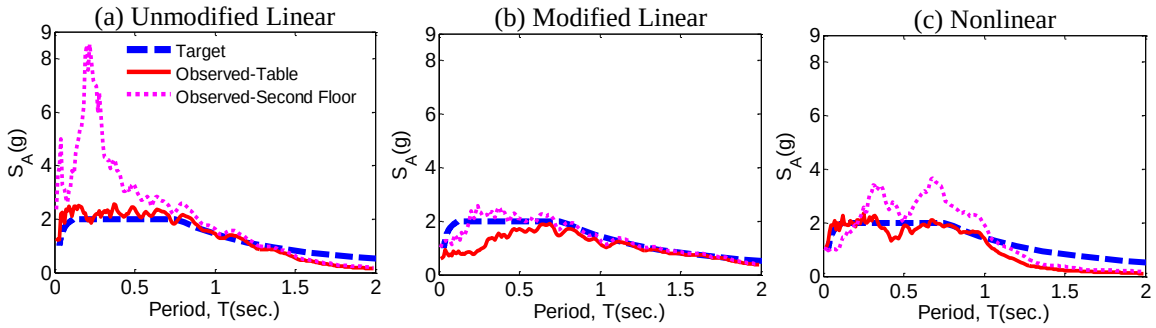

Fig. 7. Comparison between Achieved and Target 50% IM Spectrum [Source: Soroushian et al., 2014c]

A total of 8 tests were conducted in this study. Linear testing consisted of five tests named, Linear-1 through Linear-6 (example L-1). It should be mentioned that test Linear-4 was removed from testing to ensure a timely project completion. The remaining linear experiments were not consecutively updated because the schedule and documentation were already assigned. The remaining three were nonlinear, named Nonlinear-1 through Nonlinear-3 (example NL-1). The summary of peak floor accelerations and inter-story drift ratios in linear and nonlinear structures are presented in Table 2.

Table 2. Test-bed Responses during Linear and Nonlinear Configurations

Floor	Maximum Peak Floor Acceleration (g)			Maximum Story Drift Ratio (%)		
	Unmodified Linear	Modified Linear	Nonlinear	Unmodified Linear	Modified Linear	Nonlinear
First	1.59	1.16	1.22	0.75	0.66	2.79
Second	2.47	1.65	1.41	0.27	0.18	2.09

4. Damage Observation

The seismic performance of partition walls was evaluated through observed damage mechanisms. Table 3 outlines several damage mechanisms and shows which individual partition wall experienced the damage. A few of the general damage mechanisms observed during the experiment are shown in Fig. 8 and described below. Specimens with full height studs and partial height gypsum experienced damage such as

the formation of plastic hinges approximately 305mm (12 in.) below the top connection (Fig. 8a). In braced partial height partitions, failure of 45 degree stud connections was recorded (Fig. 8b). In specimens that involved institutional and commercial corner detailing, observed damage encompassed the tops of studs popping out of the track (Fig. 8c) and tape damage (Fig. 8d). Typical damage to gypsum boards near door and window openings included cracks extruding from the corners (Fig. 8e). Fig. 8f shows an example of the damage described as field screw popout (when the head of the screw dislodges from the plaster coating). Damage to the ends of wall sections (named boundary locations) included screws and/or the stud pulling out from the gypsum board, as shown in Fig. 8g. More excessive damage involved stud deformation or complete pullout from the top track (Fig. 8h).

In the partitions with full connections, plastic hinging (Fig. 8i), boundary stud damage, and field screw pop out in single ‘S’ shaped walls were observed. In addition, the corner connections with ‘C’ and ‘L’ shapes experienced separation of the return and longitudinal walls, crushing of gypsum board corners, and tape damage. Partitions with the slip track connections experienced studs sliding out of the track at boundary locations and crushing of gypsum board corners for single ‘S’ shape walls. Corner connection damage involved studs sliding out from the top track causing separation of the return and longitudinal walls and crushing of gypsum boards in the top corners (Fig. 8j). Damage observed in the sliding/frictional connection included field screw pop out, plastic hinging of studs, and boundary stud pullout (Fig. 8k) in single ‘S’ shape walls. While some minor tape damage was observed in corner connections, return and longitudinal walls never separated from each other.

Table 3. Partition Wall Damage Observed

D1	Boundary stud damage (pulled out from gypsum board, pulled out from top track, rotation, buckle).
D2	Boundary stud screws pulled from gypsum board.
D3	Studs sliding in top track.
D4	Plastic hinging forming in studs.
D5	Stud sliding or being pulled out from top track at corner connections.
D6	Tape damage and cracks in wall corners.
D7	Separation from transverse and longitudinal wall in top corner.
D8	Crushing of gypsum wall boards (corner, due to bracing system).
D9	Cracks at corners of openings.
D10	Field screw pop out of gypsum board screws.
D11	Popping out or damage of track screws.
D12	Shot pin damage.
D13	Partial height brace connection failure.

Partition	**Test NL-1**	**Test NL-2**	**Test NL-3**
P1-F	D1, D6, D7 (corner of P1-F, P8F), D8	D1, D6, D7 (corner of P1-F, P8-F), D10	D1, D6, D10
P2-F	D2, D4, D8, D10	D1, D2, D4, D10	D1, D2, D4, D10
P3-F	D1, D4, D8, D9, D10	D1, D4, D10	D1, D4, D9, D10
P4-F	D6, D9	-	-
P5-F	D4, D10, D11	D1, D4, D10	-
P6-F	D1, D2, D4, D10	D1, D2, D4, D10	D1, D2, D4, D10
P7-F	D1, D7 (corner of P7-F, P8-F).	D1, D10	D1, D5 (corner of P7-F, P8-F), D6, D10
P8-F	D7 (corner of P1-F, P8F and P7-F, P8-F)	D7 (corner of P1-F, P8-F), D11	D5 (corner of P7-F, P8-F)
P1-S	D1, D4, D7 (corner of P1-S, P9-S), D11	D1, D4, D6	D5 (corner of P1-S, P9-S), D6
P2-S	D1, D2, D3, D9, D10	D1, D4	-
P3-S	D3, D5 (corner of P3-S, P4-S), D8 (corner of P3-S, P4-S), D9	D1, D2, D8 (corner of P3-S, P4-S) D10, D12	D6, D8 (corner of P3-S, P4-S)
P4-S	D5 (corner of P3-S, P4-S and P4-S, P5-S), D7 (corner of P4-S, P5-S), D8 (corner of P4-S, P3-S and P4-S, P5-S), D9	D8 (corner of P3-S, P4-S and P4-S, P5-S)	D6, D8 (corner of P3-S, P4-S and P4-S, P5-S)
P5-S	D3, D5 (corner of P4-S, P5-S), D7 (corner of P4-S, P5-S), D8 (corner of P4-S, P5-S)	D8 (corner of P4-S, P5-S)	D8 (corner of P4-S, P5-S)
P6-S	D1, D3, D8	D1	D1, D8
P7-S	D1, D4, D6, D7 (corner of P7-S, P8-S), D11	D1	D1, D5 (corner of P7-S, P8-S)
P8-S	D6, D7 (corner of P7-S, P8-S)	-	D5 (corner of P7-S, P8-S)
P9-S	D6, D7 (corner of P1-S, P9-S)	-	D5 (corner of P1-S, P9-S)
P10-S	D13	-	-

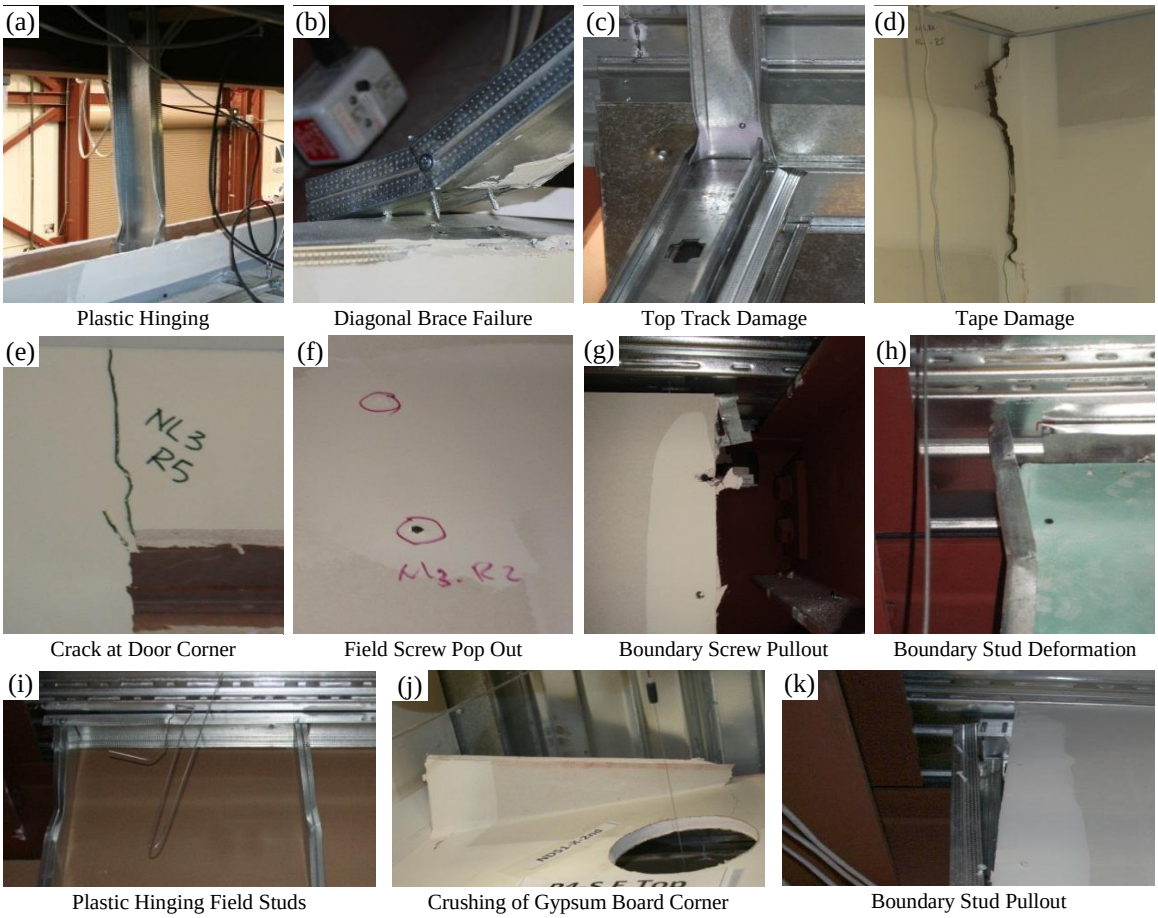

Fig. 8. Examples of Observed Damage in Partition Walls

5. Experimental Results

5.4. Performance of Top Connections

The performance of top connections was compared by considering the ratio of partition drift over the maximum story drift. Ratio values close to one correspond to a fixed connection meaning that the partition drifts were similar to the floor drifts. Values close to zero correspond to isolated partition walls, or when the partition wall experienced lower drifts than the floor drifts. Some factors that can cause a lower partition/floor drift ratio include connection detailing or damage. The performance of top connections was evaluated for the three nonlinear tests (Fig. 9). As shown, the full and

shaft wall 2 connections had the highest partition/floor drift ratio because of the stud-to-track connection. This connection forced the top and bottom of the partition wall to move like the top and bottom floors, respectively. When the drift ratio increased, the partition/floor drift ratio decreased, mainly due to the cumulative damage in the top connections. The slip track connection had the lowest partition/floor drift ratio because the top of stud was not connected to the track. Since there was no connection between the stud and track, the partition wall performed as an isolated wall causing the ratio to approach zero. It should be noted that the partition specimens used in test NL-1 were not replaced after the linear testing, therefore, the reuse of specimens and possible cumulative damage in top connections led to similar behavior regardless of the type of top connection.

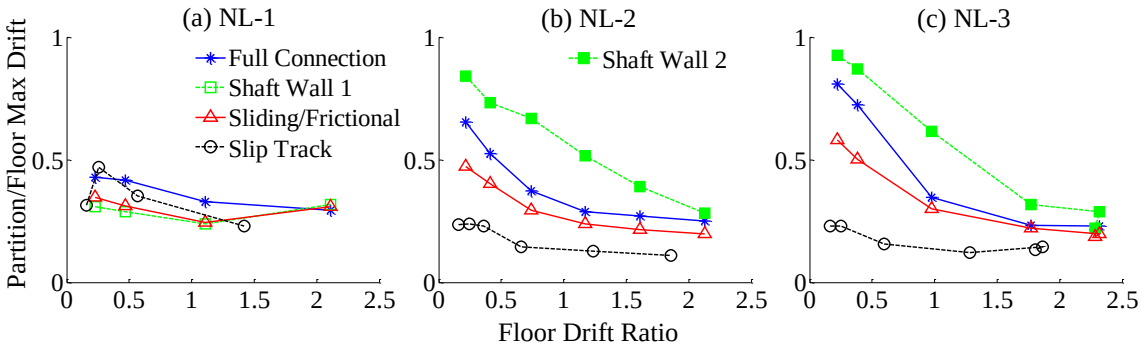

Fig. 9. Performance of Top Connections: (a) NL-1, (b) NL-2, and (c) NL-3

5.5. Partition Acceleration Amplification

Acceleration amplification (a_p) factors for ten out-of-plane partition walls were calculated for each of the ground motions applied to the structure. Table 4 shows the statistics (maximum, minimum, and median) calculated for each partition wall. The amplification factors were calculated by taking the ratio of the peak partition acceleration over the peak floor acceleration for every connection to adjacent slabs. As an example,

partitions that were full or braced partial height walls included two separate amplification factors, named “Top” and “Bottom”. Partitions with only one connection, such as free standing partitions, only had one amplification factor (Bottom). As the table shows, the amplification factors for linear tests range (approximately) from 1.5 to 2.5 with a median value of 2.1. The nonlinear tests produced similar results that range (approximately) from 1.8 to 2.5 with a median value of 2.3. ASCE 7-10 [2010] suggests that the maximum amplification is 2.5 for flexible components. The median value for both tests, labeled “All” in Table 4, was 2.2. The results justify the recommended value since the median (2.2) is less than 2.5.

Table 4. Partition Acceleration Amplification Factors

Partition	**P4-F**		**P8-F**		**P10-F**		**P11-F**		**P4-S**		**P8-S**		**P10-S**		**P11-S**		**P14-S**		**P17-S**
Location	**T**	**B**	**T**	**B**	**T**	**B**	**T**	**B**	**T**	**B**	**T**	**B**	**T**	**B**	**T**	**B**	**T**	**B**	**B**
Linear																			
Max	2.1	2.7	2.1	2.7	1.9	2.6	1.8	2.4	3.0	4.9	1.6	2.2	1.3	1.7	2.1	2.6	3.1	4.1	1.6
Min	1.6	2.1	1.8	2.3	1.4	1.8	1.8	2.4	2.1	2.8	1.3	1.8	1.2	1.7	1.9	2.6	1.3	1.7	1.4
Median	1.9	2.5	1.9	2.5	1.6	2.2	1.8	2.4	2.4	3.4	1.5	2.0	1.3	1.7	2.0	2.6	2.2	3.0	1.5
Nonlinear																			
Max	3.0	2.2	3.2	2.3	2.0	1.8	2.3	2.0	2.6	3.5	2.4	3.2	1.8	2.5	1.6	2.2	3.6	4.8	2.2
Min	2.5	2.1	2.4	2.0	2.0	1.8	2.3	2.0	2.2	2.7	1.6	2.1	1.8	2.5	1.6	2.2	3.5	4.3	1.6
Median	2.7	2.2	2.7	2.2	2.0	1.8	2.3	2.0	2.4	3.2	1.9	2.4	1.8	2.5	1.6	2.2	3.6	4.5	1.8

Summary			
	Linear	**Nonlinear**	**All**
Max	4.9	4.8	4.9
Min	1.2	1.6	1.2
Median	2.1	2.3	2.2

T = Top connected to adjacent floor

B = Bottom connected to adjacent floor

5.6. Seismic Fragility Analysis

Experimental results for cold-formed steel-framed partition walls were used to assess the seismic vulnerability of partitions through fragility functions. A fragility function is a conditional statement (Eq. (1) that relates the probability of a component exceeding a level of damage, known as damage state (DS), when subjected to a particular engineering demand parameter (EDP) [Porter et al., 2007]. The EDP considered for this study was inter-story drift due to the drift sensitive nature of partition walls. Three damage states (Table 5) were developed using the FEMA P-58 [2012] framework and the damage states suggested by the State University of New York at Buffalo (UB) [Davies et al., 2011 and Retamales et al., 2013]. The defined damage states are based on level of damage observed and the required repair action. The observed damage mechanisms during the experiments were categorized into the defined damage states. Then, the drift ratio that initiated the damage was recorded for each of the partition specimens. Table 6 shows the minimum drift ratio that triggered each damage state for the partition specimens that experienced damage.

Table 5. Damage State Definitions

Damage State	Definition	Required Repair
DS_1	**Minor Damage:** Popping out or rocking of gypsum board screws (field and boundary); Cracks forming at corners of openings; Minor gypsum cracking or crushing; Joint paper damage; Sliding of studs in top track.	Tape replacement at corners; gypsum board screw replacement at pop out locations; minor repairs to cracking.
DS_2	**Local Damage:** Boundary stud deformation (bending, twisting, pulling out from top track); Crushing of gypsum boards; Damage to partial height brace connection.	Boundary stud replacement; replacing partial sections of gypsum board; replacing partial height brace system.
DS_3	**Severe Damage:** Plastic hinging forming in field studs; tearing in steel track through slab fasteners.	Removal of full gypsum board sections and replacement of field studs; replacement of new full height gypsum wall boards; replacement of top tracks.

It should be mentioned that in this study, the damage defined as field screw pop out was considered under the first, or minor, damage state. Field screw pop out occurs

when the head of the field screw dislodges from the coating compound and can transpire at relatively low inter-story drifts. It is believed that this damage is an indication of plastic hinging occurring in field studs in which the repair actions include possible removal of gypsum boards and replacement of studs. However, the correlation between the drift ratio initiating field screw pop out and the drift ratio initiating plastic hinging could not be made until the gypsum boards were removed from the studs at the end of the test. Therefore, due to testing procedure limitations, the field screw pop out damage is considered DS1 and the plastic hinging of field stud damage is considered DS3. It is recommended that additional studies be conducted in order to better understand the correlation between the two damages.

Experimental fragility functions were developed using Method A, outlined by Porter et al. [2007], which requires that all specimens failed at a target EDP. A summary of the fragility parameters, median and dispersion, determined using Eqs. (2 and (3, respectively, are shown in Table 7. The following fragilities are deemed acceptable because the Lilliefors goodness-of-fit test passed at the 5% significance level.

$$F_{dm}(edp) = \Phi\left(\frac{\ln\left(\frac{edp}{x_m}\right)}{\beta}\right) \tag{1}$$

where Φ is the normal cumulative distribution function, *edp* is the triggering drift ratio per specimen, and x_m and β are the fragility parameters, median and dispersion, respectively.

$$x_m = \exp\left(\left(\frac{1}{M}\right)\sum_{i=1}^{M} ln(edp)\right) \tag{2}$$

$$\beta = \sqrt{\left(\frac{1}{M-1}\sum_{i=1}^{M}\left(\ln\left(\frac{edp}{x_m}\right)\right)^2\right)^2 + {\beta_u}^2} \quad (3)$$

where M is the number of specimens tested to failure, i is the specimen index, and β_u is 0.25 because the tests met at least one of the criteria listed by Porter et al. [2007].

Fig. 10(a-c) presents individual fragility curves for partition specimens as well as a combination of all specimens labeled “All”. As shown, the fragilities for DS3 (Fig. 10c) are all the same because the plastic hinging of field stud damage could not be observed until the gypsum wallboards were removed at the end of testing. Fig. 10d presents a summary of the three damage state combinations. As shown, the damage states are in consecutive order with median floor drift ratios of 0.99%, 1.61% and 2.34%.

Table 6. Minimum Triggering Drift Ratio (First Floor Partition Walls)

			P1-F			P2-F			P3-F			P5-F			P6-F			P7-F		
			1	**2**	**3**	**1**	**2**	**3**	**1**	**2**	**3**	**1**	**2**	**3**	**1**	**2**	**3**	**1**	**2**	**3**
DS1	Minor Damage	Screws pulled/rocked out from gypsum board (field)	-	0.74	0.97	0.47	0.74	0.97	1.11	0.74	0.38	2.11	1.17	0.38	2.11	0.74	0.38	-	0.74	0.97
		Screws pulled/rocked out from gypsum board (top or bottom track)	-	-	-	-	-	-	-	-	-	0.47	-	-	-	-	-	-	-	-
		Minor stud damage (includes screw to track damage)	-	1.61	-	-	-	-	-	-	-	-	-	-	-	-	-	-	-	-
		Cracks along openings (window, door)	-	-	-	-	-	-	2.11		2.32	-	-	-	-	-	-	-	-	-
		Cracks along joint paper tape, pulled tape, corner beads	2.64	2.13	0.97	-	-	-	-	-	-	2.64	-	-	-	-	-	2.64	-	1.77
		Screws pulled/rocked out from gypsum board (Boundary Stud)	-	-	-	2.64	0.74	0.97	-	-	-	-	-	0.97	1.11	1.17	0.97	-	-	-
		Crushing of gypsum board due to interaction from the beams and partitions	-	-	-	-	-	-	2.11	-	-	-	-	-	-	-	-	-	-	-
		Sliding of stud in top track	-	-	-	-	-	-	-	-	-	-	-	-	-	-	-	-	-	-
		Minimum Drift Ratio Triggering DS1	2.64	0.74	0.97	0.47	0.74	0.97	1.11	0.74	0.38	0.47	1.17	0.38	1.11	0.74	0.38	2.64	0.74	0.97
DS2	Local Damage	Crushing of gypsum board	2.64	-	-	2.11	-	-	-	-	-	-	-	-	-	-	-	-	-	-
		Out-of-plane bending and cracking of gypsum wallboards at wall intersections	-	-	-	-	-	-	-	-	-	-	-	-	-	-	-	-	-	-
		Bending of boundary studs/detached from gypsum/detached from top track	2.11	1.61	2.32	-	1.61	1.77	2.11	1.61	0.97	-	1.61	0.97	1.11	-	0.97	2.64	2.13	0.97
		Buckling of diagonal braces (partial height walls)	-	-	-	-	-	-	-	-	-	-	-	-	-	-	-	-	-	-
		Minimum Drift Ratio Triggering DS2	2.11	1.61	2.32	2.11	1.61	1.77	2.11	1.61	0.97	-	1.61	0.97	1.11	-	0.97	2.64	2.13	0.97
DS3	Severe Damage	Tears in steel tracks through slab fasteners	-	-	-	-	-	-	-	-	-	-	-	-	-	-	-	-	-	-
		Plastic hinges forming in studs	-	-	-	2.64	2.13	2.29	2.64	2.13	2.29	2.64	2.13	2.29	2.64	2.13	2.29	-	-	-
		Minimum Drift Ratio Triggering DS3	-	-	-	2.64	2.13	2.29	2.64	2.13	2.29	2.64	2.13	2.29	2.64	2.13	2.29	-	-	-

Table 6 Continued. Minimum Triggering Drift Ratio (Second Floor Partition Walls)

			P1-S			P3-S			P4-S			P5-S			P9-S		
			1	2	3	1	2	3	1	2	3	1	2	3	1	2	3
DS1	Minor Damage	Screws pulled/rocked out from gypsum board (field)	-	-	-	-	-	-	-	-	-	-	-	-	-	-	-
		Screws pulled/rocked out from gypsum board (top and bottom track)	0.57	-	-	-	-	-	-	-	-	-	-	-	-	-	-
		Minor stud damage (includes screw to track damage)	-	1.86	1.81	-	-	-	-	-	-	-	-	-	-	-	1.81
		Cracks along openings (window, door)	-	-	-	2.07	-	-	0.16	-	-	-	-	-	-	-	-
		Cracks along joint paper tape, pulled tape, corner beads	2.07	1.23	1.81	-	-	1.28	-	-	1.28	-	-	-	2.07	1.23	1.81
		Screws pulled/rocked out from gypsum board (Boundary Stud)	-	-	-	-	1.86	-	-	-	-	-	-	-	-	-	-
		Crushing of gypsum board due to interaction from the beams and partitions	-	-	-	-	1.86	-	-	-	-	2.07	-	-	-	-	-
		Sliding of stud in top track	-	-	-	2.07	-	-	-	-	-	2.07	-	-	-	-	-
		Minimum Drift Ratio Triggering DS1	0.57	1.23	1.81	2.07	1.86	1.28	0.16	-	1.28	2.07	-	-	2.07	1.23	1.81
DS2	Local Damage	Crushing of gypsum board	-	-	-	1.42	-	-	1.42	-	-	2.07	-	-	-	-	-
		Out-of-plane bending and cracking of gypsum wallboards at wall intersections	-	-	-	-	1.23	1.81	1.42	1.23	1.28	1.42	1.9	1.28	-	-	-
		Bending of boundary studs/detached from gypsum/detached from top track	2.07	1.23	-	2.07	-	-	2.07	-	-	-	-	-	-	-	-
		Buckling of diagonal braces (partial height walls)	-	-	-	-	-	-	-	-	-	-	-	-	-	-	-
		Minimum Drift Ratio Triggering DS2	2.07	1.23	-	1.42	1.23	1.81	1.42	1.23	1.28	1.42	1.86	1.28	-	-	-
DS3	Severe Damage	Tears in steel tracks through slab fasteners	-	-	-	-	1.86	-	-	-	-	-	-	-	-	-	-
		Plastic hinges forming in studs	2.07	1.86	-	-	-	-	-	-	-	-	-	-	-	-	-
		Minimum Drift Ratio Triggering DS3	2.07	1.86	-	-	1.86		-	-	-	-	-	-	-	-	-

Table 7. Summary of Fragility Parameters

DS1				DS2				DS3			
Partition	**x_m**	**β**	**Goodness-of-fit Test**	**Partition**	**x_m**	**β**	**Goodness-of-fit Test**	**Partition**	**x_m**	**β**	**Goodness-of-fit Test**
P1-F	1.24	0.51	Pass	P1-F	1.99	0.25	Pass	P2-F	2.34	0.25	Pass
P2-F	0.70	0.28	Pass	P2-F	1.82	0.25	Pass	P3-F	2.34	0.25	Pass
P3-F	0.68	0.38	Pass	P3-F	1.49	0.29	Pass	P5-F	2.34	0.25	Pass
P5-F	0.60	0.43	Pass	P7-F	1.76	0.37	Pass	P6-F	2.34	0.25	Pass
P6-F	0.68	0.38	Pass	P3-S	1.47	0.25	Pass				
P7-F	1.24	0.51	Pass	P4-S	1.31	0.25	Pass				
P1-S	1.08	0.43	Pass	P5-S	1.50	0.25	Pass				
P3-S	1.70	0.26	Pass								
P9-S	1.67	0.26	Pass								
All	0.99	0.42	-	All	1.61	0.26	-	All	2.34	0.25	-

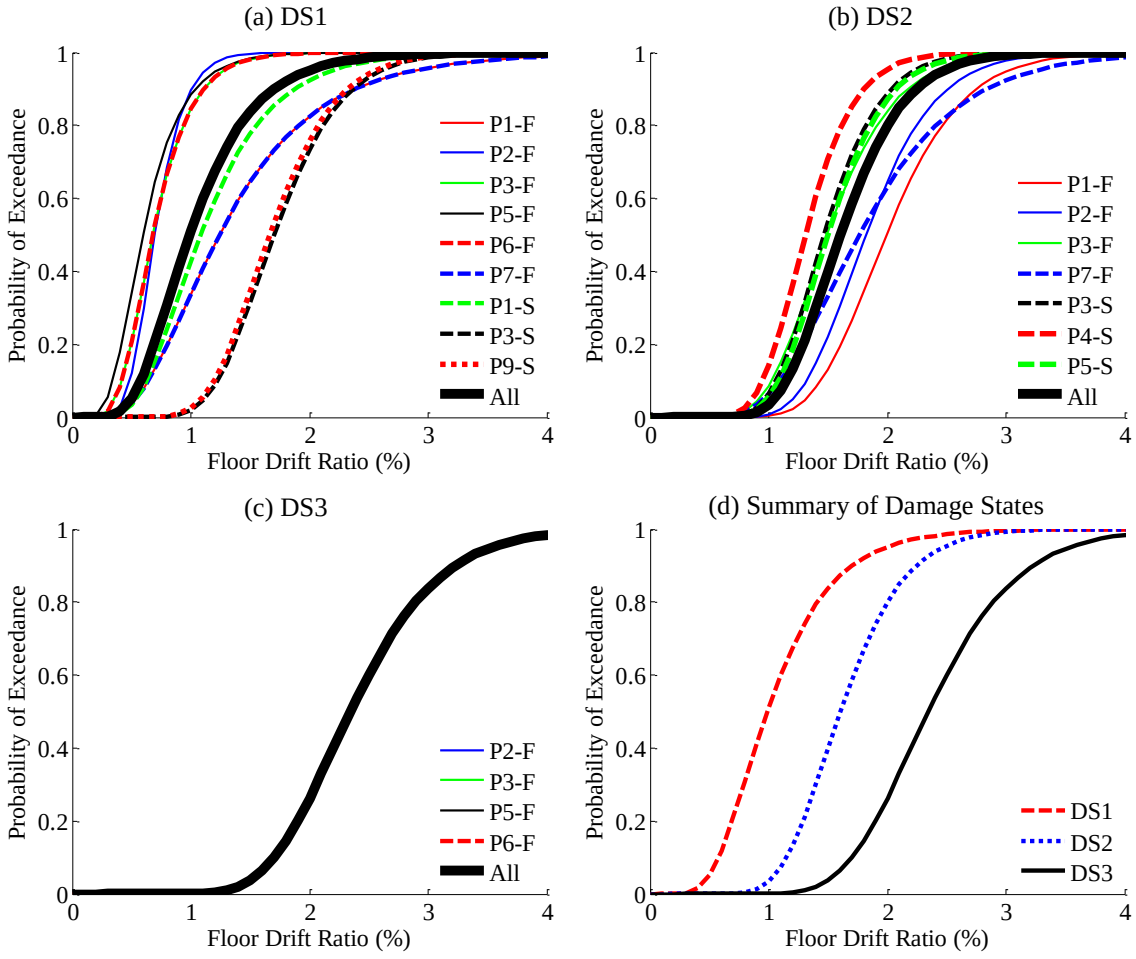

Fig. 10. Experimental Fragility Functions

5.7. Comparison to Past Experimental Studies

The ranges of inter-story drift ratios that represent the three partition wall damage states are compared for this study and past experimental studies (Table 8) [Restrepo and Bersofsky, 2011; Retamales et al., 2013; and Wang et al., 2015]. When comparing the ranges from DS1, the lower drift percentage for the experiments evaluated by Restrepo and Bersofsky [2011] and Retamales et al. [2013] are close to the drift experienced in this experiment (UNR). However, when comparing the higher drift percentage, UNR observed a much higher drift (2.64%). The range of drift percentages observed at DS2 is higher for UNR (2.64%) than all past experiments. The drift percentages recorded for DS3 are similar between all the experimental studies. The range differences between experiments can be due to distinct design variables used for each individual experiment. Examples that can contribute to these discrepancies include loading protocol, experimental setups (housing components, specimen configurations, uncertainties in material properties), detailing, or damage state definitions.

Table 8. Comparison of Drift Ratios (Correlating to Partition Damage) Reported from Various Experimental Studies (%)

Damage State	Restrepo and Bersofsky [2011]	Retamales et al. [2013]	Wang et al. [2015]	UNR [2015]
DS1	0.05-0.75	0.1-0.56	N/A	0.16-2.64
DS2	0.5-1.5	0.4-1.84	0.11-1.09	0.97-2.64
DS3	0.5-3.0	0.62-2.66	1.24-2.75	1.86-2.64

SUMMARY

This study investigated the response and failure mechanism of nonstructural components through a series of full-scale testing conducted at the University of Nevada, Reno NEES site. A two-story, two-by-one bay steel braced-frame structure, that spanned over three biaxial shake tables, was used to house the nonstructural components. The

performance of light-gauged steel-framed partition walls were evaluated through design variables including: 1) framing systems, 2) partition wall heights, 3) partition wall geometries, 4) openings in partition walls, and 5) top connections. Experimental results include the performance evaluation of top connections, out-of-plane acceleration amplification factors, and fragility curves based on damage caused by inter-story drift. The ranges of inter-story drifts observed from this experiment were compared to drifts observed in past experimental studies. The major findings are summarized as follows:

- When evaluating the performance of top connections (full, slip track, and sliding/frictional), results show that as the drift ratio increased, the partition/floor drift ratio decreased because of the cumulative damage in the top connections.
- Damage to the full connection included plastic hinging of field studs and field screw pop out.
- The slip track connection reduced the amount of plastic hinging and field screw pop out, but experienced excessive corner damage.
- Damage to the sliding/frictional connection involved plastic hinging of field studs and field screw pop out, however, it only encountered minor tape damage in corner locations.
- The computed acceleration amplification factors for out-of-plane partition walls justify the ASCE 7-10 [2010] code's recommendation of a maximum amplification factor of 2.5 for flexible components.
- Investigators were unable to observe if the field screw pop out damage was an indication of plastic hinging forming in field studs until the

gypsum boards were removed at the end of testing. Therefore, it is recommended that additional studies be conducted in order to better understand the correlation between the inter-story drift that initiates field screw pop damage and the drift that initiates plastic hinging in field studs.

- Experimental fragility curves are in consecutive order with the median drift ratios for DS1, DS2, and DS3, as 0.99%, 1.61%, and 2.34% respectively.
- Results show that after comparing the ranges of inter-story drifts (from past experimental studies to the current study), drifts observed during the UNR experiment are higher for DS1 and DS2, but are similar for DS3 than the drifts experienced from other studies.

ACKNOWLEDGEMENTS

This material is based upon work supported by the National Science Foundation under Grant No. 0721399. This Grand Challenge (GC) project to study the seismic response of nonstructural systems is under the direction of M. Maragakis from the University of Nevada, Reno and Co-PIs: T. Hutchinson, A. Filiatrault, S. French, and B. Reitherman. Any opinions, findings, conclusions or recommendations expressed in this document are those of the investigators and do not necessarily reflect the views of the sponsors.

5. SUMMARY AND CONCLUSIONS

Summary

The seismic performance of nonstructural components is crucial regarding life safety, system functionality, and economic expense. Therefore, it is vital to conduct experimental programs, such as the one described in this report, in order to better understand the behaviors and responses of these systems. The project titled, "NEESR-GC: Simulation of the Seismic Performance of Nonstructural Systems", aimed to evaluate the seismic performance of integrated ceiling-piping-partition nonstructural systems through multidisciplinary system-level studies. Experimental programs were conducted at three different facilities to assess full-scale system-level (UNR-NEES site and E-Defense facility) and full-scale sublevel (UB-NEES site) performances of nonstructural components.

The experimental series conducted at the UNR-NEES site is the main focus of this report. In this study, the nonstructural components were housed in a two-story, two-by-one bay steel braced-frame structure that spanned over three biaxial shake tables. The test-bed structure was subjected to a number of artificial uniaxial ground motions. The responses of the structure and nonstructural components were recorded through nearly 400 channels of instruments including: string potentiometers, displacement transducers, load cells, and accelerometers. Each individual component of the ceiling-piping-partition system was described and evaluated in three separate papers, submitted to various journals. Experimental data led to the determination of acceleration amplification factors, seismic fragility analyses, and overall performance of nonstructural systems. Specific

findings that correspond to each nonstructural component are described in the subsequent section.

Findings and Conclusions

The following findings and conclusions are first categorized by the nonstructural component: suspended ceiling systems, fire sprinkler piping systems, or partition wall systems. Then, the conclusions regarding the integrated ceiling-piping-partition systems are discussed.

Suspended Ceiling Systems

Experimental results regarding the ceiling systems included the acceleration amplifications for four design variables: bracing, number of attached walls, panel weight, and effects of connections to partition walls. In addition, fragility functions were developed for ceiling perimeter displacement, support axial force, and overall ceiling performance. The major findings are summarized as follows:

- Ceiling acceleration amplifications are most effected by: 1) additional attachments to partition walls (a_p = 1.57) and 2) four free (unattached) walls (a_p = 3.56).
- Ceiling systems that have all free sides (grids unattached to the wall angle) have the highest failure probability while ceilings with additional partition walls (content rooms) have the lowest failure probability when evaluating a pounding gap of 3/4 in. (19.1 mm).
- Fragility functions based on the unseating gap show that the seismic design category D-E-F governs the failure probability (high and low) compared to category C, as defined in section 1. Introduction. Unseating of grid members from

7/8 in. (22.2 mm) wall angles have the highest probability of exceedance and unseating of grid members from 2.0 in. (50.8 mm) wall angles has the lowest exceedance probability.

- From the support element fragility curves, results show that wire restrainers have a higher probability of failure compared to hangers.
- Fragility functions for the overall performance of ceiling systems show that assemblies that were unbraced, included seismic clips, or did not have additional connections to partition walls had a higher failure probability than assemblies that were braced, included pop rivets, or had additional connections.
- Overall fragility results show that systems with pop rivet connections have the lowest probability of failure compared to other ceiling system variables.
- The median fragility parameters based on overall ceiling system performance are 0.82g, 2.47g, and 3.39g for percentage of ceiling area loss of 5% (DS1), 30% (DS2), and 50% (DS3), respectively.

Fire Sprinkler Piping Systems

Experimental results from the fire sprinkler piping system led to the computation of acceleration amplification factors for three pipe segment types: main pipe run, branch line/armover, and sprinkler heads. Additionally, results also led to the development of fragility curves for pipe joint rotation, support axial force, and pipe displacement. The major findings are summarized as follows:

- Acceleration amplification factors show an increasing trend (2.7, 3.5 and 6.1) from the main pipe run to branch lines/armovers to the sprinkler heads.

- The main pipe run amplification (2.7) is comparable to the ASCE 7-10 (2010) recommended amplification value for flexible components (a_p = 2.5).
- The ASCE 7-10 (2010) value underestimates the amplifications for branch line/armover and sprinkler head pipe segments.
- Pipe joint rotation fragilities show that 2.0 in. (50 mm) diameter pipes have the greatest probability of failure compared to other diameter pipes.
- Support axial force fragilities depict that hangers supporting 3.0 in. (80 mm) diameter pipes exceed the suggested capacity value given by NFPA 13 (2011).
- Pipe segments that are 3.0 in. (80 mm) in diameter have the highest vulnerability of hanger or wire restrainer failure compared to other supported pipe diameters.
- Pipe displacement fragilities indicate that pipe segments with large diameters have greater displacements and probability of failure compared to small pipe diameters.
- Pipe displacement is the governing fragility function compared to pipe joint rotation and support axial force.
- Fire sprinkler pipe joints did not experience enough rotation to cause water leakage. Therefore, future studies should ensure that pipe joints rupture in order to acquire accurate failure capacities.

Partition Wall Systems

The performance of light-gauged steel-framed partition walls were evaluated through the following design variables: 1) framing systems, 2) partition wall heights, 3) partition wall geometries, 4) openings in partition walls, and 5) top connections.

Experimental data led to the performance evaluation of top connections, out-of-plane acceleration amplification factors, and fragility curves based on damage caused by inter-story drift. The major findings are summarized as follows:

- When evaluating the performance of top connections (full, slip track, and sliding/frictional), results show that as the drift ratio increased, the partition/floor drift ratio decreased because of the cumulative damage in the top connections.
- Damage to the full connection included plastic hinging of field studs and field screw pop out.
- The slip track connection reduced the amount of plastic hinging and field screw pop out, but experienced excessive corner damage.
- Damage to the sliding/frictional connection involved plastic hinging of field studs and field screw pop out, however, it only encountered minor tape damage in corner locations.
- The computed acceleration amplification factors for out-of-plane partition walls justify the ASCE 7-10 (2010) recommendation of a maximum amplification factor of 2.5 for flexible components.
- Investigators were unable to observe if the field screw pop out damage was an indication of plastic hinging forming in field studs until the gypsum boards were removed at the end of testing. Therefore, it is recommended that additional studies be conducted in order to better understand the correlation between the inter-story drift that initiates field screw pop out damage and the drift that initiates plastic hinging in field studs.

- Experimental fragility curves are in consecutive order with the median drift ratios for DS1, DS2, and DS3, as 0.99%, 1.61%, and 2.34% respectively.
- Results show that after comparing the ranges of inter-story drifts (from past experimental studies to the current study), drifts observed during the UNR experiment are higher for DS1 and DS2, but are similar for DS3 than the drifts experienced from other studies.

Integrated Ceiling-Piping-Partition Systems

This study was conducted as a system-level experiment, and therefore, one focus was to evaluate the performance characteristics of the integrated ceiling-piping-partition nonstructural system. The performance of the integrated system can be investigated through the observed damage caused by the interactions between nonstructural components.

- The damage observed from the interaction between ceiling-piping systems includes the tearing of ceiling tiles. Sprinkler piping drops that were rigid and included a 2.0 in. (50 mm) gap between the sprinkler head and the ceiling tile experienced the most severe tearing. However, this tearing effect was reduced in drop configurations that utilized flexible hoses or when there was no gap between the sprinkler head and ceiling tile.
- It should be noted that there was no damage reported between the piping-partition systems during this study.
- The damage from ceiling-partition interaction generated in the perimeter wall angles. Large accelerations caused the ceiling grids to unseat from the perimeter

wall angle, which ultimately led to the ends of grid members causing a punching effect in the gypsum board.

REFERENCES

ACI 355.2 (American Concrete Institute). (2004). *Qualification of Post-Installed Mechanical Anchors in Concrete (ACI 355.2-04) and Commentary (ACI 355.2R-04).* Farmington Hills, Michigan.

ANCO Engineers, Inc. (1983). *Seismic Hazard Assessment of Nonstructural Ceiling Components.* NSF Rep. No. CEE-8114155, Culver City, California.

Antaki, G., and Guzy, D. (1998). Seismic Testing of Grooved and Threaded Fire Protection Joints and Correlation with NFPA Seismic Design Provisions. *ASME 1998, PVP-Vol. 364*, pp. 69-75.

Araya-Letelier, G., and Miranada, E. (2012). Novel Sliding/Frictional Connections for Improved Seismic Performance of Gypsum Wallboard Partitions. *Fifteenth World Conference on Earthquake Engineering.* Lisbon, Portugal.

Arnold, C. (1991). The Seismic Response of Nonstructural Elements in Buildings. *Bulletin of the New Zealand National Society for Earthquake Engineering, Vol. 24*(No. 4), 306-316.

ASCE (American Society of Civil Engineers). (2005). *Minimum Design Loads for Building and Other Structures.* Reston, Virginia.

ASCE (American Society of Civil Engineers). (2010). *Minimum Design Loads for Building and Other Structures.* Reston, Virginia.

ASTM (American Society for Testing and Materials) International. (2011). *E580/E580M - Standard Practice for Installation of Ceiling Suspension Systems for Acoustical*

Tile and Lay-in Panels in Areas Subject to Earthquake Ground Motions. West Conshohocken, Pennsylvania.

ASTM (American Society for Testing and Materials) International. (2013). *C635/C635M-13a - Standard Specification for the Manufacture, Performance, and Testing of Metal Suspension Systems for Acoustical Tile and Lay-in Ceilings.* West Conshohocken, Pennsylvania.

ATC-58. (2013). *Seismic Performance Assessment of Buildings.* Redwood City, California.

Ayres, J. M., and Sun, T. Y. (1973). Nonstructural Damage. In *The San Fernando, California Earthquake of February 9, 1971.* National Oceanic and Atmospheric Administration, Washington, D.C.

Ayres, J. M., Sun, T. Y., and Brown, F. R. (1973). Nonstructural Damage to Buildings. In *The Great Alaska Earthquake of 1964.* National Academy of Sciences, Washington, D.C.

Badillo, H., Kusumastuti, D., Reinhorn, A. M., and Whittaker, A. S. (2002). *Seismic Qualification of Suspended Ceiling Systems.* Technical Report UB CSEE/SEESL-2002-01, Vol. 1, Department of Civil, Structural, and Environmental Engineering, University at Buffalo, Buffalo, New York.

Badillo, H., Whittaker, A. S., and Reinhorn, A. M. (2003a). *Seismic Qualification of Suspended Ceiling Systems.* Technical Report UB CSEE/SEESL-2003-01, Vol. 3, Department of Civil, Structural, and Environmental Engineering, University at Buffalo, Buffalo, New York.

Badillo, H., Whittaker, A. S., and Reinhorn, A. M. (2003b). *Testing for Seismic Qualification of Suspended Ceiling Systems, Part 3.* Technical Report UB CSEE/SEESL-2003-01, Department of Civil, Structural, and Environmental Engineering, University at Buffalo, Buffalo, New York.

Badillo, H., Whittaker, A. S., and Reinhorn, A. M. (2003c). *Testing for Seismic Qualification of Suspended Ceiling Systems, Part 4.* Technical Report UB CSEE/SEESL-2003-02, Department of Civil, Structural, and Environmental Engineering, University at Buffalo, Buffalo, New York.

Badillo, H., Whittaker, A. S., and Reinhorn, A. M. (2003d). Performance Characterization of Suspended Ceiling Systems. *ATC-29-2 Seminar on the Seismic Design, Performance and Retrofit of Nonstructural Components in Critical Facilities.* Irvine, California.

Badillo, H., Whittaker, A., and Reinhorn, A. (2007). Seismic Fragility of Suspended Ceiling Systems. *Earthquake Spectra, Vol. 23, No. 1*, 21-40.

Bersofsky, A. (2004). A Seismic Performance Evaluation of Gypsum Wallboard Partitions. M. S. Thesis, University of California, San Diego, San Diego, California.

Cornell, A., Jalayer, F., Hamburger, R., and Foutch, D. (2002). Probabilistic Basis for 2000 SAC Federal Emergency Management Agency Steel Moment Frame Guidelines. *J. Struct. Eng.*, 526-533. doi:10.1061/(ASCE)0733-9445(2002)128:4(526)

Dao, N. D., and Ryan, K. L. (2013). Computational Simulation of a Full-Scale Fixed-Base and Isolated Base Steel Moment Frame Building Tested at E-Defense. *Journal of Structural Engineering*. doi:10.1061/(ASCE_ST.1943-541X.0000922

Davies, R., Retamales, R., Mosqueda, G., and Filiatrault, A. (2011). *Experimental Seismic Evaluation, Model Parameterization, and Effects of Cold-formed Steel-framed Gypsum Partition Walls on the Seismic Performance of an Essential Facility.* Technical Rep. MCEER-11-0005, State University of New York, Buffalo, New York.

Dhakal, R. (2010). Damage to Non-structural Components and Contents in 2010 Darfield Earthquake. *Bulletin of the New Zealand Society for Earthquake Engineering, Vol. 43*(No. 4), 404-411.

Ding, D. and Arnold, C. (1990). Architecture, Building Contents, and Building Systems. *Chaper 9 in Earthquake Spectra, Supplement to Vol. 6*, 339-377.

FEMA (Federal Emergency Management Agency) E-74. (2012). *Reducing the Risks of Nonstructural Earthquake Damage: A Practical Guide.* Redwood City, California.

FEMA (Federal Emergency Management Agency) P-58/BD-3.9.4. (2011). *Development of Seismic Fragilities for Acoustical Tile or Lay-in Panel Suspended Ceilings: Background Document FEMA P-58/BD-3.9.4.* Redwood City, California.

FEMA (Federal Emergency Management Agency) P-58-1. (2012). *Seismic Performance Assessment of Buildings Volume 1 - Methodology.* Redwood City, California.

Filiatrault, A., Uang, C., Folz, B., Christopoulos, C., and Gatto, K. (2001). *Reconnaissance Report of the February 28, 2001 Nisqually (Seattle-Olympia)*

Earthquake. Structural Systems Research Project, Report No. SSRP-2001/02, Univ. of California, San Diego, San Diego, California.

Fleming, R. P. (1998). *Analysis of Fire Sprinkler Systems Performance in the Northridge Earthquake.* NIST-GCR-98-736, National Institute of Standards and Technology.

Gerdeen, J., Rodabaugh, E., and O'Donnell, W. (1979). A Critical Evaluation of Plastic Behavior Data and a Unified Definition of Plastic Loads for Pressure Components. *Welding Research Council Bulletin, Bulletin No. 254*.

Hoehler, M. S., Panagiotou, M., Restrepo, J. I., Silva, J. F., Floriani, L., Bourgund, U., and Gassner, H. (2009). Performance of Suspended Pipes and their Anchorages During Shake Table Testing of a Seven-Story Building. *Earthquake Spectra, 25(1)*, 71-91.

ICC Evaluation Service. (2010). *AC 156 - Acceptance Criteria for Seismic Certification by Shake-Table Testing of Nonstructural Components.* ICC Evaluation Service, Whittier, California.

Jenkins, C., Soroushian, S., Rahmanishamsi, E., Maragakis, E. M. (2015a). Experimental Fragility Analysis of Cold-Formed Steel-Framed Partition Wall Systems. *ASCE Structures Congress.* Portland, Oregon.

Jenkins, C., Soroushian, S., Rahmanishamsi, E., Maragakis, E. M. (2015b). Experimental Fragility Analysis of Cold-Formed Steel-Framed Partition Wall Systems. *Thin-Walled Structures*, Under Review.

Jenkins, C., Soroushian, S., Rahmanishamsi, E., Maragakis, E. M. (2015c). Experimental Fragility Analysis of Pressurized Fire Sprinkler Piping Systems. *Earthquake Engineering*, Under Review.

Jenkins, C., Soroushian, S., Rahmanishamsi, E., Maragakis, E. M. (2015d). Fragility Analysis of Suspended Ceiling Systems in a Full-Scale Experiment. *Journal of Structural Engineering*, Under Review.

Kusumastuti, D., Badillo, H., Reinhorn, A. M., and Whittaker, A. S. (2002). *Seismic Qualification of Suspended Ceiling Systems.* Technical Report UB CSEE/SEESL-2002-01, Vol. 2, Department of Civil, Structural, and Environmental Engineering, University at Buffalo, Buffalo, New York.

Larson, L., Stokey, W., and Frangen, W. (1975). An Approximate Model for an Elastic-Plastic Pipe Element Under Combined Loading. *ASME Journal of Pressure Vessel Technology*, 22-28.

Lavan, O., Reinhorn, A. M., Shao, X., and Pitman, M. (2006). *Seismic Qualification Test of Suspended Ceiling Systems: System H, a Study for Chicago Metallic Corporation.* Report No. CSEE/SEESL-2006-15, Department of Civil, Structural, and Environmental Engineering, University at Buffalo, Buffalo, New York, (private distribution only).

Malhotra, P., Senseny, P., Braga, A., and Allard, R. (2003). Testing Sprinkler-Pipe Seismic-Brace Components. *Earthquake Spectra, Vol. 19*(No. 1), 87-109.

Masri, S., Caffrey, J., Myrtle, R., Nigbor, R., Agbabian, M., Johnson, E., Petak, W., Shinozuka, M., Tranquada, R., and Wellford, L. (2002). Nonstructural Mitigation in Hospitals: the FEMA-USC Hospital Project. *Proceedings of the Seventh U.S. National Conference on Earthquake Engineering.* Boston.

Matzen, V., and Tan, Y. (2002). Using Finite Element Analysis to Determine Piping Elbow Bending Moment (B2) Stress Indices. *Welding Research Council Bulletin, Bulletin No. 472*.

Miranda, E., Mosqueda, G., Retamales, R., and Pekcan, G. (2012). Performance of Nonstructural Components during the 27 February 2010 Chile Earthquake. *Earthquake Spectra, 28(S1)*, 453-471.

Mizutani, K., Kim, H., Kikuchihara, M., Nakai, T., Nishino, M., and Sunouchi, S. (2012). The Damage of the Building Equipment under the 2011 Tohoku Pacific Earthquake. *9th International Conference on Urban Earthquake Engineering and 4th Asia Conference on Earthquake Engineering.* Tokyo Institute of Technology, Tokyo, Japan.

Motosaka, M., and Mitsuji, K. (2012). Building Damage during the 2011 Off the Coast of Tohoku Earthquake. *The Japanese Geotechnical Society, Soils and Foundations, 52*, 929-944.

NEES Nonstructural. (2015, September 23). *NEES Nonstructural*. Retrieved from NEES Nonstructural Website: http://www.nees-nonstructural.org

NEES Nonstructural Proposal. (2007). *NEES Nonstructural Proposal.* doi:http://www.nees-nonstructural.org

NFPA (National Fire Protection Association) 13. (2011). *Standard for the Installation of Sprinkler Systems.* Quincy, Massachusetts.

Nielson, G., and DesRoches, R. (2007). Analytical Seismic Fragility Curves for Typical Bridges in the Central and Southeastern United States. *Earthquake Spectra, 23 (3)*, 615-633.

NRC (National Research Council). (1973). *The Great Alaska Earthquake of 1964.* National Academy of Sciences, Washington, D.C.

Porter, K., Kennedy, R., and Bachman, R. (2007). Creating Fragility Functions for Performance-Based Earthquake Engineering. *Earthquake Sprectra,* 471-489.

Rahmanishamsi, E., Soroushian, S., and Maragakis, E. M. (2014). System-Level Experiments on Ceiling/Piping/Partition Systems at UNR-NEES Site. *The Tenth U.S. National Conference on Earthquake Engineering.* Achorage, Alaska.

Rahmanishamsi, E., Soroushian, S., and Maragakis, E. M. (2015a). Cyclic Behavior of Gypsum Board-to-Steel Stud Screw Connections in Nonstructural Walls. *Earthquake Spectra,* In-press.

Rahmanishamsi, E., Soroushian, S., and Maragakis, E. M. (2015b). Analytical Model for the Seismic Performance of Cold-Formed Steel-Framed Gypsum Partition Walls. *ASCE Structures Congress.* Portland, Oregon.

Ramanathan, K. N. (2012). *Next Generation Seismic Fragility Curves for California Bridges Incorporating the Evolution in Seismic Design Philosophy.* Doctoral Dissertation, School of Civil and Environmental Engineering, Georgia Institute of Technology, Atlanta.

Reinhorn, A., Ryu, K., and Maddaloni, G. (2010). *Modeling and Seismic Evaluation of Nonstructural Components: Testing Frame for Experimental Evaluation of Suspended Ceiling Systems.* Technical Rep. MCEER-10-0004, State University of New York, Buffalo, New York.

Reitherman, R., and Sabol, T. (1995). Nonstructural Damage in Northridge Earthquake of January 17, 1994 Reconnaissance Report. *Supplement C to Earthquake Spectra*, 453-514.

Repp, J., Badillo, H., Whittaker, A. S., and Reinhorn, A. M. (2003a). *Seismic Qualification of Suspended Ceiling Systems, Part 5.* Technical Report UB CSEE/SEESL-2003-03, Department of Civil, Structural, and Environmental Engineering, University at Buffalo, Buffalo, New York.

Repp, J., Badillo, H., Whittaker, A. S., and Reinhorn, A. M. (2003b). *Seismic Qualification of Suspended Ceiling Systems, Part 6.* Technical Report UB CSEE/SEESL-2003-03, Department of Civil, Structural, and Environmental Engineering, University at Buffalo, Buffalo, New York.

Restrepo, J. I., and Bersofsky, A. M. (2011). Performance Characteristics of Light Gage Steel Stud Partition Walls . *Thin Walled Struct., 49*, 317-324.

Retamales, R., Davies, R., Mosqueda, G., and Filiatrault, A. (2013). Experimental Seismic Fragility of Cold-Formed Steel Framed Gypsum Partition Walls. *Journal of Structural Engineering, 139*, 1285-1293.

Rihal, S., and Granneman, G. (1984). *Experimental Investigation of the Dynamic Behavior of Building Partitions and Suspended Ceiling During Earthquakes.* Rep. No. ARCE R84-1, California Polytechnic State University, Pomona, California.

RMS (Risk Management Solutions) Inc. (2006). *2006 Kiholo Bay, Hawaii Earthquake.* RMS Event Report, Newark, California.

Rodabaugh, E., and Moore, S. (1978). *Evaluation of the Plastic Characteristics of Piping Products in Relation to ASME Code Criteria.* USNRC NUREG Report No. NUREG/CR-0261.

Roh, H. S., Reinhorn, A. M., and Pitman, M. (2008). *Seismic Qualification Test of Suspended Ceiling Systems: System F8 of Chicago Metallic Corporation.* Report No. UB CSEE/SEESL-2008-08, Department of Civil, Structural, and Environmental Engineering, University at Buffalo, Buffalo, New York.

Ryu, K. P., and Reinhorn, A. M. (2013). *Capacity Evaluation of Suspended Ceiling Systems.* Technical Report MCEER-13-XXXX, Buffalo, New York. (in review).

Soroushian, S., Maragakis, E. M., Itani, M., Pekcan, G., and Zaghi, A. (2011). Design of a Test-Bed Structure for Shake Table Simulation of the Seismic Performance of Nonstructural Systems. *ASCE Structures Congress.* Las Vegas, Nevada.

Soroushian, S., Maragakis, E. M., Ryan, K., Sato, E., Sasaki, T., Okazaki, T., and Mosqueda, G. (2014a). Seismic Simulation of Integrated Ceiling-Partition Wall-Piping System at E-Defense, Part 2: Evaluation of Nonstructural Damage and Fragilities. *Journal of Structural Engineering*.

Soroushian, S., Maragakis, E. M., Zaghi, A., Echevarria, A., Tian, Y., and Filiatrault, A. (2014b). *Comprehensive Analytical Seismic Fragility of Fire Sprinkler Piping Systems.* Technical Report MCEER-14-0002, University of Nevada, Reno, Nevada.

Soroushian, S., Maragakis, E. M., Zaghi, A., Rahmanishamsi, E., Itani, A., and Pekcan, G. (2014c). Response of a 2-Story Test-Bed Structure for the Seismic Evaluation

of Nonstructural Systems. *Earthquake Engineering and Engineering Vibration*, Accepted.

Soroushian, S., Rahmanishamsi, E., Ryu, K., Maragakis, E., and Reinhorn, A. (2015). Experimental Fragility Analysis of Suspended Ceiling Systems. *Earthquake Spectra*, In-Press.

Soroushian, S., Ryan, K. L., Maragakis, E. M., Sato, E., Sasaki, T., Okazaki, T., Tedesco, L., Zaghi, A. E., Mosqueda, G., Alvarez, D. (2012). Seismic Response of Ceiling/Sprinkler Piping Nonstructural Systems in NEES TIPS/NEES Nonstructural/NIED Collaborative Tests on a Full Scale 5-Story Building. *Proceeding of the 43rd Structures Congress, ASCE/SEI.* Chicago, USA.

Soroushian, S., Zaghi, A. E., Maragakis, E. M., and Echevarria, A. (2014d). Seismic Fragility Study of Displacement Demand on Fire Sprinkler Piping Systems. *Journal of Earthquake Engineering, 18:7*, 1129-1150.

Soroushian, S., Zaghi, A. E., Maragakis, E. M., Tian, T., and Filiatrault, A. (2013). Analytical Seismic Fragility Analyses of Fire Sprinkler Piping Systems with Threaded Joints. *Earthquake Spectra*, In-press.

Taghavi, S., and Miranda, E. (2003). *Response Assessment of Nonstructural Building Elements.* Pacific Earthquake Engineering Research Center, PEER Report 2003/05, Univ. of California, Berkeley, California.

Takahashi, N., and Shiohara, H. (2004). Life Cycle Economic Loss Due to Seismic Damage of Nonstructural Elements. *The 13th World Conference on Earthquake Engineering.* Vancouver, B.C., Canada.

Tian, Y., Filiatrault, A., Mosqueda, G. (2013). *Experimental Seismic Study of Pressurized Fire Sprinkler Piping Subsystems.* Technical Report MCEER-13-0001, Multidisciplinary Center for Earthquake Engineering Research, State University of New York at Buffalo, Buffalo, New York.

USG Corporation (USG). (2010). *Seismic Ceiling Resources Center*. Retrieved March 12, 2015, from http://www.usg.com/rc/technicalarticles/seismic-technical-guide-hanger-wire-attachment-en-SC2522.pdf

Wais, E. (1995). Recent Changes to ASME Section III Welded Attachments (Lugs) Code Cases. *Internation Pressure Vessels and Piping Codes and Standard: Vol. 2-Current Perspectives, Vol. 313-2*, 29-31.

Wang, X., Pantoli, E., Hutchinson, T. C., Restrepo, J. I., Wood, R. L., Hoehler, M. S., Grzesik, P., and Sesma, F. H. (2015). Seismic Performance of Cold-Formed Steel Wall Systems in a Full-Scale Building. *J. Struct. Eng.*

Wittenberghe, J. V., Baets, P. D., and Waele, W. D. (2010). Nonlinear Contact Analysis of Different API Line Pipe Coupling Modifications. *ASME Journal of Pressure Vessel Technology, Vol. 132*, 1-7.

Yao, G. (2000). Seismic Performance of Direct Hung Suspended Ceiling Systems. *ASCE/Journal of Architectural Engineering, 6*, 6-11.

Yu, Q., and Gonzalez, D. (2008). Lessons Learned from the October 15, 2006 Hawaii Earthquake and the August 15, 2007 Peru Earthquake. *The 14th World Conference on Earthquake Engineering.* Beijing, China.